HYDRO-PNEUMATIC CONVEYING OF LIQUID

BY MEANS OF AN AIRLIFT PUMP

by

R.R. BERG
BSc (Civil Engineering), Cape Town

A thesis submitted to the University of Cape Town
in partial fulfillment of the requirements for the
degree of Master of Science in Engineering.

January 1988

Department of Civil Engineering
University of Cape Town

DEDICATION

To my parents.

DECLARATION

I, Rolf Rainer Berg, hereby declare that this thesis is my own work and that it has not been submitted for a degree at any other University.

Signed by candidate

R.R. BERG

January 1988

ABSTRACT

Airlift pumps operating in two-phase gas-liquid flow are investigated with a view to establishing an analytical technique to aid in theoretically modelling air-lift pump behaviour.

Extensive work on two test facilities constructed at the University of Cape Town's Hydrotransport Research facility has been done. Various components needed for the analysis are investigated. These include:

(i) static dilation;
(ii) dynamic void ratios;
(iii) two phase weight component;
(iv) two phase friction component;
(v) two phase acceleration component.

Using theoretical models for each component and combining these into the analysis technique, operating characteristics of airlift pumps with the following variables -

(i) pipe diameters;
(ii) gas injection depths;
(iii) static lift heights;
(iv) suction pipe lengths

have been successfully predicted.

ACKNOWLEDGEMENTS

I would like to express thanks to my thesis supervisor, Associate Professor J.H. Lazarus, for his guidance, enthusiasm and constant interest throughout the two year thesis period.

Also to Associate Professor F.A. Kilner, the staff of the Department of Civil Engineering and the Hydrotransport Research Unit team for helpful discussions and advice during many brainstorming sessions.

I extend thanks to the technical staff, Messrs. G. Bertuzzi, D.J. Botha and R. Edge as well as N. Hassen, A. Siko and the rest of the laboratory staff for their practical aid and assistance during construction and experimentation stages.

A particular word of thanks to R. Norman and the De Beers Marine staff involved in this project for their contributions and support and a special word of thanks to Mrs P. Jordaan for the typing of this thesis document.

Furthermore I thank the CSIR for financial support throughout the thesis period.

TABLE OF CONTENTS

LIST OF TABLES

LIST OF FIGURES

NOMENCLATURE

Symbol	Description	Unit
A	Cross-sectional area	m^2
b	Wetted perimeter	m
β	Volume flow ratio	
c	Empirical coefficient	
C_A	Armand coefficient	
D	Pipe diameter	m
ϵ_g	Dynamic void ratio	
ϵ_{go}	Static dilation	
f	Friction factor	
g	Gravitational acceleration	m/s^2
$h = \ell$	length	m
H	Hydraulic head loss	m
k_e	Entrance coefficient	
K	Constants	
η	Efficiency	
Δp	Pressure change	Pa
P	Static pressure	Pa
Q	Flow rate	m^3/s
R_e	Reynolds number	
s	Velocity ratio	
τ	Shear stress	Pa
v	Velocity	m/s
$v_{\ell s}$	Liquid superficial velocity	m/s
ν	Kinematic viscosity	m^2/s
W	Weight	N
X	Lockhart and Martinelli parameter	
Z	Height	m
ρ	Density	kg/m^3
ϕ	Two phase multiplier	

Subscripts

F	Friction
g	Gas
I	Inlet
ℓ	Liquid
m	Mixture
o	Standard conditions

CHAPTER 1

INTRODUCTION

The airlift pump in its simplest form consists of a vertical pipe submerged in a liquid. Air is introduced by means of an air injector near or at the lower end of this vertical pipe. The rising air bubbles cause a dilated air-liquid mixture to form inside the pipe which is less dense than the surrounding liquid. This pressure imbalance results in the vertical conveying of the liquid as well as, in required applications, solids up the inside of the pipe.

This method of hydro-pneumatic transport has been known since the 18th century. Throughout the 19th century towns and industries were growing rapidly and airlift pumps were successfully used to satisfy the demand for water. However, with the development of pumps of higher efficiencies, the use of airlift pumps was reduced, with the exception of uses where the reliability of the pumping operation was more important than its efficiency as well as the conveying of special materials, such as aggressive fluids.

Advantages of the air lift pump are its simple and robust nature. During operation, breakdowns rarely occur and maintenance of the pumping system is simple. These factors render it well suited for deep sea mining as well as the following applications:

- shaft and well drilling
- the lifting of fluids containing solids, wastewater and slurries
- the dredging of silt
- vertical lifting of coal in shafts
- deep sea mining of manganese modules and diamonds
- cleaning of settling tanks
- underwater exploration where pump impellers could damage recovered material
- vertical transport of aggressive and radio-active fluids
- the mixing of fluids and gases in the chemical industry.

The major disadvantages of the airlift pump are:

(i) a lower efficiency than other pumping methods. In a continuous pumping operation this could influence power costs considerably. It is for this reason that the airlift pump is rarely used for the pumping of water except in cases where sporadic pumping takes place;
(ii) a non-continuous flow at the delivery end, caused by pulsating air slugs.

Although the airlift pump is known for its simplicity of construction and maintenance, the theoretical aspects are far from simple. Various theories based on two phase flow in pipes try to model airlift pump behaviour. However, because these theories are concerned with specific airlift pump applications and are partly based on empirical values, it makes them questionable with respect to general validity.

In Southern Africa the airlift pump is extensively used for the reclamation of diamond bearing sediments off the west coast in deep water. This research project has the following objectives:

(a) An investigation into the background and available theories of the airlift pump.
(b) Design and construct airlift pump models to experimentally investigate analytical components and effects of variables on airlift pump behaviour.
(c) Refinement of two phase flow theory, with the view of establishing a correlation between theoretical approaches and prototype performances.
(d) Optimisation of the design of airlift pumps in general use.

CHAPTER 2

LITERATURE REVIEW AND THEORY

2.1 Introduction

This review is based on literature obtained from journals and books dating from 1925 to 1986. Literature has been presented in countries such as Japan, Russia, Sweden, United Kingdom and West Germany.

Various attempts have been made to analyse airlift pump behaviour theoretically. In most of these cases, the theories are concerned with specific airlift pump designs and thus the design procedures and methods of analysis vary.

After looking at the mechanism that causes and the various flow patterns encountered in two phase flow, this literature review consists of a discussion and analysis of some of the theoretical methods put forward by authors in an attempt to model airlift pump behaviour.

2.2 Two phase flow mechanism

Prior to discussing the analysis, it is necessary to understand how the airlift process works.

2.2.1 Static conditions

Figure 2.1(a) shows the layout of a typical airlift pump with no flow. It consists of a pipe, which is vertically immersed in a liquid, with its lower end a distance ($h_1 + h_2$) below the surface. The depth to which the pipe is immersed depends on the mode of operation of the airlift pump and has an effect on its pumping characteristics. If, for example, it were required to pump solid material, the lower end would have to be in contact with this solid material.

The other end of the pipe protrudes a distance h_3 vertically above the liquid's free surface, which is determined by the desired pumping height.

Gas is injected by means of a compressor or blower hose at a distance h_1 below the surface, into the vertical pipe. The distance h_2 below the injector point is referred to as the suction pipe and the distance ($h_1 + h_3$) above the injector point to the delivery outlet, is called the delivery pipe. The liquid outside the main airlift riser is termed the surrounding column and the lift height is the distance h_3.

Figure 2.1(a) shows conditions when no gas is injected at the injector point. The pressure of the surrounding column at any depth below the liquid surface is in equilibrium with the pressure inside the airlift pump. Both the liquids inside and outside the airlift pump have the same density and the system is in static equilibrium with no flow taking place.

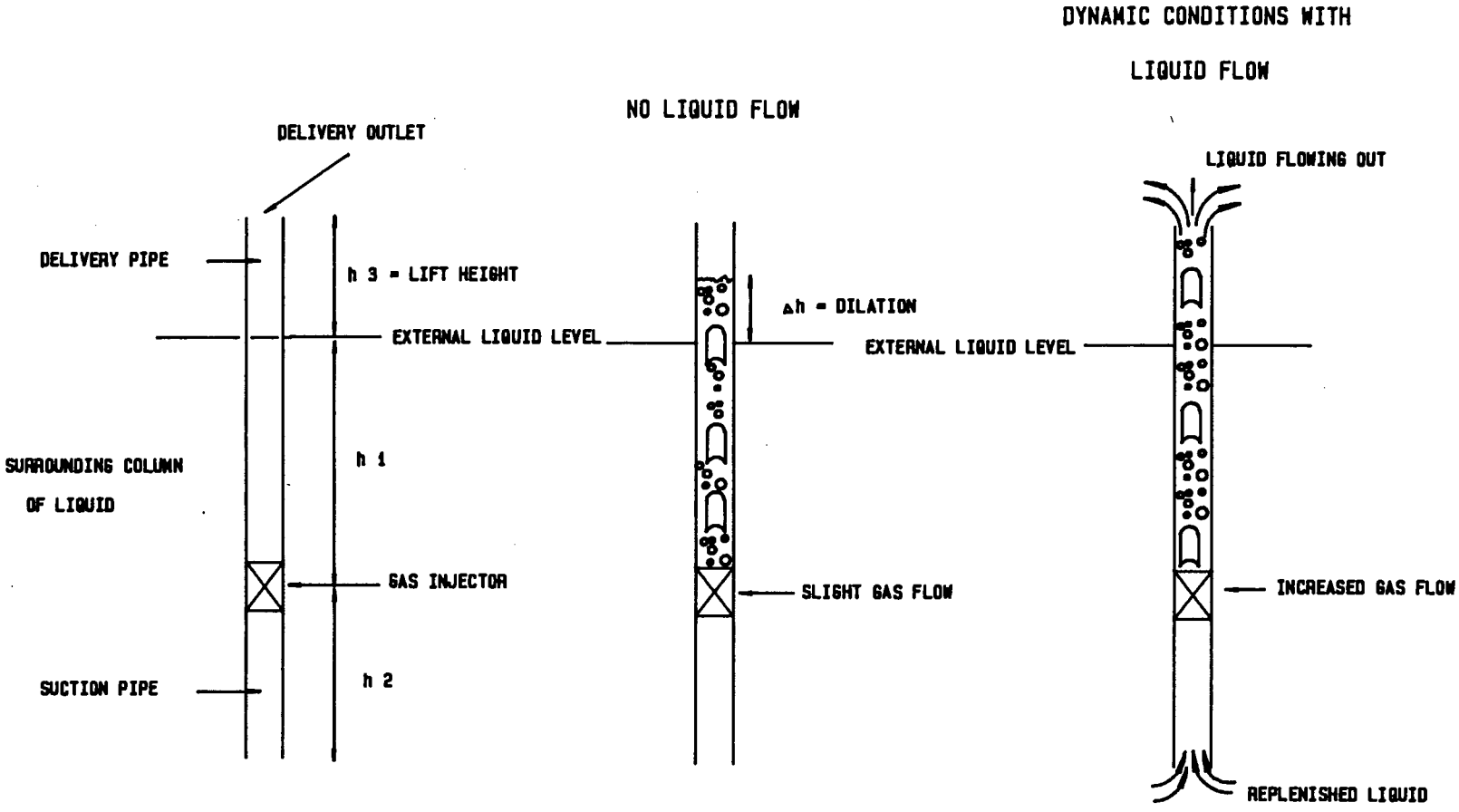

FIGURE 2.1 a

FIGURE 2.1 b

FIGURE 2.1 c

TWO PHASE FLOW MECHANISM

2.2.2 Dynamic Conditions

If gas is allowed to enter the airlift pump at the injector point, the level of the liquid inside the airlift pipe will dilate by a distance Δh as shown in Figure 2.1(b). This dilated distance is maintained until the gas input flow is altered. An increase in the gas flow results in an increased dilation and a decrease in the gas flow causes a decrease in the distance Δh. If the gas flow is increased to a point where Δh is larger than the lift height (h_s), the liquid will flow out of the delivery outlet.

The liquid which has been discharged at the delivery outlet is replenished at the bottom of the suction line, as shown in Figure 2.1(c).

A conveying system, whereby the liquid is conveyed vertically by a distance in excess of the lift height, is established. The cause of this is the gas input flow which directly influences the dilation.

In an attempt to explain the operation of the airlift process, most authors mention that a gas-liquid mixture of lesser density than the surrounding column of liquid forms inside the airlift pipe. (Weber 1976, 1982; Clark et al 1986; Alver 1954; Gibson 1925; Dedegil 1974, 1978, 1986; Giot 1986). Hence, a pressure dis-equilibrium is set up between the gas-liquid column inside the air-lift pump, and the surrounding column of liquid. To regain equilibrium, the gas-liquid mixture inside the pipe rises. If the height required to attain equilibrium is larger than the lift height, the liquid flows out the top and a dynamic equilibrium is set up.

The components of this dynamic equilibrium are:

1. The weight of the surrounding column of liquid.
2. The weight of the gas-liquid column inside the airlift pump.
3. The pressure losses due to the conveying of the gas-liquid column such as friction, isothermal expansion and entrance effects.

Very few authors actually examine the influence of the gas bubbles on the dilation. Halde et al 1981, Stenning et al 1968 and Chisholm 1985 however mention this effect in their analysis.

Consider an airlift tube with no liquid flowing and a single rising gas bubble, as shown in Figure 2.2. As soon as the gas bubble is injected, the liquid level dilates from point A to point B. As the bubble rises the liquid between the bubble and the pipe wall flows downwards. The liquid level remains at point B until the bubble emerges at this point, whereafter the level drops back down to point A. A continuous inflow of bubbles at a steady rate would cause the liquid level to rise to a point C, and remain there, as each time a bubble emerges at the top it is replaced by another at the gas injector. This effect is known as the "liquid hold-up".

Examining a control volume between points D and E inside the airlift pipe at any time interval and comparing it to a control volume at the same depth situated in the surrounding column, it is seen that the control volume inside the airlift pipe consists of a certain percentage gas, causing it to have a lower density than in the surrounding column of water. If there were no dilation and the liquid level inside the pipe were to remain at point A, then there would be a pressure dis-equilibrium between the two control volumes. To overcome this, the level inside the airlift pipe rises.

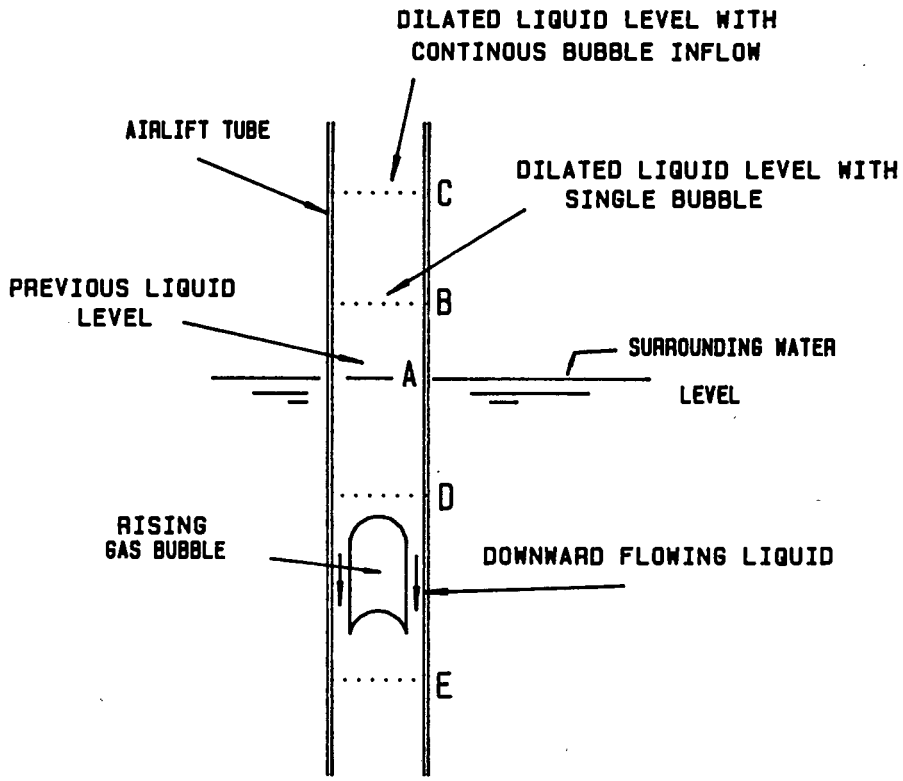

FIGURE 2.2 - LIQUID HOLD-UP

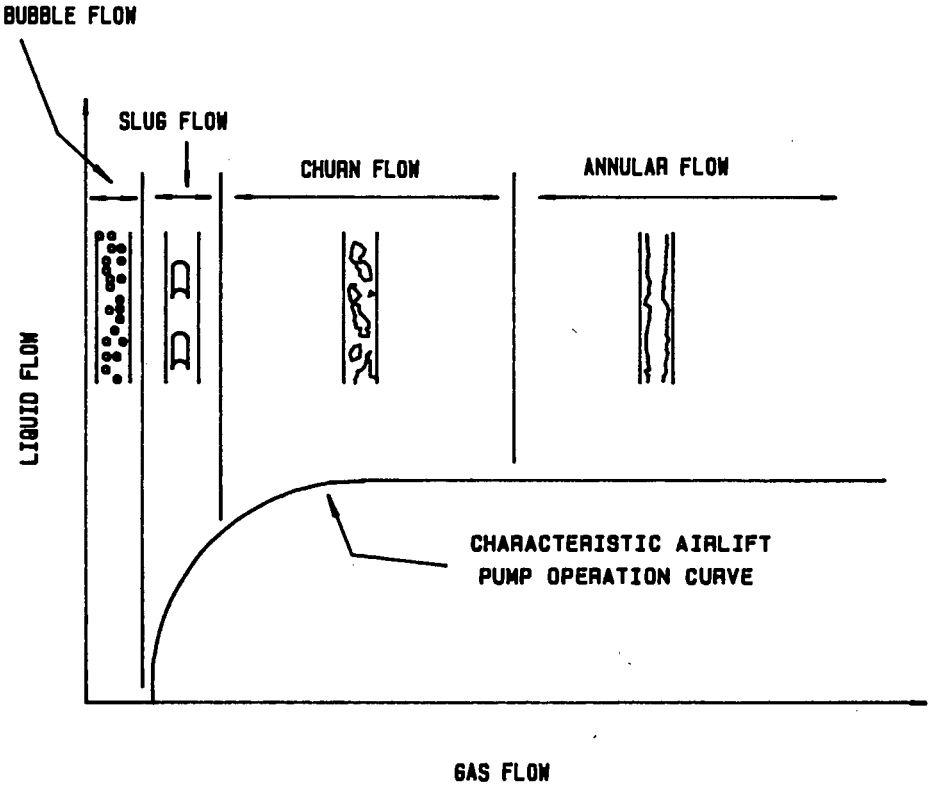

FIGURE 2.4 - TWO PHASE FLOW PATTERNS

The operation of the airlift process is thus directly related to the dilation of the gas-liquid column. This dilation could be the result of

(a) the "liquid hold-up" effect; and
(b) a density difference between the two control volumes inside and outside the airlift pipe.

These two conditions will result in the conveying of liquid in an airlift pump.

2.3 Two Phase Gas-Liquid Flow Patterns

There are many flow patterns that can occur in vertical two phase flow. In the literature a variety of classifications exist in order to distinguish between these flow patterns. Authors such as Govier et al and Taitel et al have produced formulas (Chisholm 1983) to model these classifications; however, because of the large amount of variables encountered in two phase flow, these become questionable.

Chisholm (1983) and Clark et al (1986) present four primary classifications for vertical two phase flow. These being:

1. Bubble flow
2. Slug flow
3. Churn flow
4. Annular flow.

Photographs of these four classifications, taken in the 40 mm airlift pump test facility at the University of Cape Town, are shown in Figures 2.3(a), (b), (c) and (d).

Referring to Figure 2.4, bubble flow is defined as very small bubbles of gas in a continuous liquid phase. This flow classification usually exists at very small gas flow rates and is not often encountered in operational airlift pumps. Increasing the gas flow rate results in the formation of slug-flow, which are bullet shaped slugs of gas known as the "Taylor Bubble" in a continuous liquid phase. Again this classification occurs at low gas flow rates. As the gas flow rate is increased, the slug flow changes to churn flow which is a highly mixed oscillatory flow, and is common to all airlift pumps. At very high gas flow rates the churn flow transforms into annular flow, where the liquid forms a film around the wall and the gas is located in a central core.

It is difficult to distinguish visually the point where one flow classification changes to another. This is the reason why so many other classifications are encountered in the literature. Table 2.1 presents some of these classifications which are often encountered when dealing with vertical two phase gas-liquid flow.

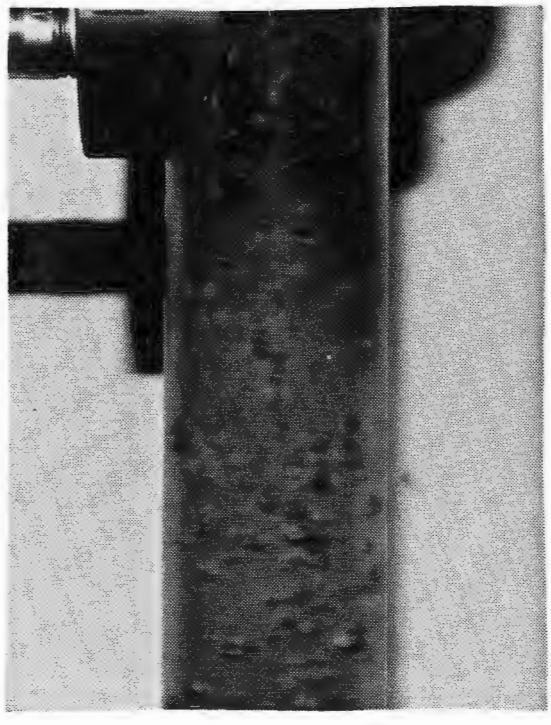

FIGURE 2.3a - BUBBLE FLOW

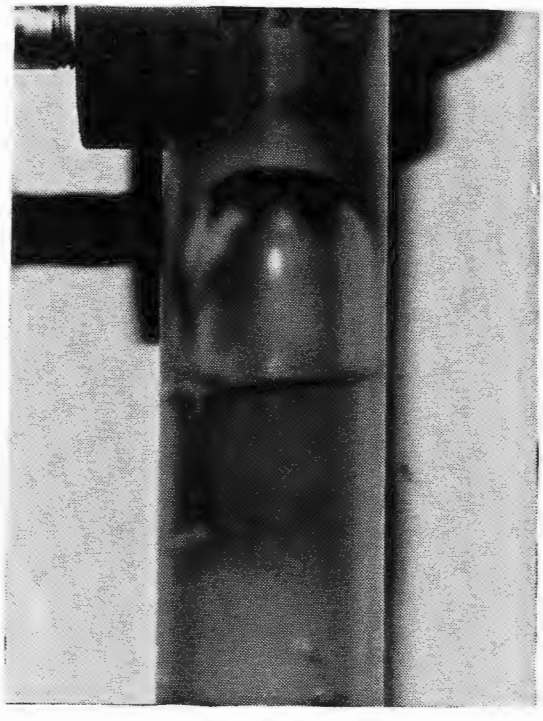

FIGURE 2.3b - SLUG FLOW

FIGURE 2.3c - CHURN FLOW

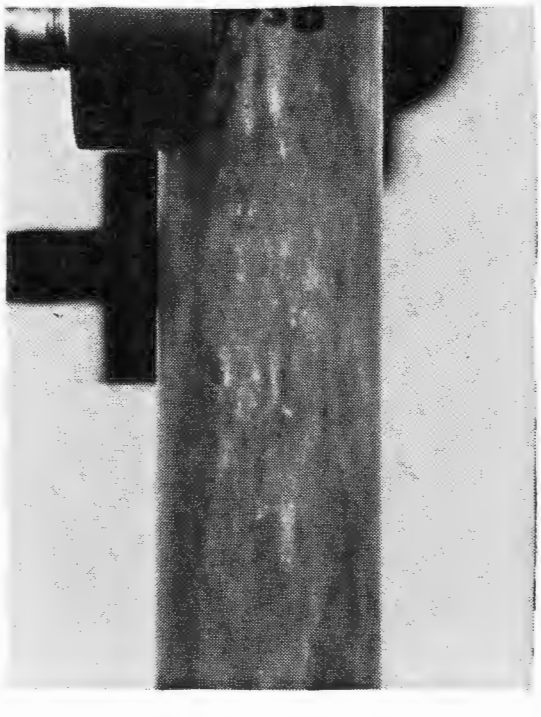

FIGURE 2.3d - ANNULAR FLOW

General classification	Alternative descriptions	Source	Alternative general classification	
1 Bubble	Froth	Hoogendoorn and Buitelar	Homogeneous	1
	Stratified bubble Pulsating bubble	Johnson and Abou-Sabe		
2 Plug	Elongated bubble	Gregory , Govier and Aziz	Intermittent	2
	Stratified plug	Sternling		
	Plug froth	Kosterin		
3 Slug	Stratified slug	Sternling , Johnson and Abou-Sabe		
	Splashing flow	Krasyakova		
	Frothy slug	Oshinowo and Charles		
	Plug	Chierici *et al.*		
4 Churn	Froth	Oshinowo and Charles		
	Dispersed	Kosterin		
5 Stratified	Divided	Kosterin	Separated	3
	Cresting flow	White and Huntington		
6 Annular	Film	Govier and Omer	Annular	4
	Mist annular	Hoogendoorn and Buitela		
	Ripple flow	White and Huntington		
	Slug annular	Sternling		
	Wispy annular	Collier		
	Ripple flow	White and Huntington		

TABLE 2.1 - CLASSIFICATIONS AND DESCRIPTIONS (CHISHOLM 1983)

2.4 Airlift Pump Analysis Technique

Most analysis techniques presented in the literature are based on balancing pressures. As stated before, an operating airlift pump is in dynamic equilibrium. That is, the pressure at a point near the entrance of the suction pipe (the static pressure gain Δp_1) located in the surrounding column of liquid is in balance with the pressure losses due to the conveying of the liquid up the inside of the pipe. The pressure losses due to the conveying of the liquid are given as:

1. Pressure losses in the suction pipe (Δp_2)
2. Pressure losses across the gas injector (Δp_3)
3. Pressure losses in the delivery pipe (Δp_4)

Once the three pressure drops and the static pressure gain have been obtained it is possible to perform a pressure balance, i.e.

$$\Delta p_1 = \Delta p_2 + \Delta p_3 + \Delta p_4 \qquad (2.1)$$

2.4.1 Static pressure gain

Referring to Figure 2.5, it is necessary to first obtain the pressure at a point B which is at the same elevation as the suction inlet of the airlift tube. This is done using Bernouilli's energy equation, i.e.

$$\frac{P_A}{w} + z_A + \frac{v_A^2}{2g} = \frac{P_B}{w} + z_B + \frac{v_B^2}{2g} + \Delta H_F \qquad (2.2)$$

where P_A = atmospheric pressure = P_o
z_A = 0 ; reference height
v_A = 0
P_B = pressure at point B
z_B = $-(h_1 + h_2)$
v_B = 0
ΔH_F = 0; pressure losses due to friction
w = ρg; where ρ is the liquid density

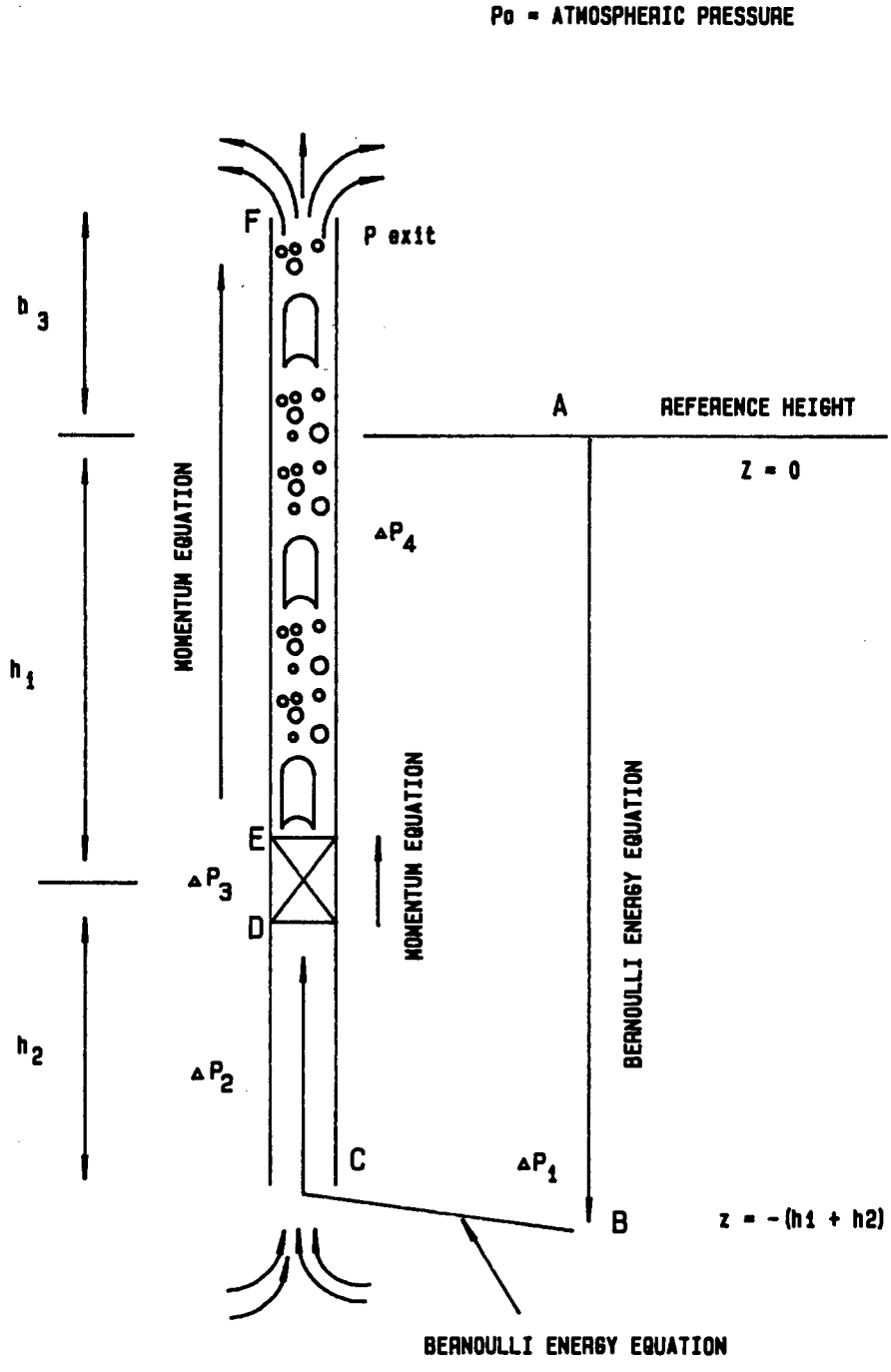

FIGURE 2.5 - AIRLIFT PUMP ANALYSIS

Equation (2.2) can be rewritten as

$$\Delta p_1 = P_B - P_o = w\,(h_1 + h_2) \qquad (2.3)$$

where Δp_1 = the static pressure gain obtained when moving from point A to point B in the surrounding column of liquid

This pressure gain must balance the following pressure losses.

2.4.2 Pressure losses in the suction line

To obtain the pressure losses in the suction line (Δp_2), Bernouilli's Energy Equation is applied between points B and D, namely

$$\frac{P_B}{w} + z_B + \frac{v_B^2}{2g} = \frac{P_D}{w} + z_D + \frac{v_D^2}{2g} + \Delta H_F + \Delta H_I \qquad (2.4)$$

where P_B = pressure at point B

$z_B = -(h_1 + h_2)$

$v_B = 0$

P_D = pressure at point D

v_D = velocity of the liquid at point D = $v_{\ell s}$ (liquid superficial velocity)

$z_D = -(h_1)$

ΔH_F & ΔH_I = pressure losses due to the suction pipe inlet at point C and due to friction in the suction pipe between points C and D.

Thus $$\Delta H_F + \Delta H_I = \frac{v_{\ell s}^2}{2g}\left(\frac{4f\ell}{D} + k_e\right) \qquad (2.5)$$

where f = friction factor

ℓ = pipe length h_2

D = internal pipe diameter

k_e = head loss coefficient for entrance (typically $k_e = 0.5$)

Combining equations (2.4) and (2.5), the pressure loss in the suction line can be obtained from

$$\Delta p_2 = P_B - P_D = w \left[h_2 + \frac{v_{\ell s}^2}{2g} \left(1 + \frac{4fh_2}{D} + k_e\right)\right] \qquad (2.6)$$

where Δp_2 = the pressure loss in the suction pipe.

2.4.3 Pressure losses across the gas injector

The gas injector pressure losses are obtained by applying the momentum equation to a control volume between points D and E on Figure 2.5. This control volume is taken to be very small and the gas-liquid weight as well as friction losses are assumed to be negligible.

Therefore: $$P_D A + \rho_D v_D^2 A = P_E A + \rho_E v_E^2 A + W + \Delta p_f A \qquad (2.7)$$

where:
- P_D = pressure at point D
- A = pipe area
- ρ_D = density of liquid = ρ_ℓ
- v_D = velocity of the liquid at point D
- $\Delta p_f A$ = friction of the gas-liquid mixture $\neq 0$
- W = weight of the gas-liquid mixture $\neq 0$
- $P_E A$ = force at point E, consisting of the pressure of the liquid as well as the pressure of the gas acting over their respective areas.

$$P_E A = P_\ell A_\ell + P_g A_g \qquad (2.8)$$

It is however assumed that the difference between liquid pressure P_ℓ and the gas presssure P_g is negligible.

$\rho_E v_E^2 A$ = momentum force of the gas-liquid mixture, which can be written as

$$\rho_E v_E^2 A = \epsilon_g \rho_g v_g^2 A + (1 - \epsilon_g) \rho_\ell v_\ell^2 A \qquad (2.9)$$

where ϵ_g = dynamic void ratio, which is an indication of the percentage of gas present at that section. This term will be examined in Section 2.5.1.1.

ρ_ℓ and ρ_g = densities of liquid and gas respectively

v_ℓ and v_g = velocities of liquid and gas respectively.

The velocities of the liquid and gas can be obtained from

$$v_\ell = \frac{Q_\ell}{(1 - \epsilon_g)A} \qquad (2.10)$$

and

$$v_g = \frac{Q_g}{\epsilon_g A} \qquad (2.11)$$

where Q_ℓ = liquid flow rate

Q_g = gas flow rate.

Combining equations (2.7) and (2.9) and assuming the liquid and gas pressures are the same after gas injection, the following equation is obtained to calculate the pressure drop (Δp_s) across the gas injector:

$$\Delta p_s = P_D - P_E = -\rho_\ell v_D^2 + \left[\epsilon_g \rho_g v_g^2 + (1 - \epsilon_g) \rho_\ell v_\ell^2\right] \qquad (2.12)$$

At this stage it is important to distinguish between the velocities v_g, v_ℓ and $v_{\ell s}$.

$v_{\ell s}$ = the liquid superficial velocity, defined as the velocity if the liquid were to flow across the whole pipe section. This quantity relates to the liquid velocity in the suction pipe, before gas injection.

$$v_{\ell s} = \frac{Q_\ell}{A} \qquad (2.13)$$

Velocities v_ℓ and v_g are velocities after gas injection and can be obtained from equations (2.10) and (2.11).

2.4.4. Pressure losses in the delivery line

To obtain the pressure losses in the delivery pipe, Δp_4, the momentum equation is again applied to a control volume between points E and F.

Moving up the delivery pipe from points E to F, the pressure decreases, resulting in the isothermal expansion of the gas bubbles. This effect can be modelled using Boyle's Law

$$Q_{gx} = \frac{Q_{go} P_o}{P_x} \qquad (2.14)$$

where Q_{gx} = gas flow rate at section x in the delivery pipe.

Q_{go} = gas flow rate at S.T.P.

P_o = atmospheric pressure.

P_x = pressure at section x.

To allow for this effect, it is necessary to analyse the pressure losses over small increments up the pipe and then to integrate over the pipe length. Assuming that the control volume E to F makes up one such increment, the Momentum Equation can be written as:

$$P_E A + \rho_E v_E^2 A = P_F A + \rho_F v_F^2 A + W + \Delta p_f A \qquad (2.15)$$

where

$P_E A$ and $P_F A$ = forces at points E and F consisting of the pressures of liquid and gas multiplied by their respective areas as in (2.8)

$\rho_E v_E^2 A$ and $\rho_F v_F^2 A$ = momentum forces of the gas-liquid mixture which can be written as in (2.9) with its components as in (2.10) and (2.11).

W = weight of the gas-liquid mixture

$\Delta p_f A$ = friction force of the moving gas-liquid mixture.

Thus equation (2.15) can be written as

$$\Delta p_4 = P_E - P_F = - \left[\epsilon_g \rho_g v_g^2 + (1 - \epsilon_g) \rho_\ell v_\ell^2\right]_E + \left[\epsilon_g \rho_g v_g^2 + (1 - \epsilon_g) \rho_\ell v_\ell^2\right]_F + W + p_f A \qquad (2.16)$$

2.4.4.1 Two phase weight and friction components

To calculate the weight (W) and friction ($\Delta p_f A$) of the two phase gas-liquid mixture, various models have been presented in the literature, which will be examined and modified in further detail.

Firstly, models to calculate the weight component presented by Giot et al (1986), Stenning et al (1968), Clark et al (1986), Chisholm (1983) and Weber (1976, 1982) will be discussed. Thereafter friction models presented by Stenning et al (1968), Clark (1986), Weber (1976, 1982) and a two phase multiplier model presented by Chisholm (1983) will be examined.

2.5 Two Phase Weight Models

2.5.1 Introduction

In order to calculate the pressure losses in the delivery line using equations (2.15) or (2.16), one of the components that has to be evaluated is the weight of the gas-liquid mixture.

In the evaluation methods presented by Chisholm (1983), Clark et al (1986), Giot et al (1986) and Weber (1976, 1982) use is made of the dynamic void ratio mentioned in equation (2.9). To calculate the weight component, the dynamic void ratio has to be predicted and for this reason various methods have been used in the literature. Stenning et al (1968) suggests a different method, and does not use dynamic void ratios.

After defining the dynamic void ratio, and presenting the equation used for calculating the weight of the two phase gas-liquid mixture, the various void ratio models and the method presented by Stenning et al will be examined.

2.5.1.1 Dynamic void ratio

A column of vertically moving two phase mixture is made up of a certain percentage gas and a remaining percentage of liquid.

The definition of dynamic void ratio (ϵ_g) is the area of gas divided by the total area of the pipe cross-section at any point up the delivery pipe under conditions of mixture flow.

Thus

$$\epsilon_g = \frac{A_g}{A} \qquad (2.17)$$

where A_g = area occupied by the gas

A = cross-sectional area of the pipe

The remaining percentage of liquid present can be obtained from

$$\epsilon_\ell = 1 - \epsilon_g = \frac{A_\ell}{A} \qquad (2.18)$$

To calculate the dynamic void ratio, it is necessary to determine the fractional areas of the gas and liquid present at a control section. This presents a certain amount of difficulty because:

1. the gas volume and liquid volume move relative to each other;
2. the gas volume expands isothermally as the pressure decreases up the air-lift pipe length;
3. the gas volume is influenced by the rate of movement of the liquid volume;
4. both the gas and liquid volumes present are influenced by the airlift pump parameters such as pipe dimension, lift height and suction pipe depths.

From this it can be seen that in each airlift-pump, determination of the dynamic void ratio is dependent on the system characteristics and is a function of:

1. the gas flow
2. the liquid flow
3. the delivery pipe area
4. the pressure at any section along the delivery pipe

2.5.2 Weight model presented by Stenning et al (1968)

To calculate the weight component of the two phase mixture, Stenning does not use dynamic void ratios. Instead he presents the following method:

The weight of the gas-liquid mixture can be calculated from

$$W = hg\,(\rho_\ell A_\ell + \rho_g A_g) \tag{2.22}$$

also

$$Q_\ell = A_\ell v_\ell \tag{2.23}$$

$$Q_g = A_g v_g \tag{2.24}$$

$$A_g + A_\ell = A \tag{2.25}$$

Substituting equations (2.23), (2.24) and (2.25) into equation (2.22) and neglecting ρ_g in comparison to ρ_ℓ, the following equation is obtained

$$W = h\,g\,\frac{\rho_\ell A}{\left[1 + \frac{Q_g}{s\,Q_\ell}\right]} \tag{2.26}$$

where s is the ratio of the gas velocity to the liquid velocity

$$s = \frac{v_g}{v_\ell} \tag{2.27}$$

To determine the value of s, Stenning uses a method presented by Griffith et al for slug flow

$$s = \frac{v_g}{v_\ell} = 1.2 + 0.2\,\frac{Q_g}{Q_\ell} + \frac{0.35\,\sqrt{g\,d}}{\frac{Q_\ell}{A}} \tag{2.28}$$

Using equation (2.28) and (2.26) Stenning calculates the weight component of the two phase mixture.

2.5.3 Weight model presented by Chisholm (1983)

Chisholm in his calculations to model the weight of the two phase mixture predicts the dynamic void ratio.

Using an approach presented by Armand in 1946, Chisholm suggests that for pressures close to atmospheric, the dynamic void ratio is given by

$$\epsilon_g = C_A \beta \tag{2.29}$$

where C_A = Armand coefficient

β = volume flow ratio, which is defined as the flow rate of gas divided by the total flow rate of the mixture.

Thus $$\beta = \frac{Q_g}{Q_g + Q_\ell} \tag{2.30}$$

To calculate the Armand coefficient, Chisholm derives the following equation (see Appendix B):

$$\frac{1}{C_A} = \beta + \frac{1 - \beta}{\left[1 - \beta \left(1 - \frac{\rho_g}{\rho_\ell}\right)\right]^{1/2}} \tag{2.31}$$

2.5.4 Weight model presented by Giot et al (1986)

In analysing his airlift pump, Giot uses the same approach as Chisholm for predicting the dynamic void ratio.

To calculate this quantity as well as the volume flow ratio (β), Giot uses equations (2.29) and (2.30). However, for predicting the Armand coefficient Giot suggests a constant value of 0.8 which he states would be applicable to most operating airlift pumps. Thus

$$\epsilon_g = 0.8 \beta \tag{2.32}$$

2.5.5 Weight model presented by Clark et al (1985, 1986)

Clark, for predicting dynamic void ratios, uses a drift flux model presented by Zuber and Findlay in 1962.

Zuber and Findlay, in their analysis, suggest that for vertical two phase flow, the following equation can be used to obtain the dynamic void ratio of a moving gas-liquid column.

$$\left(\frac{1}{\epsilon_g}\right)\left(\frac{Q_g}{A}\right) = K_1 \left(\frac{Q_g}{A} + \frac{Q_\ell}{A}\right) + K_2 (gd)^{1/2} \qquad (2.33)$$

where $K_2(gd)^{1/2}$ = drift velocity of a Taylor bubble mentioned in Section 2.3

K_2 = 0.35

K_1 = empirically obtained factor used in correcting for the central position of the gas slug in the pipe = 1.2

2.5.6 Weight model presented by Weber et al (1976, 1982)

In the above models, expressions are given to calculate the dynamic void ratios directly.

Weber in his analysis of the airlift pump uses a quantity called the static dilation and presents a technique for converting the static dilation to the dynamic void ratio.

2.5.6.1 **Static dilation**

To determine this quantity it is necessary to measure the dilation of a gas-liquid column under conditions of no liquid flow.

Considering a column as in Figure 2.1b, the static dilation is given by the following equation.

$$\epsilon_{go} = \frac{\Delta h}{h_1 + \Delta h} \qquad (2.34)$$

Unlike the dynamic void ratio, the static dilation is defined as the volume concentration of gas enclosed in a column of liquid and gas during conditions of no mixture flow.

Research by Pichert (1931), Schuring (1934), Bath (1963) and Weber (1965) has shown that knowledge of the static dilation has the advantage of being a function of gas flow and pipe area only. This makes it possible to construct curves for static dilation which would be applicable to all pipe sizes.

2.5.6.2 **Weber et al conversion technique (1976, 1982)**

Having obtained the static dilation for one particular delivery pipe size over a range of gas flow rate values, Weber suggests the following method of converting the static dilation to the dynamic void ratio.

Under non-flowing conditions, the "mean relative velocity" between gas and liquid is given by:

$$v_{go} = \frac{Q_g}{\epsilon_{go} A} \qquad (2.35)$$

Assuming that this relative velocity is not affected when both the liquid and gas flow, then the following equation can be used to obtain the "mean absolute velocity" of the gas:

$$v_g = v_{go} + v_\ell \qquad (2.36)$$

Also from continuity, equations (2.10), (2.11) and (2.18) apply. Furthermore

$$\epsilon_g = \frac{A_g}{A} \qquad (2.37)$$

$$\text{and } \epsilon_\ell = (1 - \epsilon_g) = \frac{A_\ell}{A} \qquad (2.38)$$

Substituting equations (2.35), (2.37), (2.38), (2.10), (2.11) and (2.18) into equation (2.36), the following equation is obtained for converting the static dilation to the dynamic void ratio in a vertically moving gas-liquid column.

$$\epsilon_g = \frac{1}{2}\left[1 + \epsilon_{go}\left(\frac{Q_g+Q_\ell}{Q_g}\right) - \sqrt{\left(1 + \epsilon_{go}\left(\frac{Q_g+Q_\ell}{Q_g}\right)\right)^2 - 4\,\epsilon_{go}}\right] \quad (2.39)$$

The weight of the gas-liquid mixture in the delivery pipe can be evaluated using one of the above mentioned models. The applicability of each of the models presented above will be examined in further detail (Refer section 7.2.3).

2.6 TWO PHASE FRICTION MODELS

2.6.1 Introduction

To be able to calculate the pressure loss in the delivery pipe (Δp_4) using equation (2.16), the other component that has to be modelled is the pressure drop due to friction of the moving two phase mixture.

In the literature, various techniques are presented. These range from statements such as "the friction pressure loss of gas-liquid flow is six times that of liquid flow only" (Gibson, 1925) to complex models using two phase multipliers (Chisholm, 1983).

Two phase friction models presented by Stenning et al, Clark et al, Weber et al and Chisholm, will be examined in further detail, in order to establish their validity in the airlift pump analysis.

2.6.2 Friction model presented by Stenning et al (1968)

To calculate the friction in a gas-liquid control column of length (ℓ), Stenning suggests:

$$\Delta p_f A = \tau \ell b \qquad (2.40)$$

where τ = average wall shear stress
b = wetted perimeter of the pipe = πD
ℓ = pipe length = h

to calculate the average wall shear stress (τ), Stenning uses an equation presented by Griffith et al:

$$\tau = f_\ell \frac{\rho_\ell}{2} \left(\frac{Q_\ell}{A}\right)^2 \left(1 + \frac{Q_g}{Q_\ell}\right) \qquad (2.41)$$

where f_ℓ = the friction factor to be obtained assuming that the mixture flows as liquid through the pipe with a volume flow rate of $(Q_g + Q_\ell)$, (see Figure 2.6).

Combining equations (2.40) and (2.41), Stenning's friction pressure model becomes:

$$p_f = f_\ell \frac{\rho_\ell}{2} \left(\frac{Q_\ell}{A}\right)^2 \left(1 + \frac{Q_g}{Q_\ell}\right) \frac{h \pi d}{A} \qquad (2.42)$$

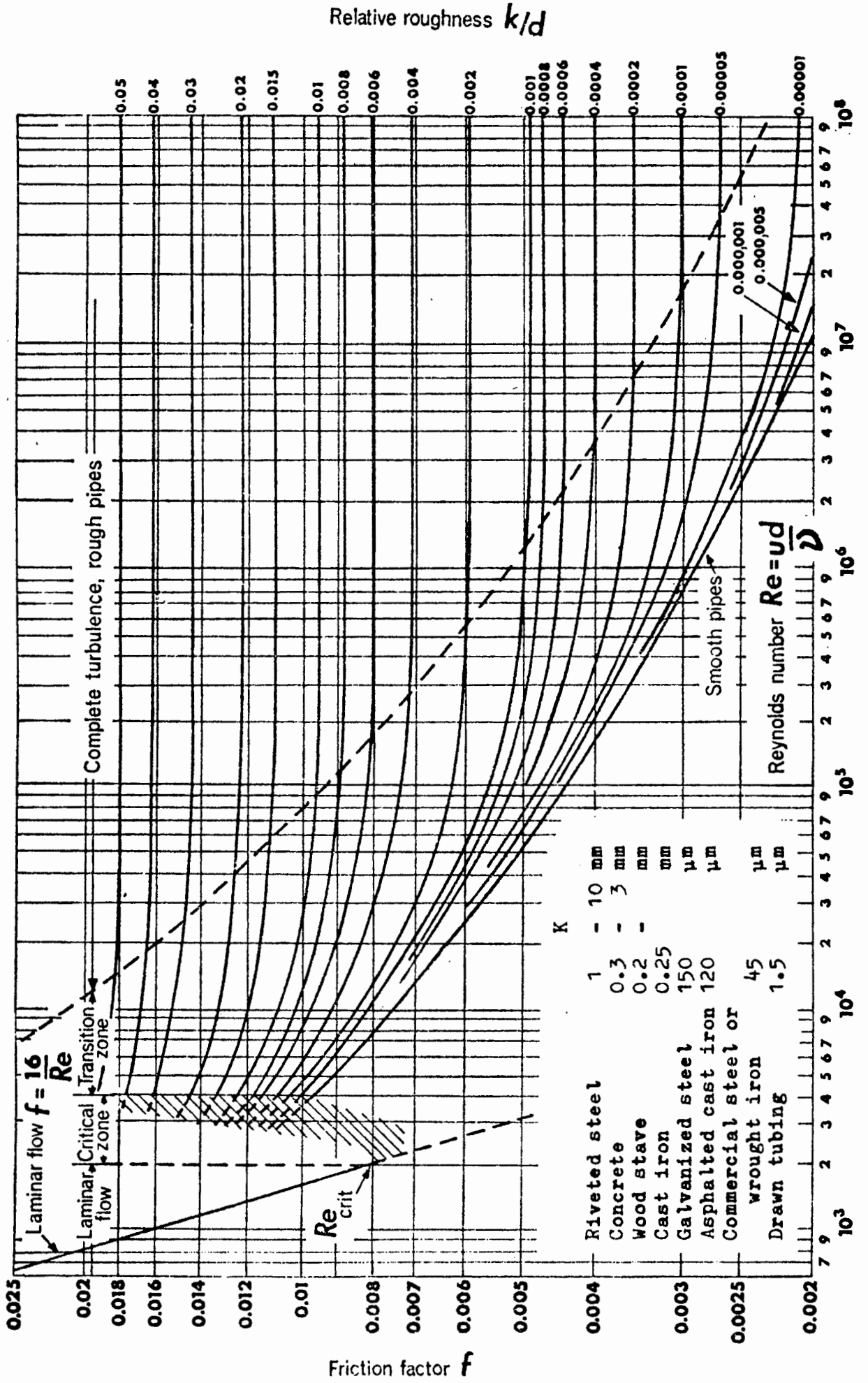

FIGURE 2.6 - FRICTION FACTOR VS REYNOLDS NUMBER DIAGRAM

2.6.3 Friction model presented by Clark et al (1986)

Clark, in his analysis, uses an approach suggested by Lockhart and Martinelli (1949) in which they state, that the friction pressure loss is a product of the friction head loss if liquid alone were flowing in the pipe and a two phase multiplier ϕ^2. Thus

$$p_f = \frac{2 f_\ell \rho_\ell h v_{\ell s}^2}{D} \phi^2 \qquad (2.43)$$

where f_ℓ = friction factor to be obtained assuming liquid alone flows through the pipe with a volume flow rate of Q_ℓ.
ϕ^2 = two phase multiplier
$v_{\ell s}$ = liquid superficial velocity
D = pipe diameter

To obtain the two phase multiplier ϕ^2, Clark suggests that in slug flow this quantity can be approximated using:

$$\phi^2 = (1 + 1.5\, \epsilon_g) \qquad (2.44)$$

Substituting equation (2.44) into (2.43), Clark's friction pressure loss equation becomes:

$$\Delta p_f = \frac{2 f_\ell \rho_\ell h v_{\ell s}^2}{D} (1 + 1.5\, \epsilon_g) \qquad (2.45)$$

2.6.4 Friction model presented by Weber et al (1976, 1982)

In his airlift pump analysis, Weber uses the following approach to calculate the friction pressure loss due to the gas-liquid mixture

$$\Delta p_f = \frac{2 f_\ell h}{D} \left(\epsilon_g \rho_g v_g^2 + (1 - \epsilon_g) \rho_\ell v_\ell^2 \right) \qquad (2.46)$$

where f_ℓ = friction factor to be obtained as in Section 2.6.2.
ϵ_g = dynamic void ratio
v_ℓ = velocity of liquid
v_g = velocity of gas
D = pipe diameter

2.6.5 Friction model presented by Chisholm (1983)

Chisholm uses a similar approach to Clark, in stating that the friction pressure loss is the product of the friction pressure loss under liquid flow conditions and a two phase multiplier ϕ^2 as in equation (2.43).

However, to calculate the two phase multiplier ϕ^2, Chisholm uses the following expression based on work done by Lockhart and Martinelli:

$$\phi^2 = 1 + \frac{c}{X} + \frac{1}{X^2} \qquad (2.47)$$

where X = the Lockhart and Martenelli parameter
c = empirical coefficient.

The Lockhart and Martenelli parameter X is defined as the square root of the ratio of the friction pressure loss if the liquid component flows alone to the loss if the gas component flows alone.

$$X^2 = \left(\frac{p_{f\ell}}{p_{fg}}\right) \qquad (2.48)$$

from this it can be shown that

$$X^2 = \frac{f_\ell \rho_\ell v_\ell^2}{f_g \rho_g v_g^2} \qquad (2.49)$$

where f_ℓ and f_g are calculated using Reynolds numbers as follows:

$$\text{for } f_\ell : \quad Re_\ell = \frac{v_\ell d}{\nu_\ell} \qquad (2.50)$$

$$\text{for } f_g : \quad Re_g = \frac{v_g d}{\nu_g} \qquad (2.51)$$

where ν_ℓ and ν_g represent the kinematic viscosity of the liquid and gas respectively.

The empirical coefficient c, is obtained by Chisholm from research conducted in a 27 mm bore pipe at pressures close to atmospheric. His results are shown in Figure 2.7.

From this log plot of the Lockhart and Martinelli parameter X and the value of (ϕ-1), it is seen that the curve to fit the data is given by equation (2.47) with c as 26.

Thus by combining equation (2.43) and (2.47), Chisholm's friction pressure loss model becomes:

$$\Delta p_f = \frac{2 f_\ell \rho_\ell h v_{\ell s}^2}{D} \left(1 + \frac{26}{X} + \frac{1}{X^2}\right) \qquad (2.52)$$

where X is defined by equation (2.49).

It is now possible to calculate the friction pressure loss by using one of the above models. The applicability of each will be researched in further detail (Refer section 7.2.4).

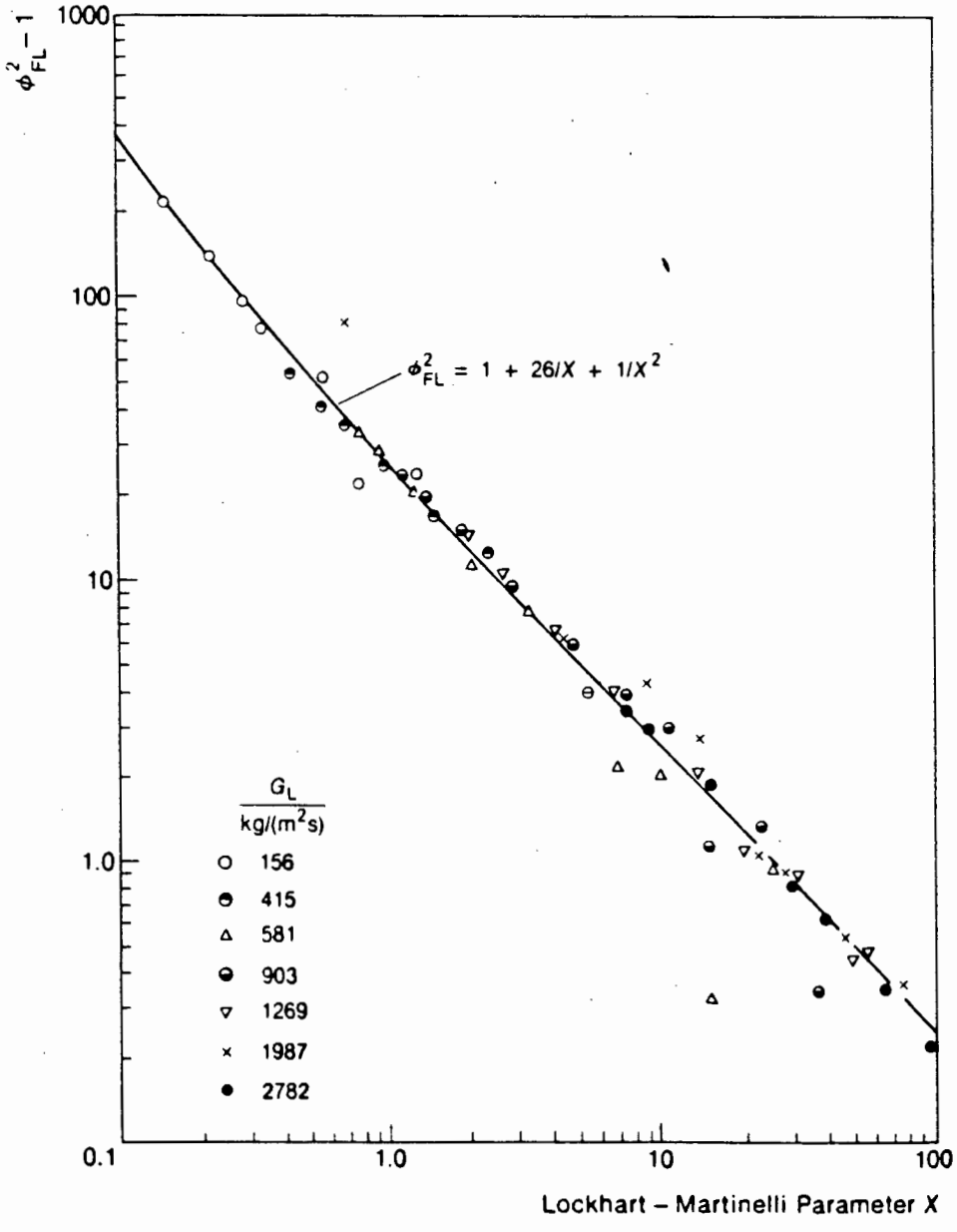

FIGURE 2.7 - TWO PHASE MULTIPLIER (CHISHOLM 1983)

2.7 Two Phase Acceleration Model

As stated in Section 2.4.4, the pressure decreases up the delivery pipe. This decrease results in isothermal expansion of the gas according to Boyles Law (equation 2.14).

Because the liquid flow remains constant and the area occupied by the liquid decreases due to the expanding gas, the velocity of the liquid increases by continuity. This results in the liquid accelerating up the delivery pipe causing a pressure drop.

Referring to equation (2.9) and (2.16), this effect is modelled in the momentum equation by the terms:

$$- \left[\epsilon_g \rho_g v_g^2 + (1 - \epsilon_g) \rho_\ell v_\ell^2\right]_{\text{before}}$$

$$+ \left[\epsilon_g \rho_g v_g^2 + (1 - \epsilon_g) \rho_\ell v_\ell^2\right]_{\text{after}} \qquad (2.53)$$

In the literature other equations which reduce to equation 2.53 are presented to model the acceleration effect (Chisholm, 1983).

2.8 Conclusion

To analyse airlift pumps it is necessary to calculate pressures throughout the system. These include -

1. pressure gain due to static head;
2. pressure loss in the suction pipe;
3. pressure loss across the air injector; and
4. pressure loss in the delivery pipe.

Pressure losses in the delivery pipe are due to -

1. the weight of the two phase mixture;
2. the friction of the two phase mixture with the pipe wall;
3. the acceleration of the two phase mixture caused by the expanding gas bubbles.

Various models exist in the literature to calculate the components of the delivery pipe pressure losses. Table 2.2 shows models presented to analyse the weight of the gas-liquid mixture and Table 2.3 shows the models presented to analyse the friction of the gas-liquid mixture.

Having calculated all the pressures throughout the system, it is now possible to apply a pressure balance using equation (2.1) and to solve for the gas and liquid flow rates in a particular airlift pump.

TABLE 2.2 : TWO PHASE WEIGHT MODELS

Author	Method	Models	Equation No.
Stenning et al (1968)	Direct weight	$w = hg \dfrac{\rho_\ell A}{\left[1 + \dfrac{Q_g}{sQ_\ell}\right]}$	2.6
	Griffith et al	$s = \dfrac{v_g}{v_\ell} = 1.2 + 0.2 \dfrac{Q_g}{Q_\ell} + \dfrac{0.35\sqrt{g\,d}}{\dfrac{Q_\ell}{A}}$	2.28
Chisholm (1983)	Dynamic void ratio prediction using Armand coefficient	$W = A\,g\,h\,[\rho_g \epsilon_g + \rho_\ell (1-\epsilon_g)$	2.21
		$\epsilon_g = C_A \beta$	2.29
		$\beta = \dfrac{Q_g}{Q_g + Q_\ell}$	2.30
		$\dfrac{1}{C_A} = \beta + \dfrac{1-\beta}{\left[1 - \beta(1 - \dfrac{\rho_g}{\rho_\ell})\right]^{1/2}}$	2.31
Giot et al (1986)	Dynamic void ratio prediction using Armand coefficient	$W = A\,g\,h\,[\rho_g \epsilon_g + \rho_\ell(1 - \epsilon_g)]$	2.21
		$\epsilon_g = 0.8\,\beta$	2.32
		$\beta = \dfrac{Q_g}{Q_g + Q_\ell}$	2.30
Clark et al (1986)	Dynamic void ratio prediction using Zuber and Finlay	$W = A\,g\,h\,[\rho_g \epsilon_g + \rho_\ell(1 - \epsilon_g)]$	2.21
		$\left(\dfrac{1}{\epsilon_g}\right)\left(\dfrac{Q_g}{A}\right) = 1.2\left(\dfrac{Q_g}{A} + \dfrac{Q_\ell}{A}\right) + 0.36\,(gd)^{1/2}$	2.33
Weber et al (1976, 1982)	Static to dynamic void ratio conversion	$\Delta H_w = g\,h\,[\rho_g \epsilon_g + \rho_\ell(1 - \epsilon_g)]$	2.21
		$\epsilon_{go} = f_n\,(Q_{go};\, A) = \dfrac{\Delta h}{h_1 + \Delta h}$	2.34
		$\epsilon_g = \dfrac{1}{2}\left[1 + \epsilon_{go}\left(\dfrac{Q_g + Q_\ell}{Q_g}\right) - \sqrt{\left(1+E_{go}\left(\dfrac{Q_g + Q_\ell}{Q_g}\right)\right)^2 - 4\,\epsilon_{go}}\right]$	2.39

TABLE 2.3 : TWO PHASE FRICTION MODELS

Author	Method	Models	Equation No.
Stenning et al (1968)	Griffith	$\Delta p_f = f_\ell \dfrac{\rho_\ell}{2}\left(\dfrac{Q_\ell}{A}\right)^2 \left(1 + \dfrac{Q_g}{Q_\ell}\right) \dfrac{h\pi d}{A}$	2.42
Clark et al (1986)	Lockhart and Martinelli	$\Delta p_f = \dfrac{2\,f_\ell\,\rho_\ell h\,v_{\ell s}^2}{D}(1 + 1.5\,\epsilon_g)$	2.45
Weber et al (1976, 1982)		$\Delta p_f = \dfrac{2\,f_\ell\,h}{D}(\epsilon_g\,\rho_g\,v_g^2 + (1-\epsilon_g)\,\rho_\ell\,v_\ell^2)$	2.46
Chisholm (1983)	Lockhart and Martinelli	$\Delta p_f = \dfrac{2\,f_\ell\,\rho_\ell h\,v_{\ell s}^2}{D}\left(1 + \dfrac{26}{x} + \dfrac{1}{x^2}\right)$	2.52
		$x^2 = \dfrac{f_\ell}{f_g}\dfrac{\rho_\ell}{\rho_g}\dfrac{v_\ell^2}{v_g^2}$	2.49

2.9 Pumping efficiency

The efficiency of a system is defined as the energy output divided by the energy input.

$$\eta = \frac{\text{energy output}}{\text{energy input}} \tag{2.54}$$

The energy output in the case of airlift pumps operating in two-phase flow consists of the potential energy gained in raising a volume of liquid by a unit height. Referring to figure 2.1a, and expressing the potential energy gain in terms of power, the output consists of the power gain in lifting the liquid by a distance (h_s) as well as the power of the liquid jet at the delivery outlet.

$$\text{output} = Q_\ell \; g \; \rho_\ell \; h_s + Q_\ell \; g \; \rho_\ell \; \frac{v_\ell^2}{2g} \tag{2.55}$$

where Q_ℓ = liquid flow rate
ρ_ℓ = liquid density
v_ℓ = liquid velocity at the delivery outlet given by equation (2.10)
h_s = lift height

The energy input expressed in terms of power consists of the power input by the compressor given by

$$\text{input} = Q_{go} \; p_o \; \ln \frac{p_i}{p_o} \tag{2.56}$$

where Q_{go} = air flow rate
p_o = atmospheric pressure
p_i = injector pressure

Combining equations (2.54), (2.55) and (2.56) results in the following equation for calculating the efficiency of an airlift pump operating in two phase flow.

$$\eta = \frac{Q_\ell \; g \; p_\ell \; (h_s + \frac{v_\ell^2}{2g})}{Q_{go} \; p_o \; \ln \frac{p_i}{p_o}} \tag{2.57}$$

CHAPTER 3

RESEARCH APPARATUS

3.1 Introduction

To aid in modelling and analysing airlift pump behaviour, two research facilities have been constructed in the hydraulics laboratory of the University of Cape Town. Both systems are airlift pumps with the following delivery pipe diameters:

1. 40 mm o.d. and 36 mm i.d.
2. 90 mm o.d. and 86 mm i.d.

In the operation of an airlift pump the static pressure mentioned in Section 2.4 is a vital component. To provide this static pressure both airlift pumps were constructed as recirculating systems with constant head tanks. Both systems have delivery pipes constructed of clear P.V.C. in order to observe visually the behaviour of airlift pumps.

The facilities were designed to investigate the performance of airlift pumps under the following independent variable conditions:

(a) varying the static lift;
(b) different gas injection techniques;
(c) varying the gas injection depths;
(d) changing apertures of an annular gas injector;
(e) different pipe diameters.
(f) varying the gas flow rate.

During operation, the following dependant variables can be monitored:

(a) pressure losses in the suction line;

(b) pressure losses of the two phase, gas-liquid mixture in the delivery pipe;

(c) pressure losses across the gas injectors;

(d) static dilations;

(e) dynamic void ratios;

(f) two phase flow patterns.

In this chapter, the two research facilities will be described in detail, with reference to the three components characteristic to airlift pumps. These being the suction pipe, the gas injectors and the delivery pipe.

3.2 40 mm Research Apparatus

3.2.1 Overall layout

Figure 3.1 shows a photograph, and Figure 3.2 shows a drawing of the 40 mm airlift pump research apparatus.

Referring to Figure 3.2, this apparatus is constructed of 40 mm o.d., 36 mm i.d. clear P.V.C. pipe throughout. A constant head tank is used -

(i) to provide a static pressure at the gas injection point;

(ii) to alter the lift height;

(iii) to alter the gas injection depth.

The constant head tank is linked directly to the gas injectors via the suction pipe.

3.2.2 Suction pipe

Referring to Figure 3.2, the suction pipe starts at the base of the constant head tank and ends at the bottom of the gas injectors, forming the return line of the recirculating system. Located along its length are pressure tappings, of which pressure tapping (1) is used to monitor losses through the constant heat tank outlet. Pressure tapping (2) provides the absolute pressure in the system before gas injection and tappings (3) and (4) are used to monitor pressures in a bend meter for liquid flow determination. An air release valve is provided to facilitate filling and emptying of the apparatus.

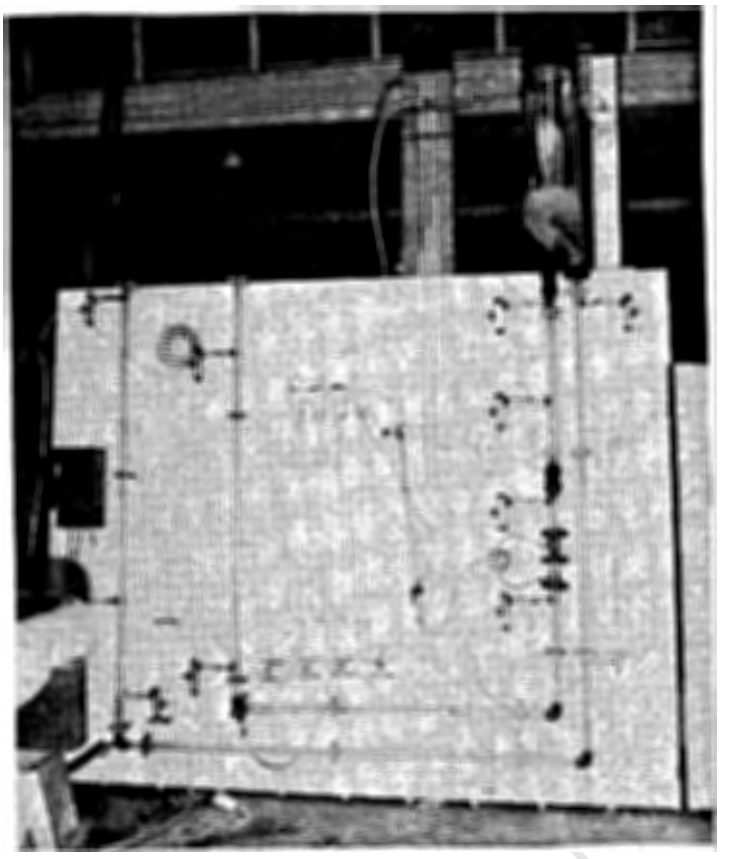

FIGURE 3.1 - 40mm RESEARCH APPARATUS

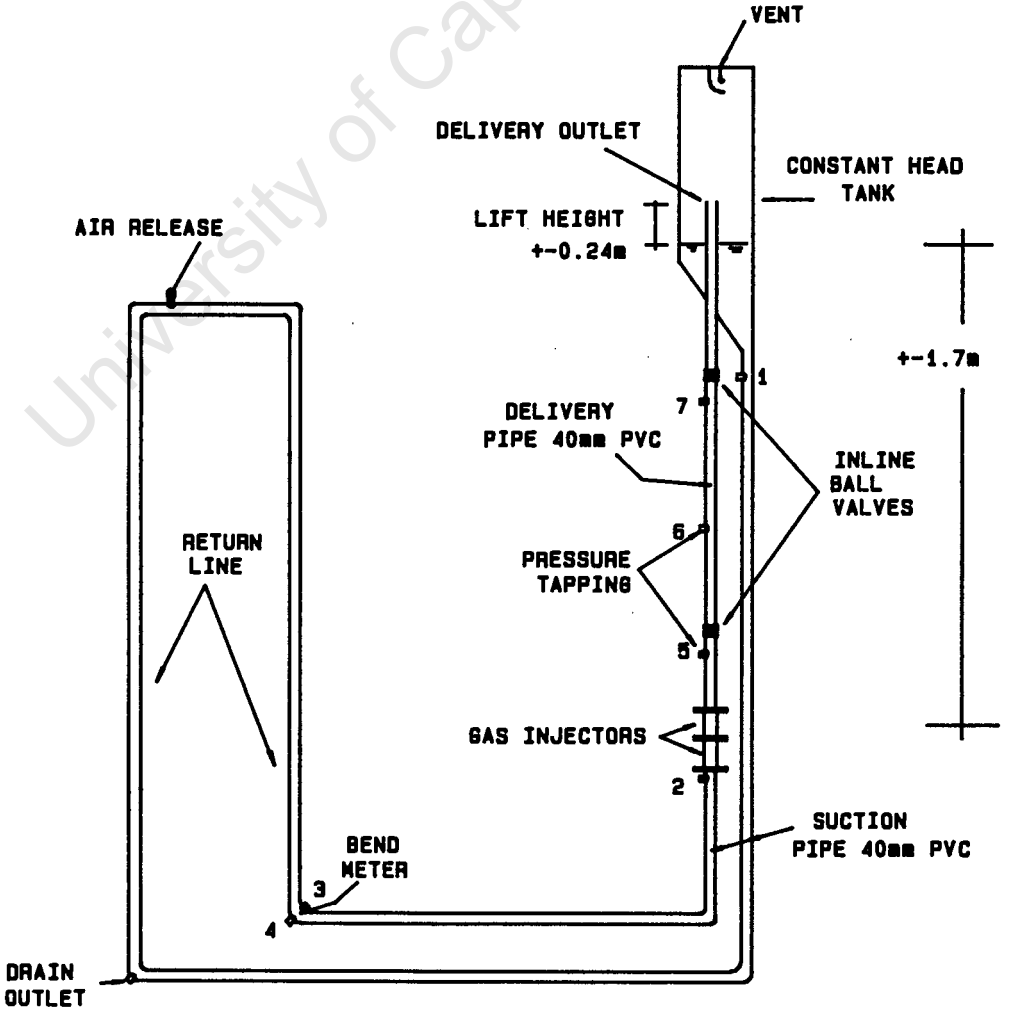

FIGURE 3.2 — 40mm AIRLIFT PUMP RESEARCH APPARATUS

3.2.3 Gas injectors

Two inline gas injectors, a horizontal injector through holes, and a vertical annular injector are provided on the 40 mm research apparatus. Figure 3.3 shows a photograph and Figure 3.4a and b show sectional drawings of these two gas injectors. Both injectors have the same internal diameters as the suction and delivery pipe, preventing flow obstruction.

Figure 3.4a shows a section of the horizontal gas injector. It consists of an 40 mm i.d. pipe section surrounded by a 50 mm o.d. pipe section. Gas is injected at the gas injection point into the annular chamber between the two pipes. The gas fills the annular chamber, and enters the inside 40 mm pipe section, through 5 mm holes drilled at regular intervals, in a horizontal direction.

Figure 3.4b shows a section of the vertical annular gas injector. It also consists of a 40 mm o.d. pipe section surrounded by an outside pipe section. The outside pipe section in this case consists of 40 mm o.d.expanded to 50 mm o.d. clear P.V.C., to give an annular gap of 4 mm between the two pipes. Gas is injected into the bottom of the annulus, at the gas injection point. The injected gas fills the annular gap and enters the system through the annular opening in a vertical direction.

Both gas injectors are located between flanges. This facilitates easy removal from the system in order to exchange them. For ease of operation, both injectors are connected to the air supply simultaneously and the flow can be alternated between them by operating a two-way diverter valve.

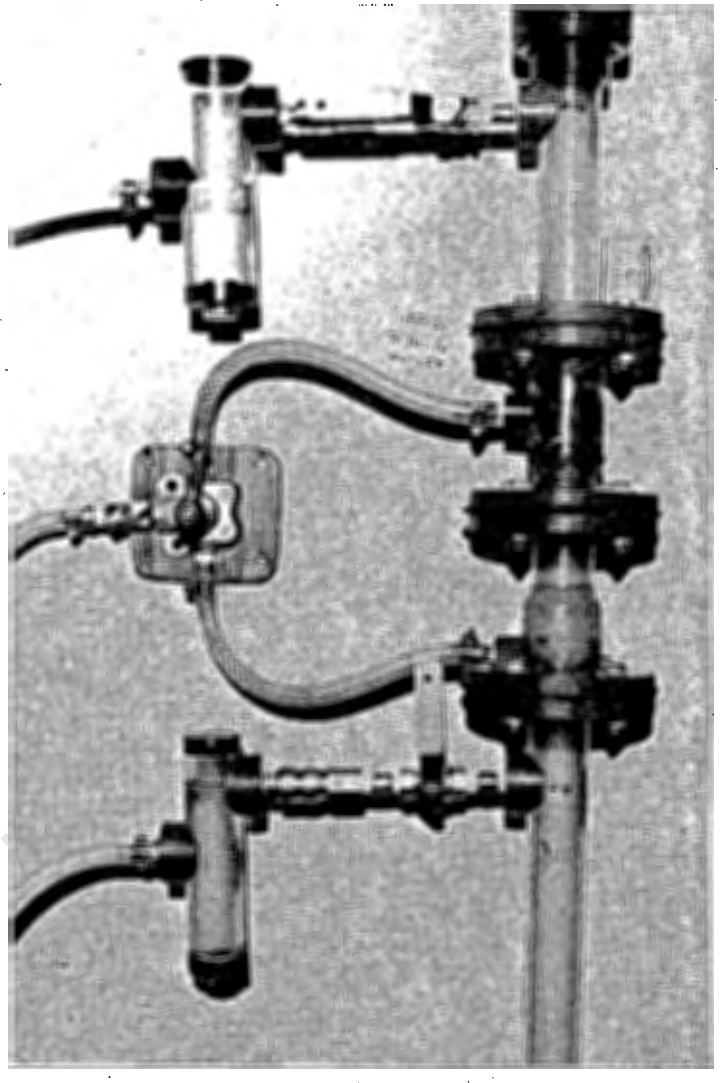

FIGURE 3.3 - 40mm GAS INJECTORS

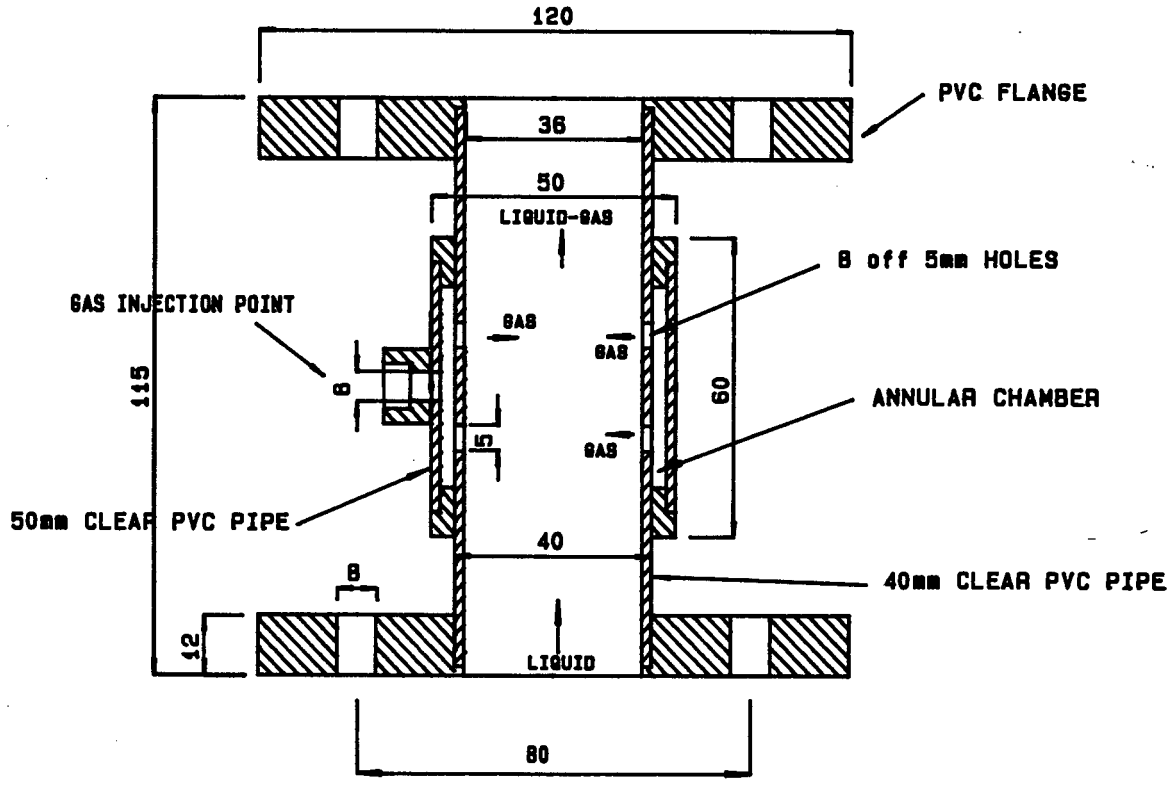

FIGURE 3.4 a — HORIZONTAL INJECTOR

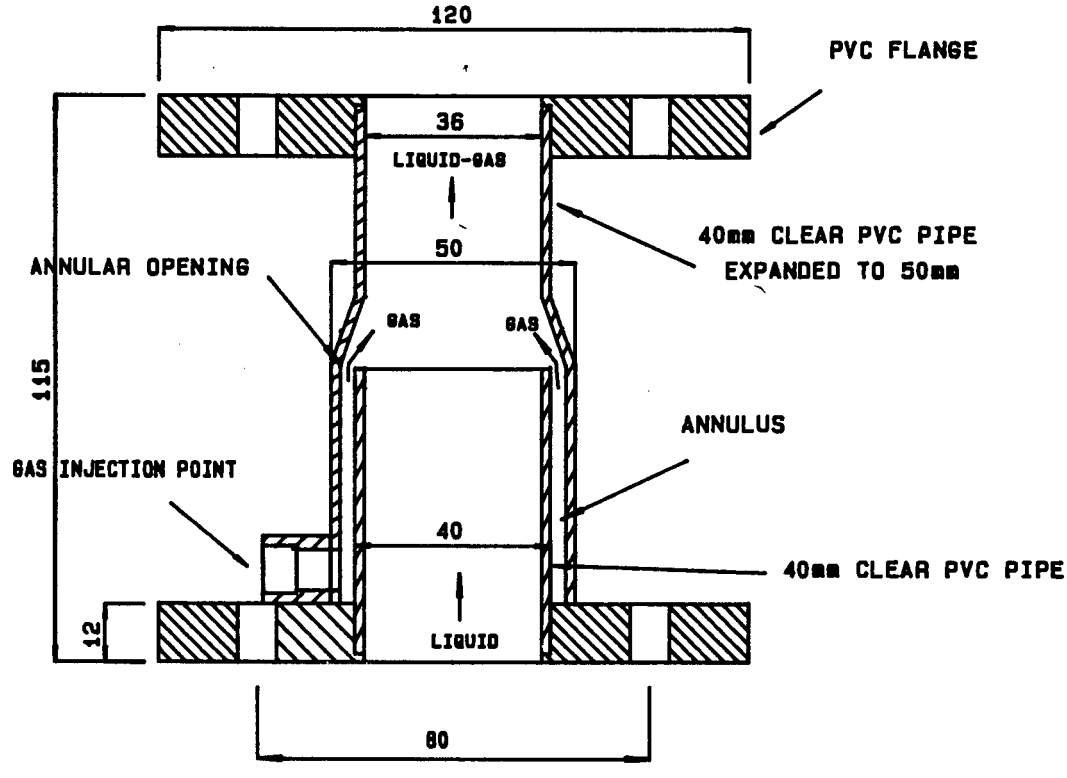

FIGURE 3.4 b — VERTICLE ANNULAR GAS INJECTOR

3.2.4 Delivery pipe

Referring to Figure 3.2, the delivery pipe has a length of approximately 1.94m depending on the preset lift height and gas injection depth. It starts at the top of the gas injectors, and ends inside the constant head tank, entering through its base.

Located along its length are pressure tappings (5), (6) and (7) to monitor pressures in the gas-liquid mixture. These pressure tappings and two inline ball valves are shown in the photograph on Figure 3.5. The ball valves situated 0.909 m apart have the same internal diameters as the delivery pipe and are used to investigate dynamic void ratios.

The delivery outlet is situated in the constant head tank, which is vented to atmosphere through a 40 mm P.V.C. elbow.

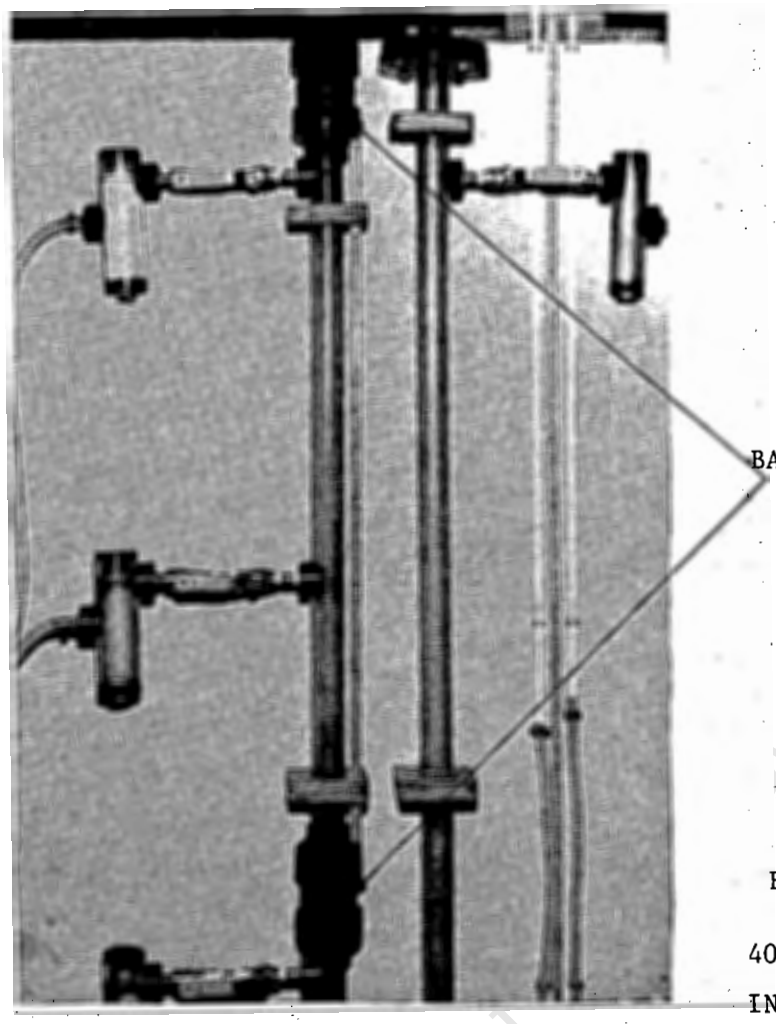

FIGURE 3.5 -

40mm AIRLIFT PUMP
INLINE BALL VALVE AND
PRESSURE TAPPINGS

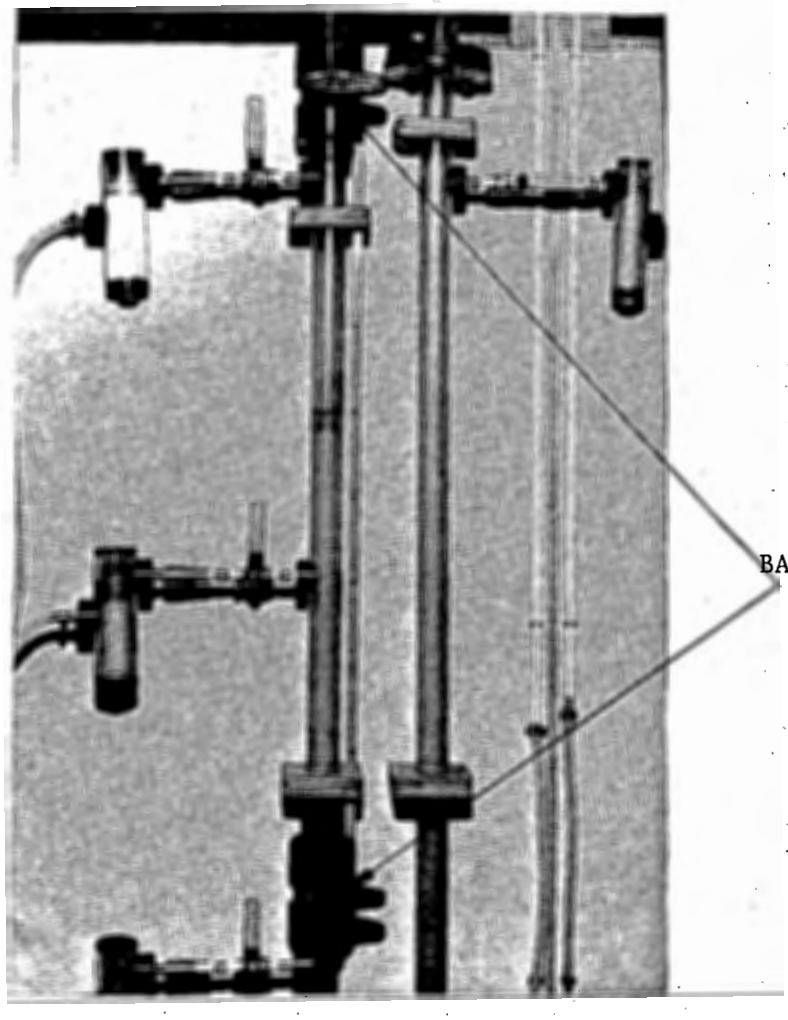

3.3 90 mm Research Apparatus

3.3.1 Overall layout

Figure 3.6a shows a photograph and a diagrammatic layout of the 90 mm research apparatus. A constant head tank provides static pressure to a pressure vessel which houses the suction inlet and part of the suction pipe.

At the delivery outlet, flow can be diverted either via a sample tank for measurement or via a 200 mm return hose back to the constant head tank, which is approximately 4.5 m above the gas injector.

3.3.2 Suction pipe

Referring to Figure 3.6 the suction pipe is partly located inside the pressure vessel to provide a static pressure at the suction inlet. 470 mm of its length is constructed from 90 mm P.V.C. pipe and the remaining 840 mm is constructed from 75 mm N.B. mild steel pipe.

Pressure tapping (1) is provided to monitor pressures at the base of the gas injectors.

3.3.3 Gas injector

The 90 mm research apparatus is fitted with a vertical annular gas injector similar to the one discussed in Section 3.2.3. Figure 3.7 shows a photograph and Figure 3.8 shows a section through the gas injector.

It consists of an inner pipe sleeve which can be moved up or down by means of a hand wheel. This movement in relation to the outer pipe sleeve causes the annular aperture to vary. Gas is injected equally at four points around the circumference of the outer sleeve. The gas fills the annulus which then enters the delivery pipe through the annular aperture in a vertical direction.

Figure 3.26 a-90mm Research Apparatus

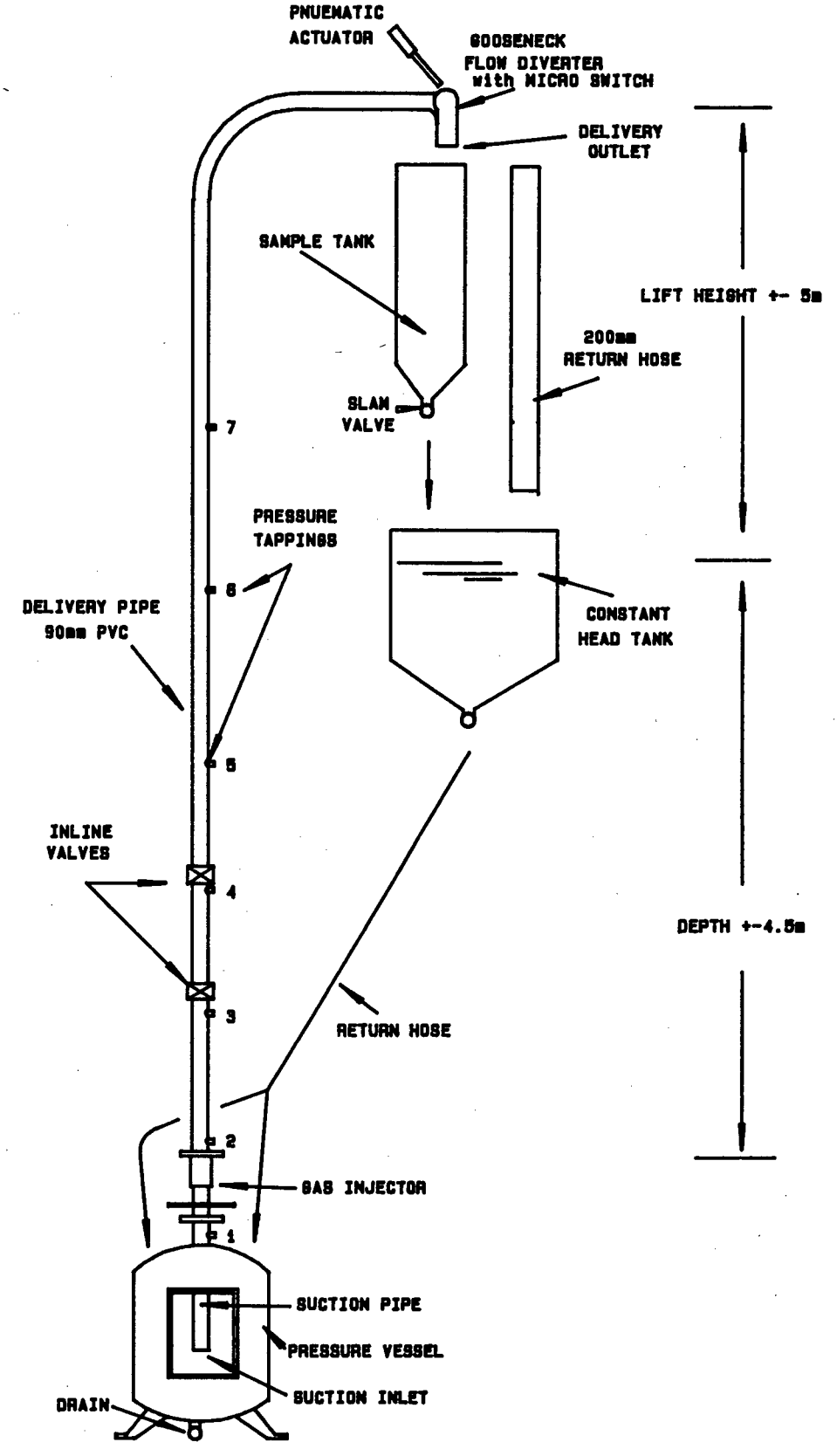

FIGURE 3.6 b — 90mm AIRLIFT PUMP RESEARCH APPARATUS

Table 3.1 gives the relationship of the numbers marked on the inner pipe sleeve to the annular aperature area.

Marked number	Annular gap distance (mm)	Aperture area (mm^2)
0	closed	0
1	1.0	384.1
2	2.5	647.9
3	3.5	918.1
4	4.5	1335.2
5	6.0	1621.1
6	7.0	1766.36
7	8.0	2437.9
8	9.0	2770.9
9	9.5	2939.7

Table 3.1 : 90 mm gas injector : annular areas

3.3.4 Delivery pipe

Referring to Figure 3.6, the delivery pipe is attached to the top of the gas injector and runs vertically for a distance of approximately 9.5 m depending on the liquid level in the constant head tank.

It is constructed of 90 mm o.d., 86 mm i.d. clear P.V.C. pipe. Two inline ball valves, located 1.376 m apart, with inside diameters the same as the delivery pipe, are used to monitor the dynamic void ratio in the delivery pipe.

Pressure tappings (2), (3), (4), (5), (6) and (7) are provided to measure pressures during operation.

The outlet of the delivery pipe leads to a gooseneck flow diverter which is operated by a pneumatic actuator. A micro switch is located halfway through the travel of the gooseneck, for time measurement while sampling.

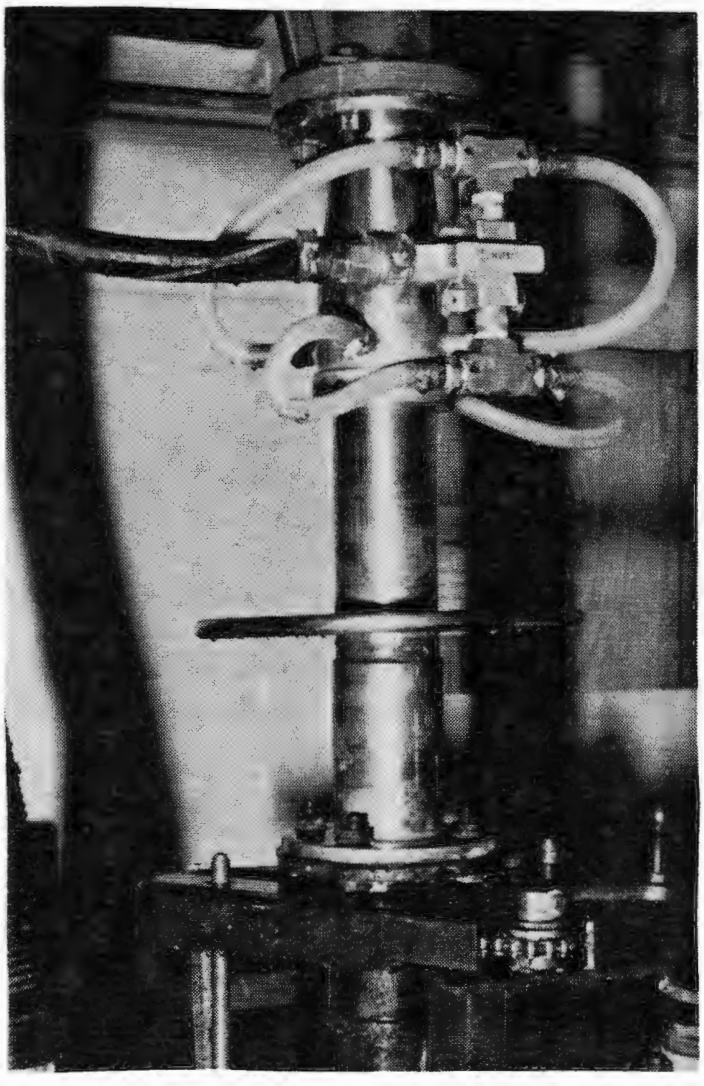

FIGURE 3.7 - 90mm GAS INJECTOR

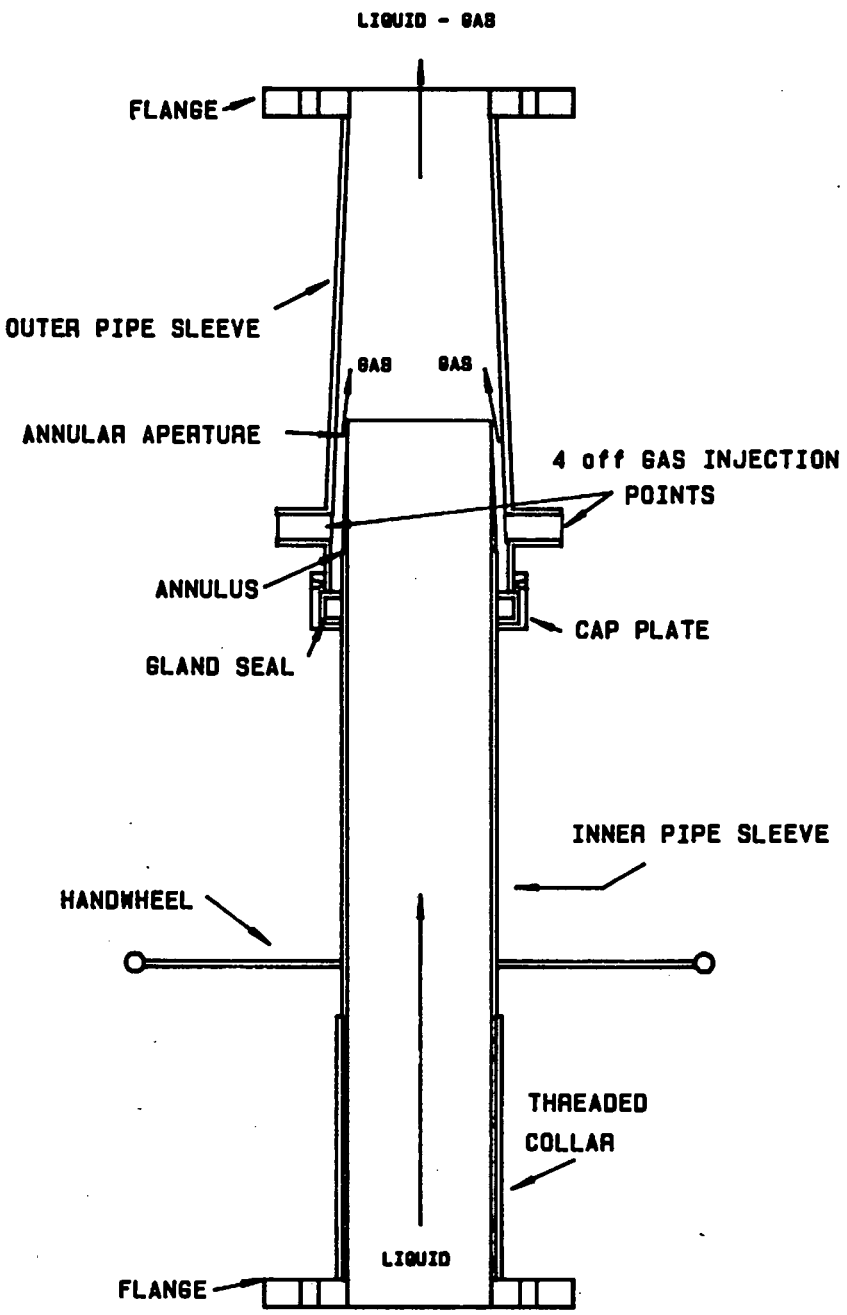

FIGURE 3.8 — 90mm GAS INJECTOR

CHAPTER 4

MEASUREMENT TECHNIQUES, CALIBRATIONS AND ACCURACY OF COLLECTED DATA

4.1 Introduction

To analyse the behaviour of airlift pumps, it is necessary to monitor:

1. pressures,
2. gas flow rates, and
3. liquid flow rates

during operation.

This chapter discusses the techniques used for the measurement of these components, as well as measurement of static dilations and dynamic void ratios. Also presented are calibrations and calculations to determine the accuracy of the collected data.

4.2 Pressure measurement

Pressure tappings are provided to monitor pressure differences and absolute pressures on the test apparatus. These tappings consist of 3 mm holes drilled into the pipe section. Pressures are monitored on manometer tubes. The manometer tubes are linked to the tappings via separation pods for separating the gas and the liquid to obtain liquid only for pressure measurement.

Figure 4.1 shows a photograph and Figure 4.2 shows a section, of a typical separation pod, used to supply the manometer board with clear liquid for pressure measurement. Valves and quick couple connectors are installed to allow removal for cleaning and priming of these pods.

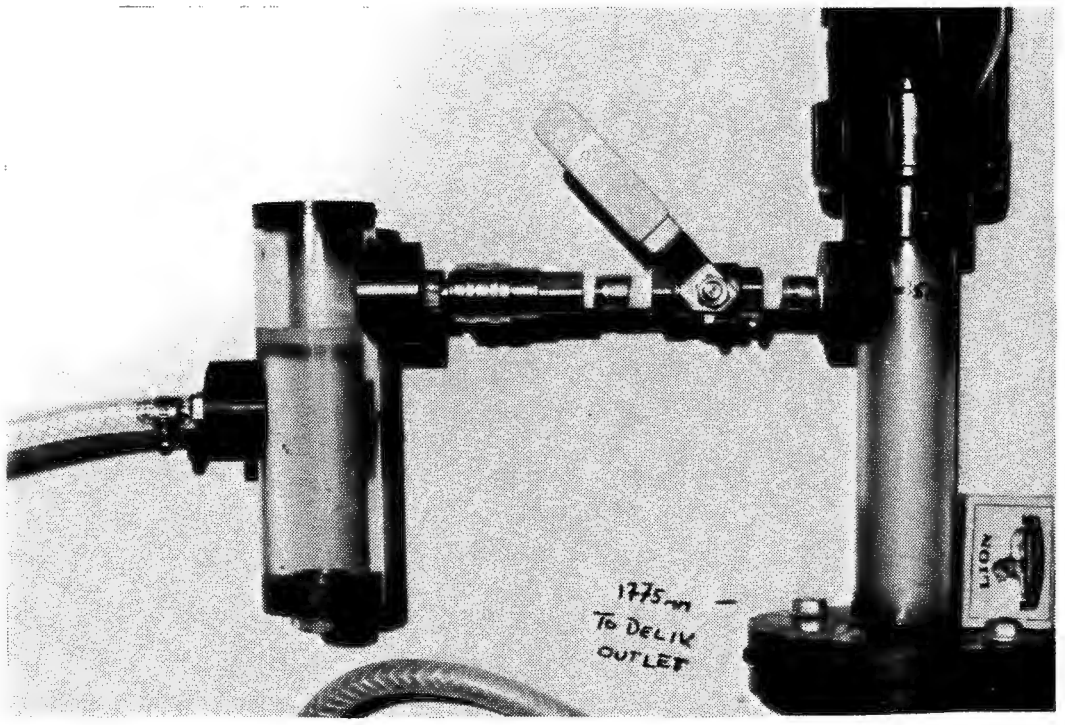

FIGURE 4.1 - SEPARATION POD

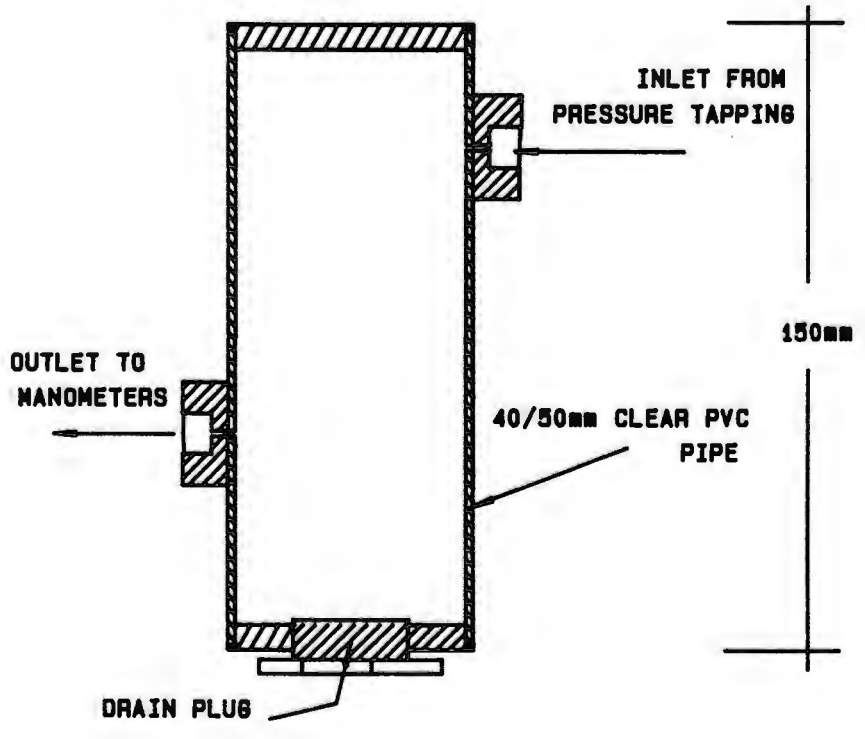

FIGURE 4.2 — SEPARATION POD

4.2.1 Absolute pressure measurement

Figure 4.3 shows a diagram of the manometer arrangement for measuring absolute pressures. To prime the manometer, valve (B) is closed and valves (A) and (C) are opened. Liquid is used to flush the air through the manometer and separation pods into the pipe. Having flushed all the air out of the manometer tube and pod, valve (C) is closed and valves (A) and (B) are opened, for pressure measurement under atmospheric conditions.

4.2.2 Differential pressure measurement

The manometer arrangement for measuring differential pressure is shown in Figure 4.4. To prime the manometers, firstly valve (A) is closed and valve (D) and (B) are opened. Liquid is used to flush the air through the top pod into the pipe. Then valve (B) is closed and valve (A) opened, now flushing through the bottom pod. Having flushed all the air out the manometer tubes and pods, valve (D) is closed and valves (A) and (B) are opened for pressure measurement. To bring the levels into a readable range, the tops of the manometer tubes are pressurised by blowing air in through a pressurising nipple at (C).

All measurements are converted into pressures using:

$$P = \rho_\ell \, g \, \Delta h \qquad (4.1)$$

where ρ_ℓ = the density of the liquid in the manometer

Δh = the actual or differential heights measured on the manometer tubes

P = pressure

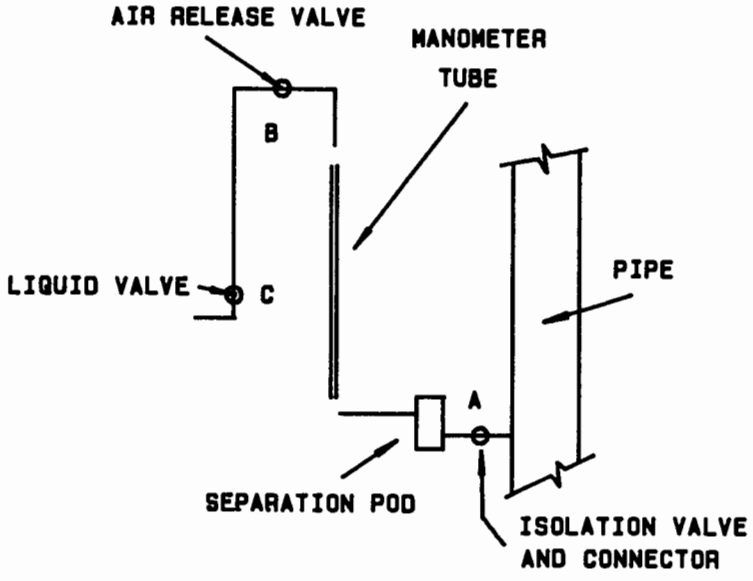

FIGURE 4.3 — ABSOLUTE PRESSURE MANOMETER

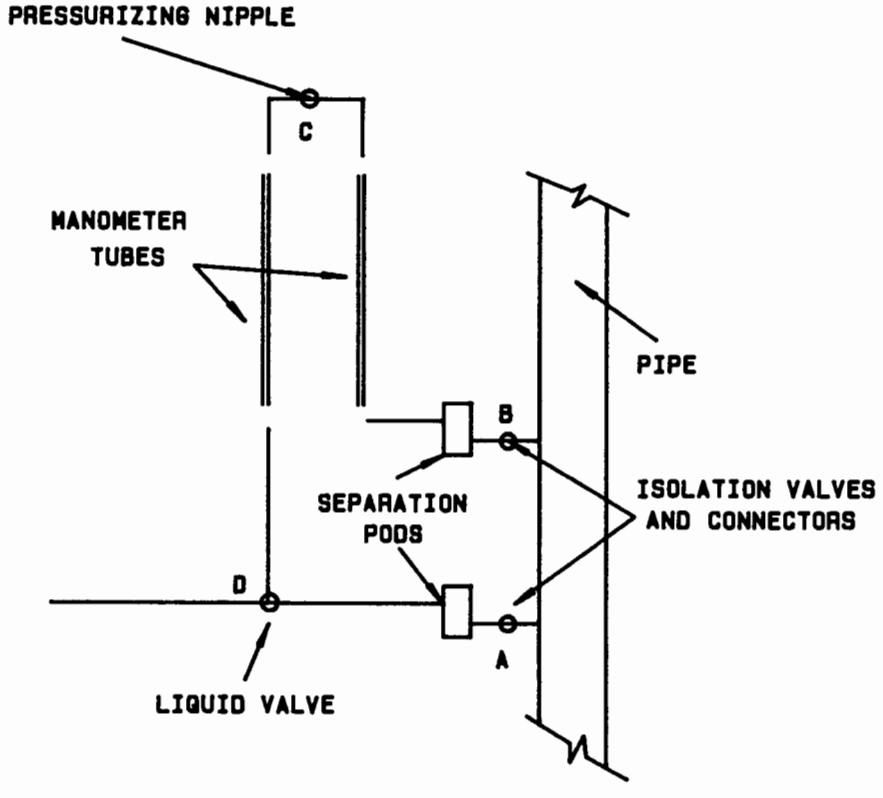

FIGURE 4.4 — DIFFERENTIAL PRESSURE MANOMETER

4.2.3 Accuracy of pressure measurement

To determine the accuracy of collected data and the effect on subsequent calculations, the equation used is partially differentiated with respect to each of the measured variables (Lazarus 1984).

$$\frac{\partial P}{P} = \frac{\partial h}{\Delta h} \qquad (4.2)$$

where ∂h = accuracy obtained when reading data

Δh = lowest measured value of the data

$\frac{\partial h}{\Delta h} \times 100\%$ = percentage error incurred

In taking absolute pressure measurements, fluctuations in the manometers were averaged to the accuracies given in Table 4.1.

Apparatus	Accuracy	Lowest measurement Δh (mm)	% error
90 mm	50 mm	3227	1.5
40 mm	5 mm	390	1.2

Table 4.1 - Pressure measurement accuracy

4.3 Gas flow rate measurement

Gas flow rates on both the 40 mm and 90 mm airlift pumps are monitored using orifice plates. The plates were designed according to ISO standards (Millar) with design data shown in Table 4.2.

Apparatus	40 mm	90 mm
Orifice diameter (mm)	6.549	20.6474
Pipe diameter (mm)	17	28.7
β	0.3853	0.727
Max. flow (m^3/hr at STP)	17	170
Deflection at max. flow (m)	1	1
Operating temperature (°C)	35	35
Operating gauge pressure (kPa)	300 .	200

Table 4.2 - Orifice Data

Pressure tappings from the orifice plates lead to air over water differential manometers. Figure 4.5 shows a photograph and Figure 4.6 a section of the orifice arrangement installed in the airline of the 90 mm test apparatus. Both the 90 mm and 40 mm test facilities are fitted with pressure regulators and gas flow regulating valves.

Measurements are converted into gasflow rates at STP using

$$Q_{go} = 170 \sqrt{\frac{\Delta h}{1000}} \qquad (4.3)$$

on the 90 mm airlift pump, and:

$$Q_{go} = 17 \sqrt{\frac{\Delta h}{1000}} \qquad (4.4)$$

on the 40 mm airlift pump.

where Δh = head difference recorded on the manometers in mm

Q_{go} = gas flow rate in m^3/hr at STP

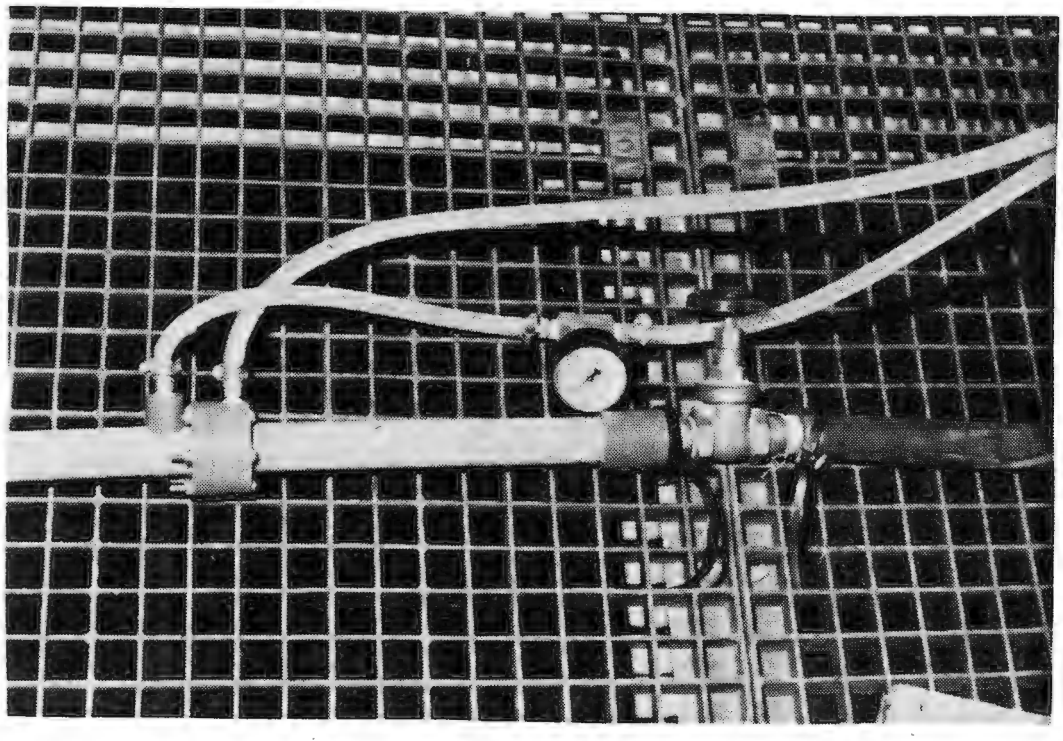

FIGURE 4.5 - 90mm ORIFICE ARRANGEMENT,
PRESSURE GAUGE AND
FLOW REGULATING VALVE

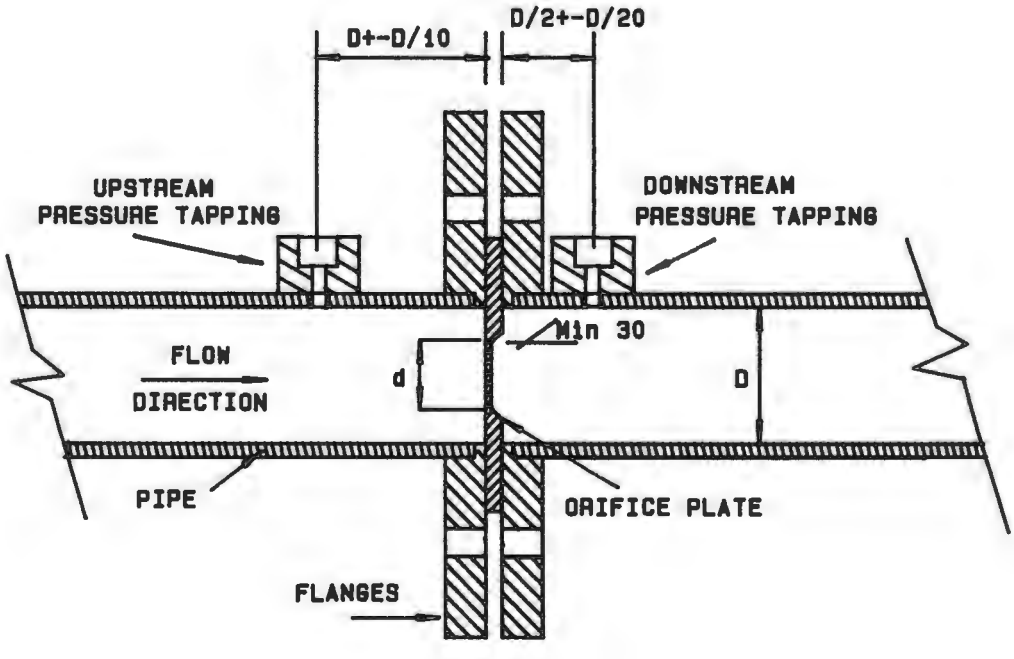

FIGURE 4.6 — ORIFICE PLATE ARRANGEMENT

4.3.1 Accuracy of gas flow measurements

Calculations to determine the accuracy are as outlined in 4.2.3. The following equation can be used to determine the percentage accuracy obtained during measurement.

$$\frac{\partial Q_{go}}{Q_{go}} = \frac{\partial h}{2\Delta h} \qquad (4.5)$$

All gas flow rates are read to 1 mm. Figure 4.7 shows graphically the variation of accuracy of the data across the measured gas flow ranges for the 90 mm and 40 mm test facilities. From Figure 4.7 it is seen that for head differences (Δh) in excess of 50 mm, the percentage error incurred is less than 1%.

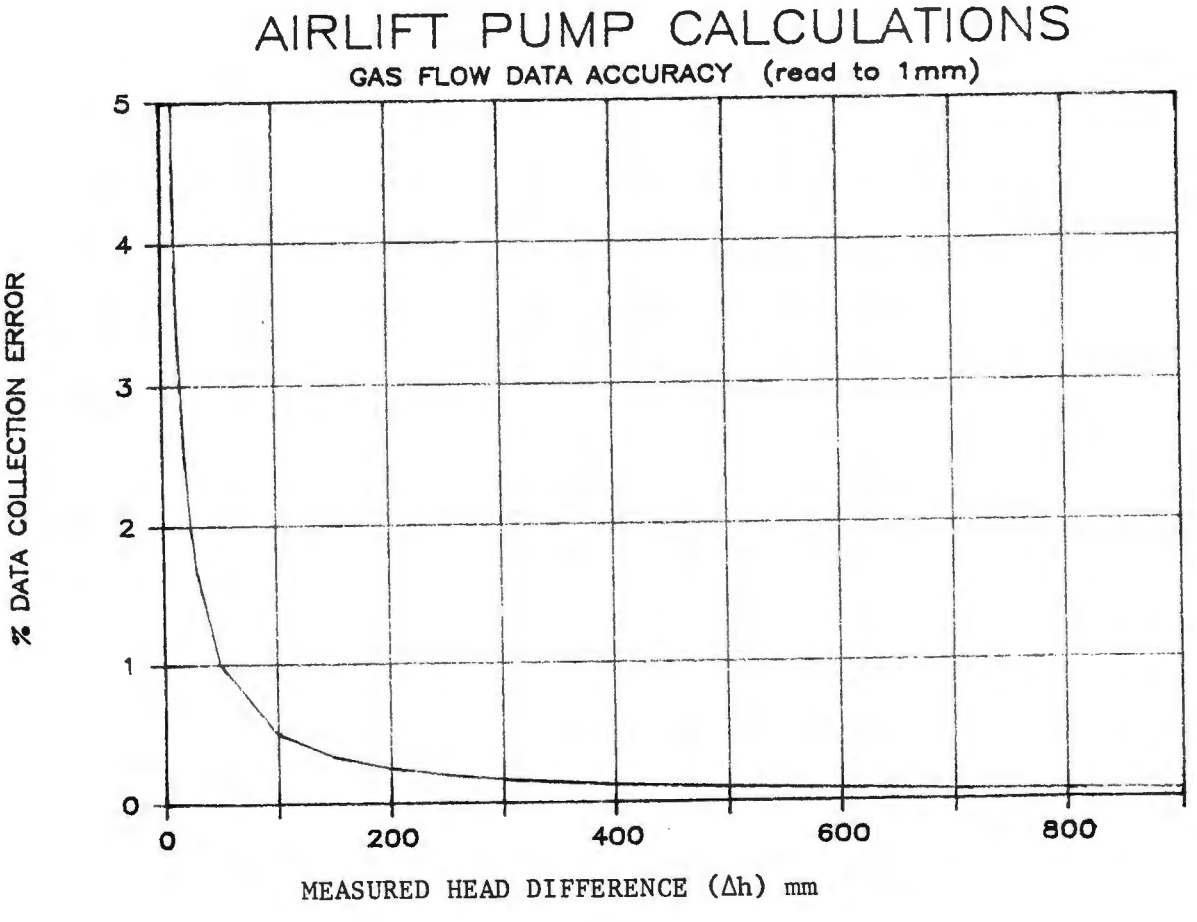

FIGURE 4.7 - GAS FLOW DATA ACCURACY

4.4 Liquid flow rate measurement

4.4.1 90 mm airlift pump

Liquid flow rates are monitored using a calibrated sample tank and a micro-switch timing facility. As the gooseneck flow diverter at the delivery outlet is swung from the return hose to the sample tank in Figure 3.6, the micro-switch is activated which starts a stopwatch. Swinging the gooseneck back to the return hose reactivates the switch and the stopwatch is stopped. The time recorded, combined with the volume of liquid in the sample tank, yields the liquid flow rate.

$$Q_\ell = V_T/t \qquad (4.7)$$

where V_T = volume of liquid in sample tank (ℓ)
t = time of sample (s)
Q_ℓ = liquid flow rate (ℓ/s)

Figure 4.8 shows the calibration curve obtained for the sample tank, where the height (H) measured on a standpipe mounted on the side of the tank is related to the liquid volume in the tank.

4.4.2 40 mm airlift pump

Liquid flow measurements on this apparatus are obtained using a bend meter (refer Figure 3.2) consisting of a 40 mm P.V.C. bend. Calibration of the bend was done using a sample tank and readings of pressure differences were recorded on a differential pressure manometer as in 4.2.2.

Figure 4.9 shows the calibration curve obtained for the bend meter. From a linear regression curve fit, the following equation can be used to relate differential manometer readings to liquid flow rates.

$$Q_\ell = 6.386 \times 10^{-3} + 9.183 \times 10^{-2} \sqrt{\Delta h} \qquad (4.7)$$

where Q_ℓ = liquid flow rate in ℓ/s
Δh = head difference on the manometer in mm.

4.4.3 Accuracy of liquid flow rate measurements

4.4.3.1 **90 mm airlift pump**

From equation 4.7 and Figure 4.8, the equation used to calculate the liquid flow rate is given as:

$$Q_\ell = \frac{(-1164.62 + 0.11947\ H)}{t} \qquad (4.8)$$

Using the procedure as outlined in 4.2.3, the accuracy obtained from height measurement (H) is given by

$$\frac{\partial Q_\ell}{Q_\ell} = \frac{0.119474\ \partial H}{(-1164.62 + 0.119474\ H)} \qquad (4.9)$$

and by time measurement (t) is given by

$$\frac{\partial Q_\ell}{Q_\ell} = -\frac{\partial t}{t} \qquad (4.10)$$

Data collection errors are shown in Table 4.3.

Measured Quantity	Accuracy	Lowest measurement	% error
H	1 mm	10045 mm	0.33
t	0.01 sec	5.70 sec	0.17

Table 4.3 - Liquid Flow Rate Accuracy

4.4.3.2 40 mm airlift pump

The equation derived, using the procedure as outlined in 4.2.3, which can be used to determine the accuracy obtained by measuring Δh on the manometers is given by:

$$\frac{\partial Q_\ell}{Q_\ell} = \frac{6.386 \times 10^{-3}\ \partial h}{2\sqrt{\Delta h}\,(6.386 \times 10^{-3} + 9.183 \times 10^{-2}\sqrt{\Delta h})} \qquad (4.11)$$

Fluctuations in the manometers were averaged to 5 mm. The lowest measured Δh is 23 mm resulting in 0.73% error.

4.5 Static Dilation Measurement

Weber (1976, 1982), in his analysis, requires knowledge of static dilations discussed in Section 2.5.6.1. Static dilations are monitored by direct measurement with fluctuations being averaged visually. Equation (2.34) is used to calculate the dilations and equation (4.12) is used to predict the accuracy of the measured data.

$$\frac{\partial\, \epsilon_{go}}{\epsilon_{go}} = \frac{h}{\Delta h\,(h_1 + h_2)}\ \partial \Delta h \qquad (4.12)$$

It is possible to average the fluctuations of the liquid surface to an accuracy of less than 100 mm. The lowest measured Δh recorded was 220 mm, with h_1 being 435 mm. This results in a 0.3% data collection error.

4.6 Dynamic Void Ratio Measurement

For calculation of the weight of the two phase gas-liquid column inside the delivery pipe, it is necessary to measure the dynamic void ratio discussed in 2.5.1.1. To determine dynamic void ratios, two inline ball valves on either of the test facilities are shut off simultaneously, trapping a column of gas and liquid. Once the gas and liquid have separated, the ratio of pipe length occupied by air to total pipe length between the ball valves yields the dynamic void ratio. Direct measurements are converted into void ratios by using

$$\epsilon_g = \frac{1308 - H}{1376} \tag{4.13}$$

on the 90 mm airlift pump, and

$$\epsilon_g = \frac{858 - H}{909} \tag{4.14}$$

on the 40 mm airlift pump

where H = the height of liquid measured to the top of the stub on the bottom valve in mm

ϵ_g = dynamic void ratio

Figure 4.10 and 3.5 show the layout and dimensions of the two valves on the 40 mm and 90 mm airlift pumps respectively.

4.6.1 Accuracy of dynamic void ratio measurement

The following equations can be used to determine the accuracy obtained during measurement. For the 40 mm airlift pump:

$$\frac{\partial \epsilon_g}{\epsilon_g} = \frac{\partial h}{909\left(\frac{858}{909} - \frac{H}{909}\right)} \tag{4.15}$$

For the 90 mm airlift pump:

$$\frac{\partial \epsilon_g}{\epsilon_g} = \frac{\partial h}{1376\left(\frac{1308}{1376} - \frac{H}{1376}\right)} \tag{4.16}$$

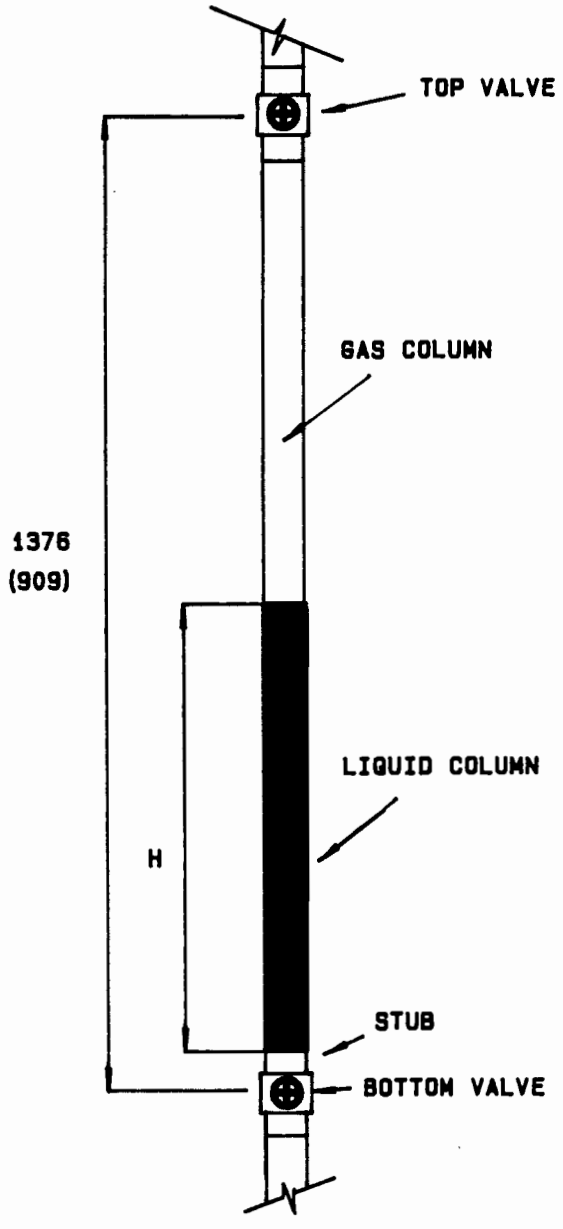

BRACKETS = 40mm
AIRLIFT PUMP

FIGURE 4.10 — BALL VALVE ARRANGEMENT FOR DYNAMIC VOID RATIO TESTS

Data collection errors are given in Table 4.4.

Apparatus	Accuracy	Lowest measurement (H)	% error
40 mm	1 mm	348 mm	1.9×10^{-3}
90 mm	1 mm	382 mm	1.5×10^{-3}

Table 4.4 - Dynamic Void Ratio Accuracy

CHAPTER 5

EXPERIMENTAL PROCEDURE

5.1 Introduction

To research analytical models for predicting airlift pump operation, tests were conducted on both the 90 mm and 40 mm research facilities. During the tests, physical parameters such as

(a) the lift height

(b) the gas injection depth

(c) gas injection techniques

(d) gas injection apertures on the 90 mm vertical annular gas injector

were varied. The influence of these parameters on the airlift pump operation were monitored by measurement of pressures, gas flow rates and liquid flow rates.

Further tests that were conducted included monitoring

(a) static dilations in 150 mm, 90 mm and 40 mm pipe diameters

(b) dynamic void ratios in 90 mm and 40 mm pipe diameters.

This chapter covers the experimental procedure adopted while conducting tests to research the above effects during airlift pump operation.

5.2 Static dilation tests

The static dilation discussed in Section 2.5.6.1 is required for Weber's (1976, 1982) analytical model.

To monitor static dilation, tests were performed in pipe sizes:

(i) 40 mm o.d., 36 mm i.d.

(ii) 90 mm o.d., 86 mm i.d.

(iii) 150 mm o.d., 142 mm i.d.

The experimental procedure adopted for each pipe is as follows:

(a) Fill the pipe to a reference height (h_1), on Figure 2.1, depending on the maximum dilation.

(b) Allow gas to bubble into the bottom of the pipe at a constant rate.

(c) Record the dilate height (Δh).

(d) Choose a different gas flow rate and repeat item c until the dilations for a range of gas flow rates are obtained.

Record all gas flow rates at S.T.P.

5.3 40 mm Airlift pump operating tests

5.3.1 Preparation

Referring to Figure 3.2, the following procedure is adopted for preparing the 40 mm airlift pump for operation:

(a) Open the air release valve in the return line.

(b) Open the inline ball valves in the delivery pipe.

(c) Open the isolation valves at all the pressure tappings.

(d) Close the air release valves on the absolute pressure manometers.

(e) Fill the apparatus by flushing water through the manometers and separation pods into the pipe, at the same time priming them of air.

(f) Close the air release valve in the return line when liquid flows out.

(g) Fill the constant head tank to the required lift height.

(h) Close the isolation valves at all the pressure tappings.

(i) Set the pressure regulator on the airline to 300 kPa.

(j) Set the two way diverter valve to the required gas injector.

(k) Slowly open the gas flow regulating valve, allowing gas to enter the airlift delivery pipe.

(l) Open the isolation valves at all pressure tappings.

(m) Open the air release valves on the absolute pressure manometers.

(n) Adjust the manometers for pressure measurement as prescribed in Section 4.2.1 and 4.2.2.

(o) Record all pressure readings, gas flow rates and liquid flow rates.

5.3.2 Varying the lift height and injector depth

The 40 mm airlift pump can be operated at different lift heights and corresponding injection depths. This is done by changing the liquid level in the system at item (g) in Section 5.3.1.

Lift heights of 80 mm, 160 mm, 240 mm and 320 mm were researched using the annular gas injector. The corresponding injector depths are given in Table 5.1.

Lift Height (m)	Injector Depth (m)
0.08	1.924
0.16	1.844
0.24	1.764
0.32	1.684

Table 5.1 - 40 mm Lift Height Test Data

At each lift height, the experimental procedure is as follows:

(a) Prepare the apparatus as in 5.3.1.

(b) Choose a low gas flow rate.

(c) Record the liquid flow rate.

(d) Choose a different gas flow rate and repeat item (c) until the liquid flow rates for a range of gas flow rates are obtained.

(e) Fill the apparatus to the next lift height. Repeat from item (a) onwards until the required number of lift heights are investigated.

5.3.3 Injection technique comparison

To monitor the difference between horizontal gas injection and vertical gas injection, tests were conducted on the two gas injectors described in Section 3.2.3.

The tests were run at a 240 mm lift height with the following operating procedure:

(a) Prepare the apparatus as in 5.3.1.

(b) Choose the vertical annular gas injector.

(c) Choose a low gas flow rate.

(d) Record the liquid flow rate.

(e) Choose a different gas flow rate and repeat from item (c) onwards, until the liquid flow rates for a range of gas flow rates are obtained.

(f) Exchange the gas injectors and repeat from item (c) onwards, now using the horizontal gas injector.

5.4 90 mm Airlift pump operating tests

5.4.1 Preparation

Referring to Figure 3.6, the following procedure is adopted for preparing the 90 mm airlift pump for operation:

(a) Close the drain valve at the base of the pressure vessel.

(b) Open the inline ball valves in the delivery pipe.

(c) Fill the system to the required injector depth through the constant head tank.

(d) Move the gooseneck flow diverter at the delivery outlet to the return hose.

(e) Prime all manometers for pressure measurement as outlined in sections 4.2.1 and 4.2.2.

(f) Set the pressure regulator on the airline to 200 kPa.

(g) Slowly open the gas flow regulating valve allowing gas to enter the airlift pipe.

(h) Record all pressure readings and gas flow rates from the manometers.

(i) Record liquid flow rates by diverting to a sample tank and measuring the height on a standpipe with the sample time on a self-activated stopwatch.

5.4.2 Operation

Tests on the 90 mm airlift pump were conducted at a lift height of 4.280 m and an injection depth of 5.240 m using the following experimental procedure:

(a) Prepare the apparatus as in 5.4.1.

(b) Choose a low gas flow rate.

(c) Record the liquid flow rate.

(d) Choose a different gas flow rate and repeat item (c) until the liquid flow rates for a range of gas flow rates are obtained.

5.4.3 Varying the injector aperature

The 90 mm airlift pump can be operated with the annular gas injector set at different aperatures. Tests were conducted at settings 8,6 and 4 corresponding to aperature areas of 2770.9 mm², 1766.36 mm² and 1335.2 mm² respectively (Refer to Table 3.1)

The experimental procedure is the same as outlined in 5.4.2, repeated for each aperature setting.

5.5 Dynamic Void Ratio Tests

To aid in modelling the weight of the two phase mixture in the delivery pipe, dynamic void ratios were monitored in the 40 mm and 90 mm airlift pumps.

The experimental procedure adopted for each airlift pump was as follows:

1. Operate the airlift pump at a particular gas flow rate.
2. Record the water flow rate.
3. Record the absolute pressures at each of the two ball valves.
4. Shut the two ball valves simultaneously trapping a gas-liquid column.
5. Record the height of water in the trapped column.
6. Choose a different gas flow rate and repeat from item 2 onwards until the dynamic ratios for a range of gas flow rates are obtained.

Record all gas flow rates at S.T.P.

For the analysis, an average gas flow rate between the valves is calculated using the air flow rate at S.T.P., the absolute pressures at the two valves and equation 2.14 The water flow rate is obtained directly from measurement, and the dynamic void ratio is obtained from the ratio of air volume to total volume of the column between the two valves.

CHAPTER 6

EXPERIMENTAL RESULTS AND ANALYSIS

6.1 Introduction

In this chapter, results obtained from experiments and analysis on the 90 mm and 40 mm airlift pumps are presented.

6.1.1 Results of experiments conducted on both the 40 mm and the 90 mm airlift pumps to find an analytical two phase flow model are given in Figures 6.1 to 6.19. These experiments are conducted under controlled conditions and specific components used in the analysis are monitored.

6.1.2 Measured and calculated airlift pump performance curves for the 40 mm and 90 mm airlift pumps operating under the conditions discussed in Section 3.1, as well as results of additional airlift pumps obtained from literature sources are given in Figures 6.20 to 6.29.

6.2 Results for analytical components

6.2.1 Static dilations

Figure 6.1a, with an enlargement shown in Figure 6.1b, presents plots of static dilation obtained in 36 mm, 86 mm and 142 mm i.d. pipes. Figure 6.2 shows dilation results of Pickert, Schuring, Weber and results obtained from Figure 6.1a and b, plotted against the gas flow rate in each test divided by the pipe area as proposed by Weber (1976).

Figure 6.3 also shows the dilation results, however plotted against the gas flow rates divided by $\pi/4\ d^{2.7}$.

6.2.2 Dynamic void ratios

Figure 6.4 shows graphs of the dynamic void ratio plotted against the average airflow rate between the two inline valves. The data points are compared with predictions by Giot (1986), Chisholm (1983), Clark (1986) and Weber (1976, 1982) in the 40 mm airlift pump. Figure 6.5 is a graph comparing the predicted dynamic void ratios by the above authors with the measured void ratio in the 40 mm airlift pump.

Figure 6.6 and Figure 6.7 show the above for the 90 mm airlift pump.

6.2.3 Weight pressure loss

Figure 6.8 is a plot of the total pressure loss between the two ball valves, during dynamic void ratio tests. Also shown is the weight pressure loss component calculated using the measured dynamic void ratio results and the weight pressure loss as calculated using the dynamic void ratios predicted by the authors mentioned above (refer Equation 2.21).

The difference between the total pressure loss and weight pressure loss components consists of the friction and acceleration pressure losses. All pressure losses are plotted against average gas flow rates between the valves for the 40 mm airlift pump. Figure 6.9 shows a comparison of the weight pressure loss calculated using the measured dynamic void ratio and the weight pressure loss calculated using the predicted dynamic void ratios.

Figure 6.10 and 6.11 show the above for the 90 mm airlift pump.

6.2.4 Friction pressure loss

Figure 6.12 shows the combined friction and acceleration pressure losses as obtained from the difference between the total pressure loss and the weight pressure loss on Figure 6.8. Shown also are theoretical friction pressure loss predictions by Chisholm (1983), Stenning (1968), Weber (1976, 1982), Clark (1986) and a modification of Clark's method.

The modification presented by the present author is to replace the superficial liquid velocity term ($v_{\ell s}$ - equation 2.13) by the liquid velocity (v_{ℓ} - equation 2.10) when applying Clark's friction pressure loss equation (equation 2.45).

Friction pressure losses are plotted against the average gas flow rates between the valves for the 40 mm airlift pump. Figure 6.13 is a comparison of the measured data and calculated values using the methods presented by the above authors.

Figure 6.14 and 6.15 show the above results for the 90 mm airlift pump.

6.2.5 Total pressure loss

Figure 6.16 is a plot of the total pressure loss, measured and predicted, between the valves on the 40 mm airlift pump, for a range of gas flow rates.

The predicted total pressure loss is calculated using

- the dynamic void ratio model presented by Clark for the weight component (equation 2.33);
- the modified Clark model for the friction component (equation 2.45 with modification as discussed in section 6.2.4);
- a standard two phase model for the acceleration component (equation 2.53).

Figure 6.17 shows a comparison between the measured data and the predicted total pressure loss model.

Figures 6.18 and 6.19 show the above for the 90 mm airlift pump.

6.3 Performance Curves

The following graphs show airlift pump performance curves calculated theoretically using the procedure outlined in Section 2.4.

Pressure losses due to the moving two-phase mixture in the delivery pipe are calculated using the following models:

1. Weight pressure loss component - void ratio model used by Clark (1986).
2. Friction pressure loss component - modification to the model used by Clark.
3. Acceleration pressure loss component - standard two phase model.

6.3.1 General operating curves

Figure 6.20 is a graph of measured and theoretically calculated liquid flow rates for a range of gas flow rates in the 40 mm airlift pump. A comparison of the measured and predicted liquid flow rates is given in Figure 6.21.

Figures 6.22 and 6.23 show the above comparisons for the 90 mm airlift pump.

6.3.2 40 mm airlift pump-static lift and injector depth variation

Figure 6.24 shows a comparison of the measured and predicted liquid flow rates in the 40 mm airlift pump operating at various lift heights and corresponding injector depths as outlined in Section 5.3.2. Theoretically predicted liquid flow rates are plotted against measured liquid flow rates.

6.3.3 40 mm airlift pump-injection technique comparison

Figure 6.2.5 shows the 40 mm airlift pump performance curves for the two types of gas injectors installed on the system. Plotted are liquid flow rates against gas flow rates for the horizontal gas injectors and the vertical annular gas injector. The experimental procedure is outlined in Section 5.3.3.

6.3.4 90 mm airlift pump-injection aperture variation

The results of the experiments outlined in Section 5.4.3 are given in Figure 6.26. Measured liquid flow rates are plotted for a range of gas flow rates at the three aperture areas used for experiments.

6.3.5 Operating curves using literature sources compared with the present analysis

Figures 6.27, 6.28 and 6.29 show comparisons of liquid flow rate data to calculated liquid flow rates for various pipe sizes. The data is obtained from literature sources and was presented by Clark, Gibson and Weber respectively.

The operating conditions and airlift pump pipe diameters are given on the figures.

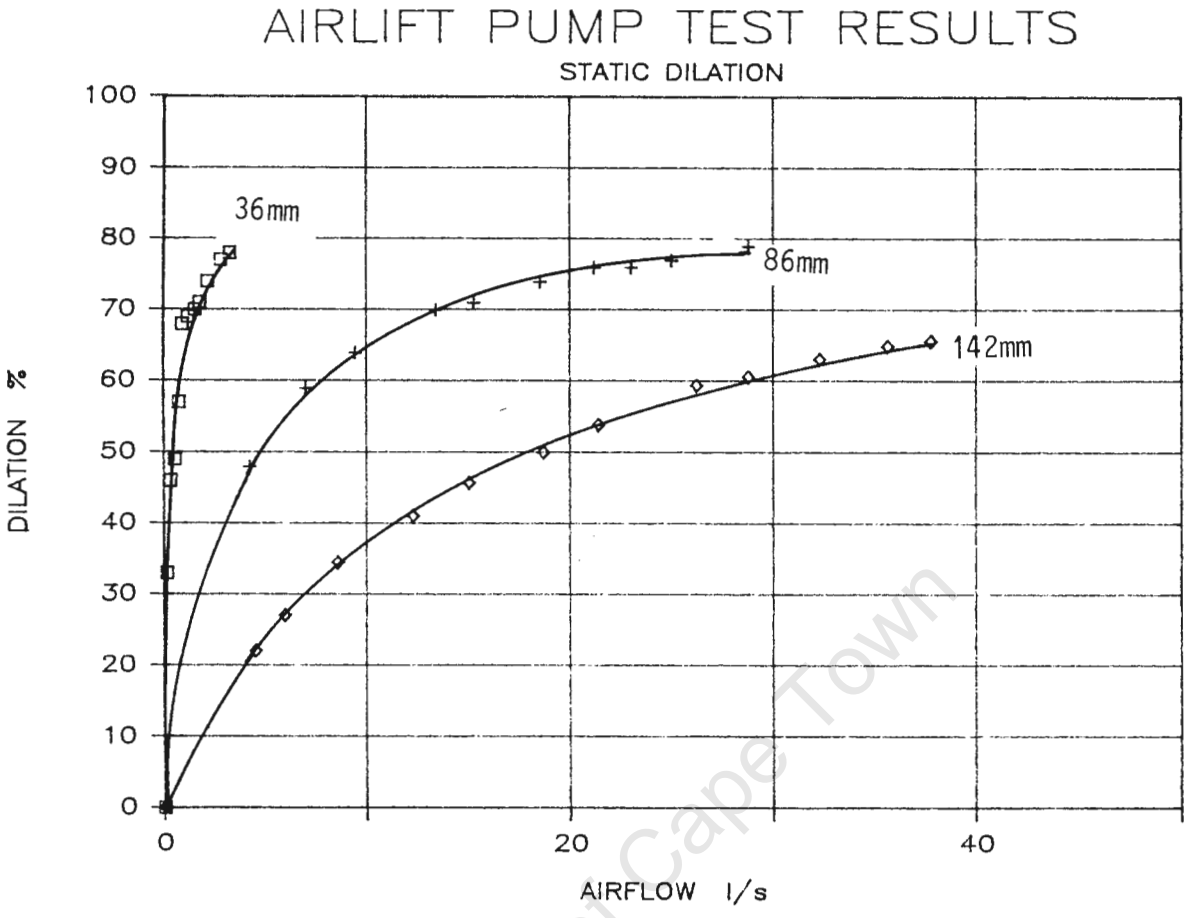

FIGURE 6.1a

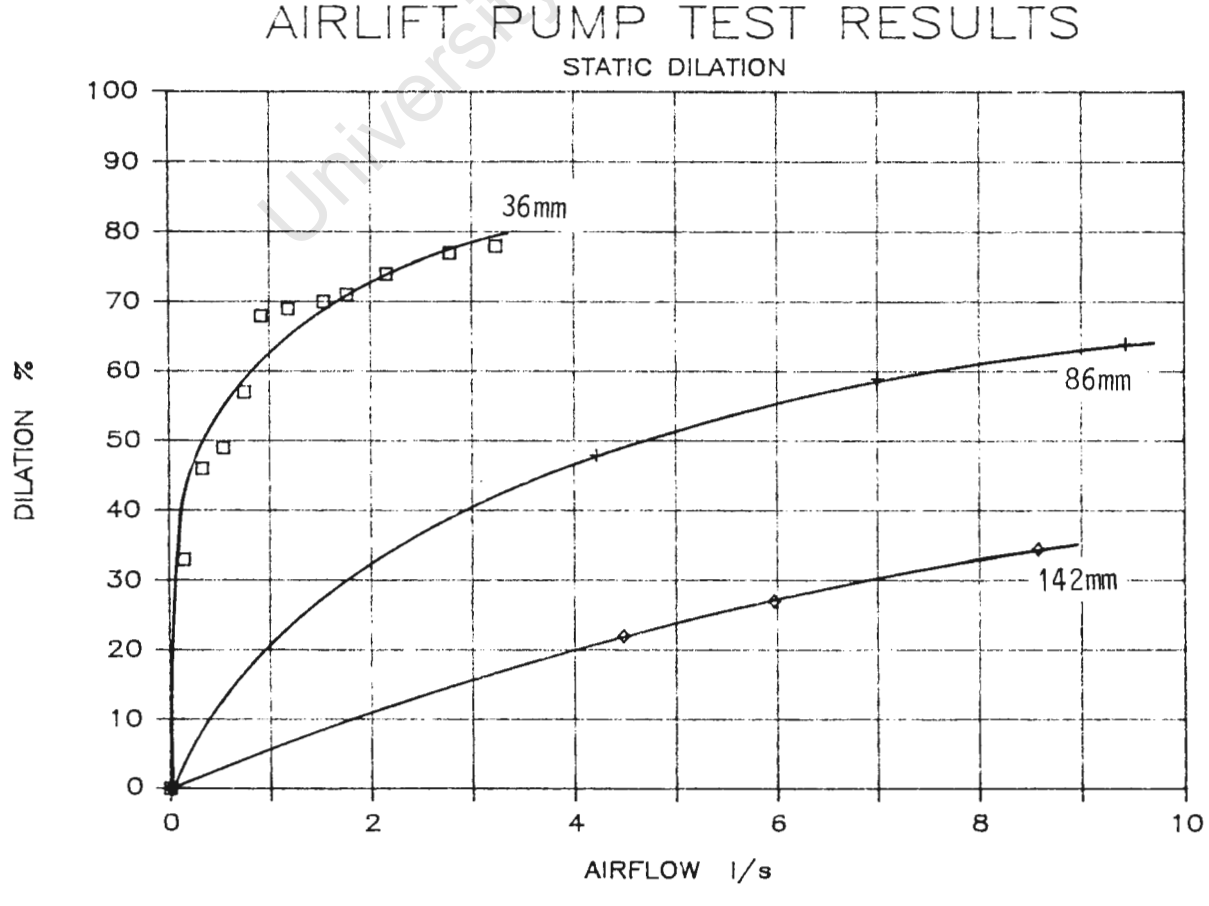

FIGURE 6.1b

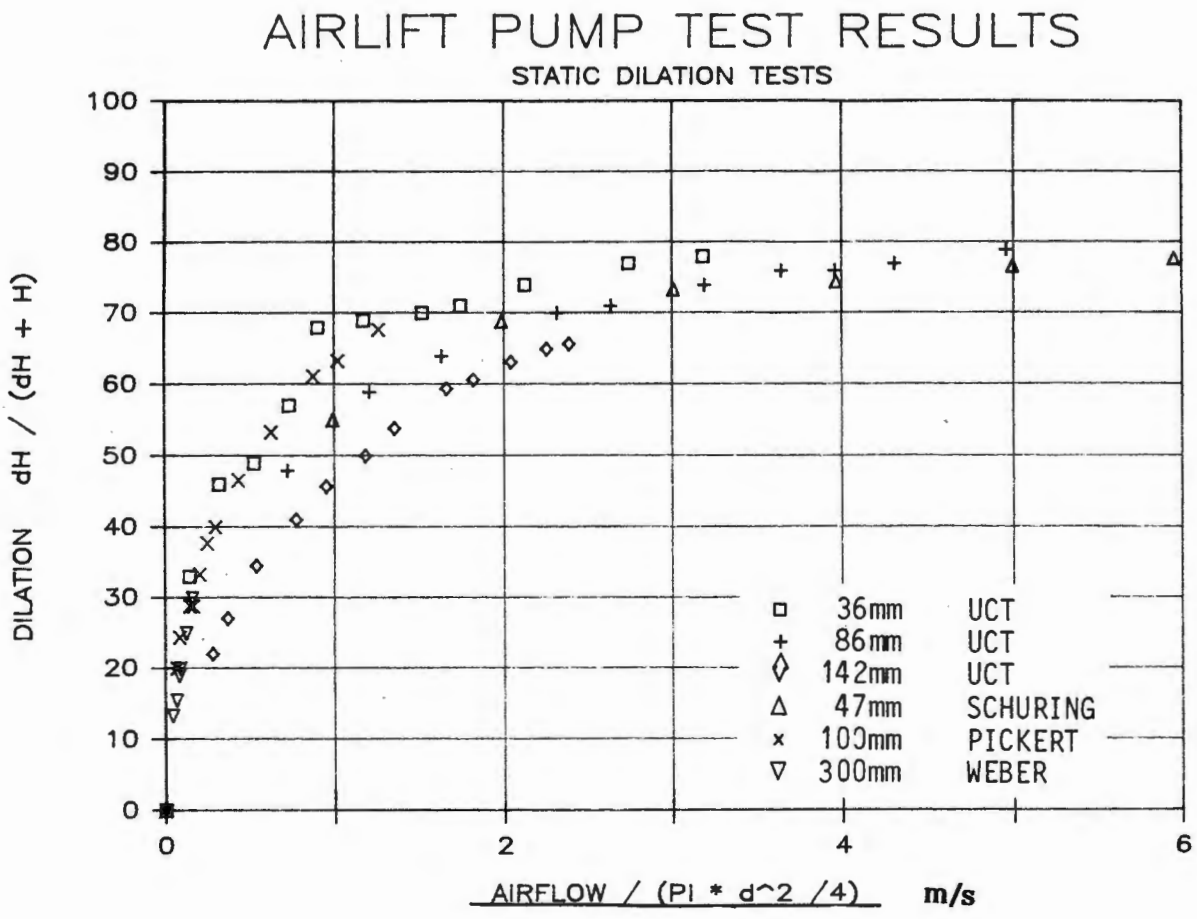

FIGURE 6.2

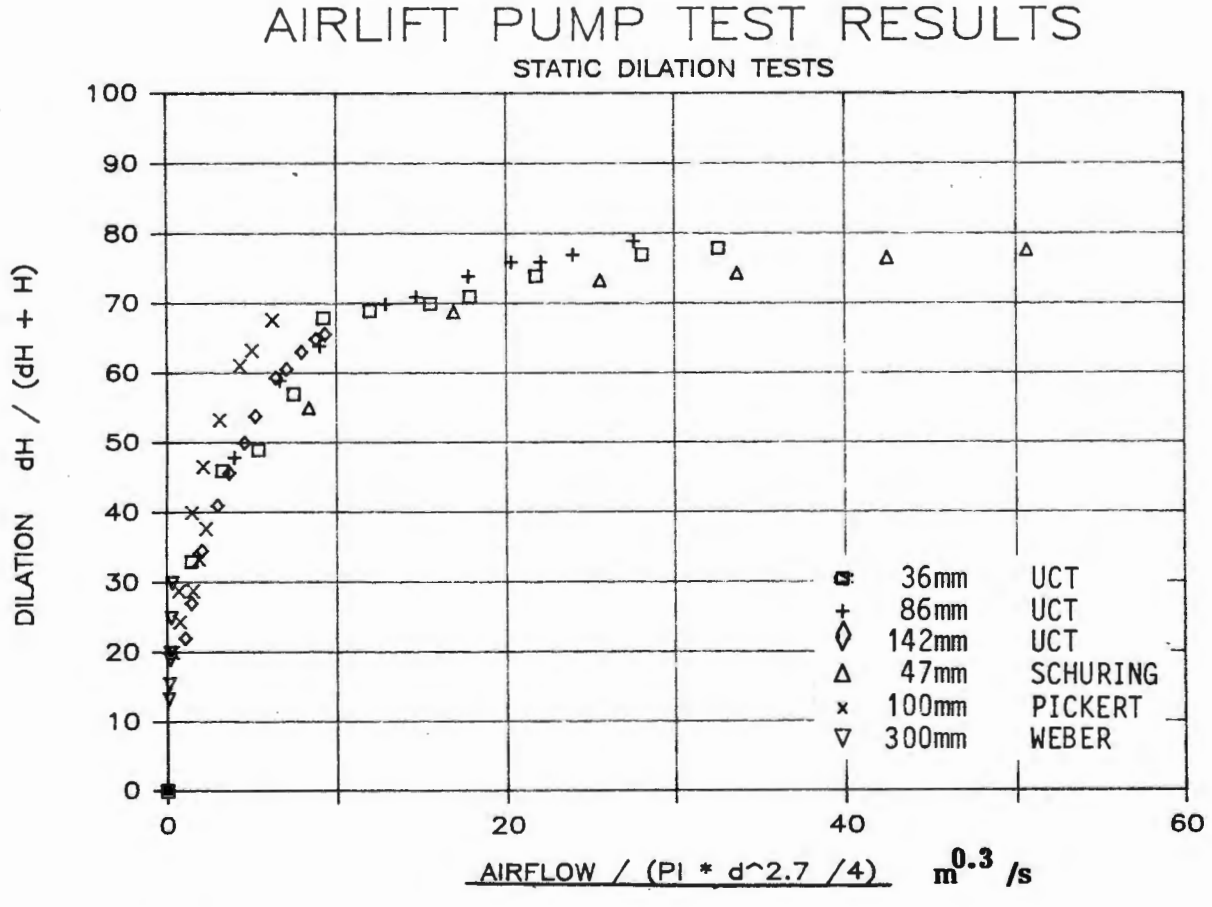

FIGURE 6.3

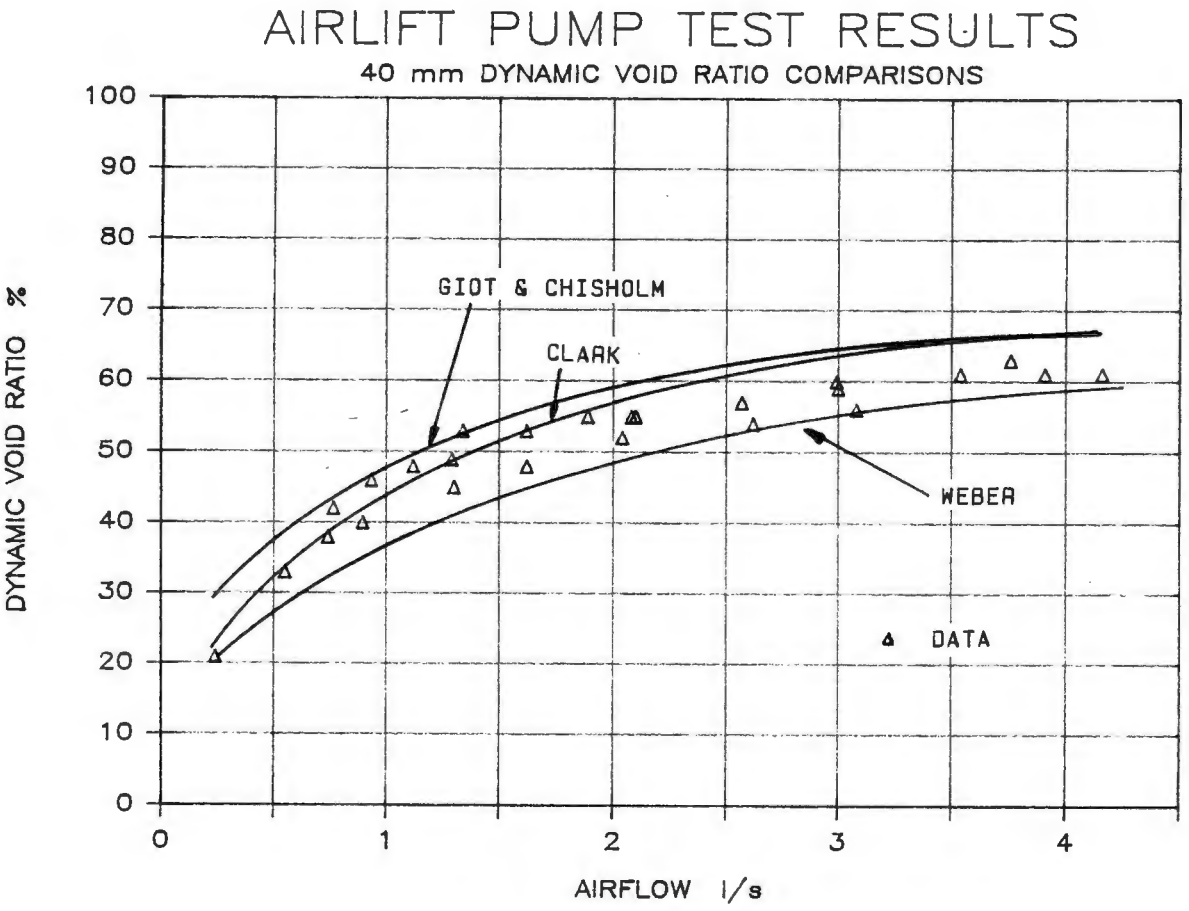

FIGURE 6.4

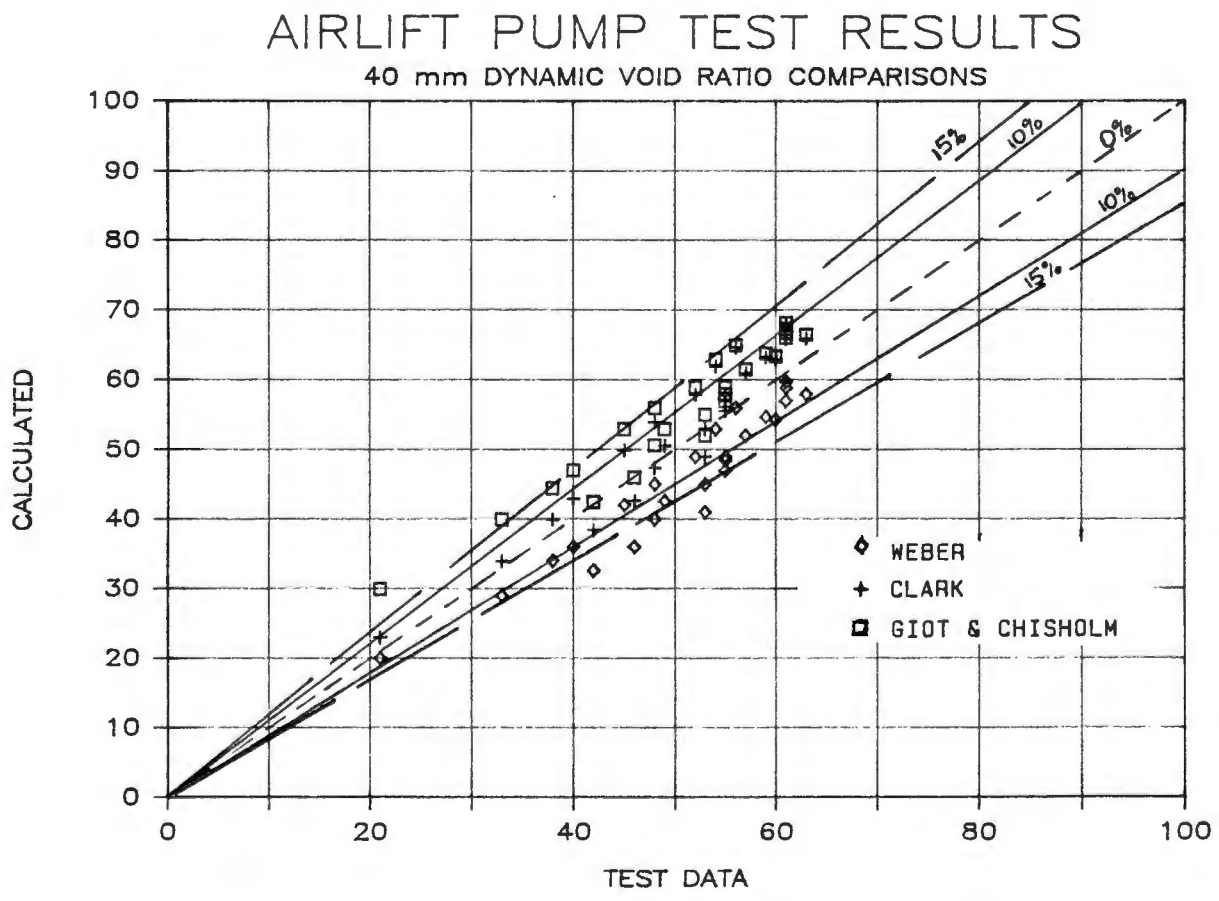

FIGURE 6.5

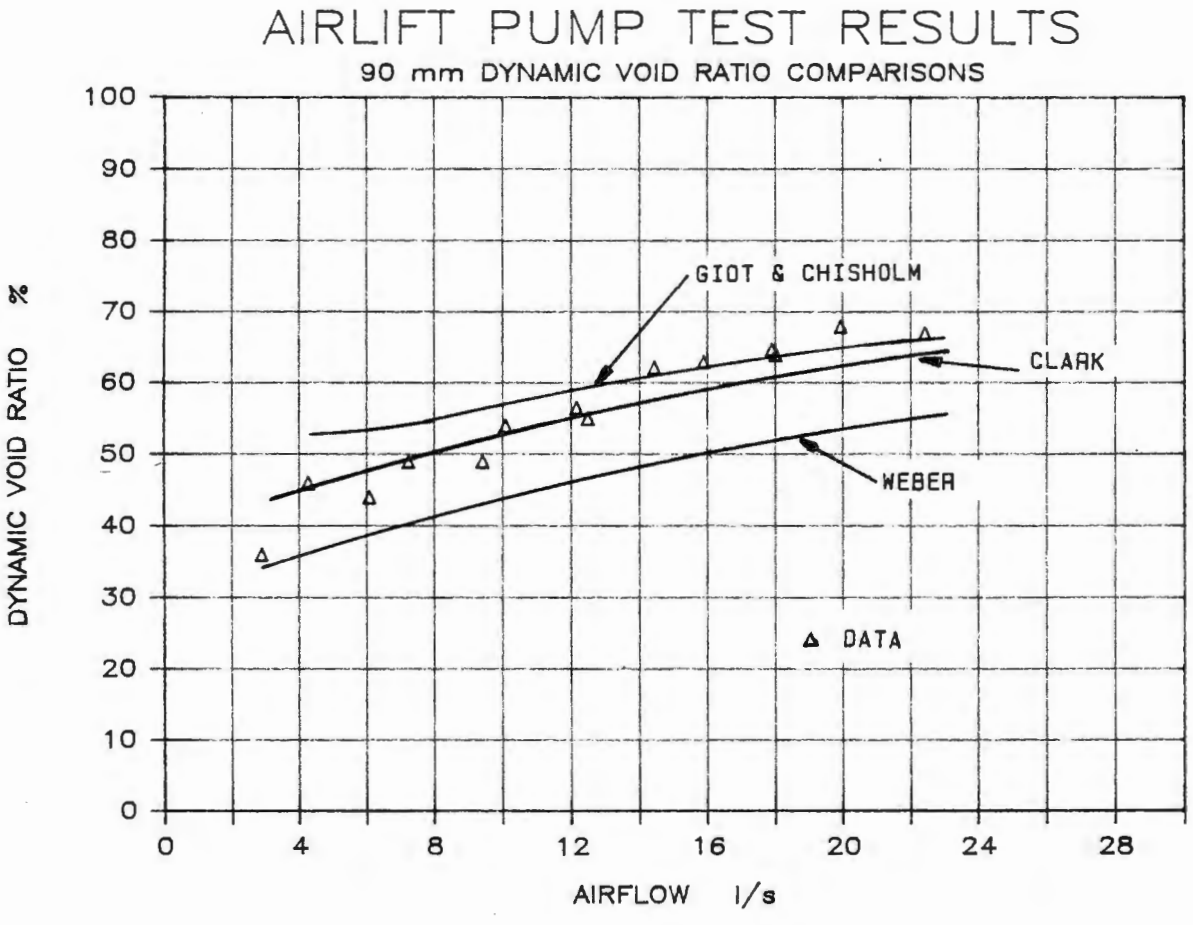

FIGURE 6.6

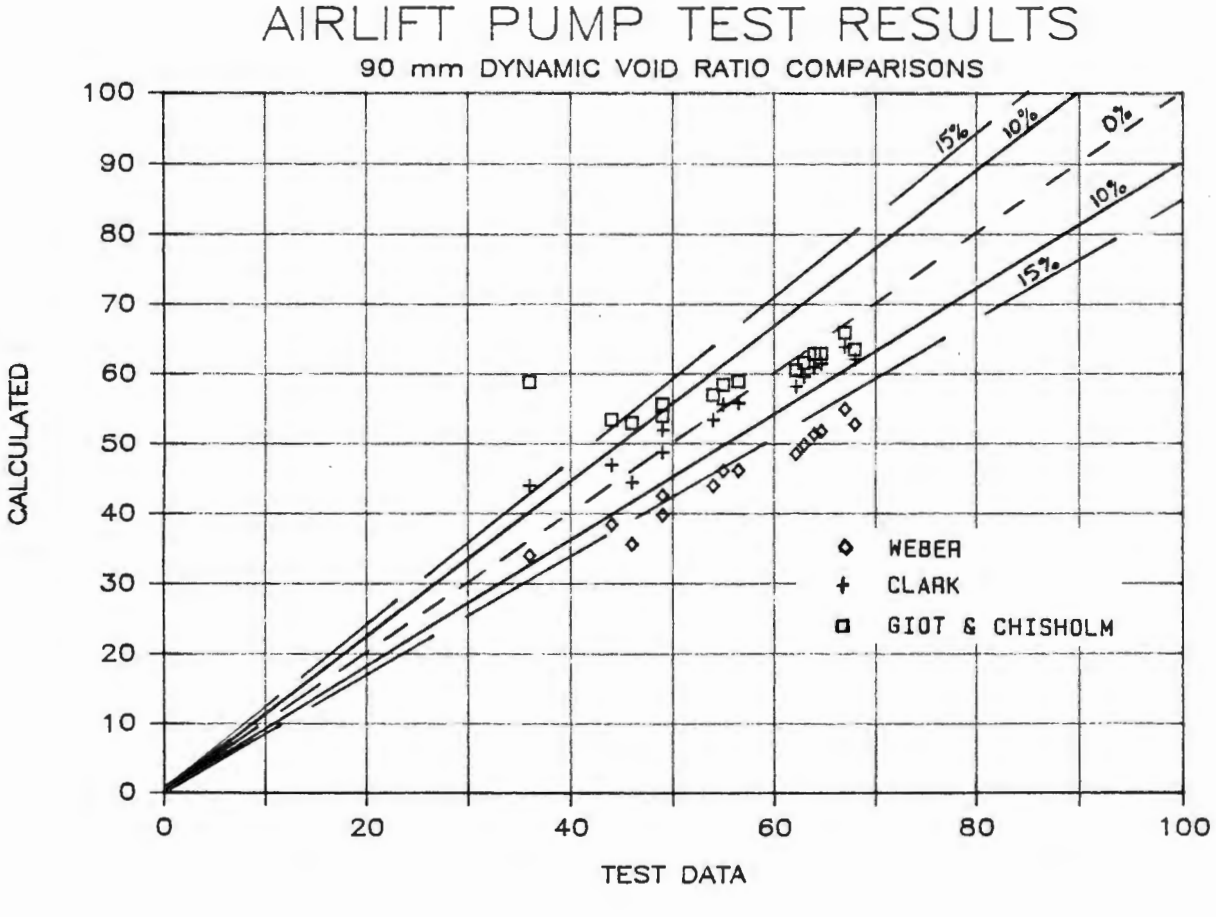

FIGURE 6.7

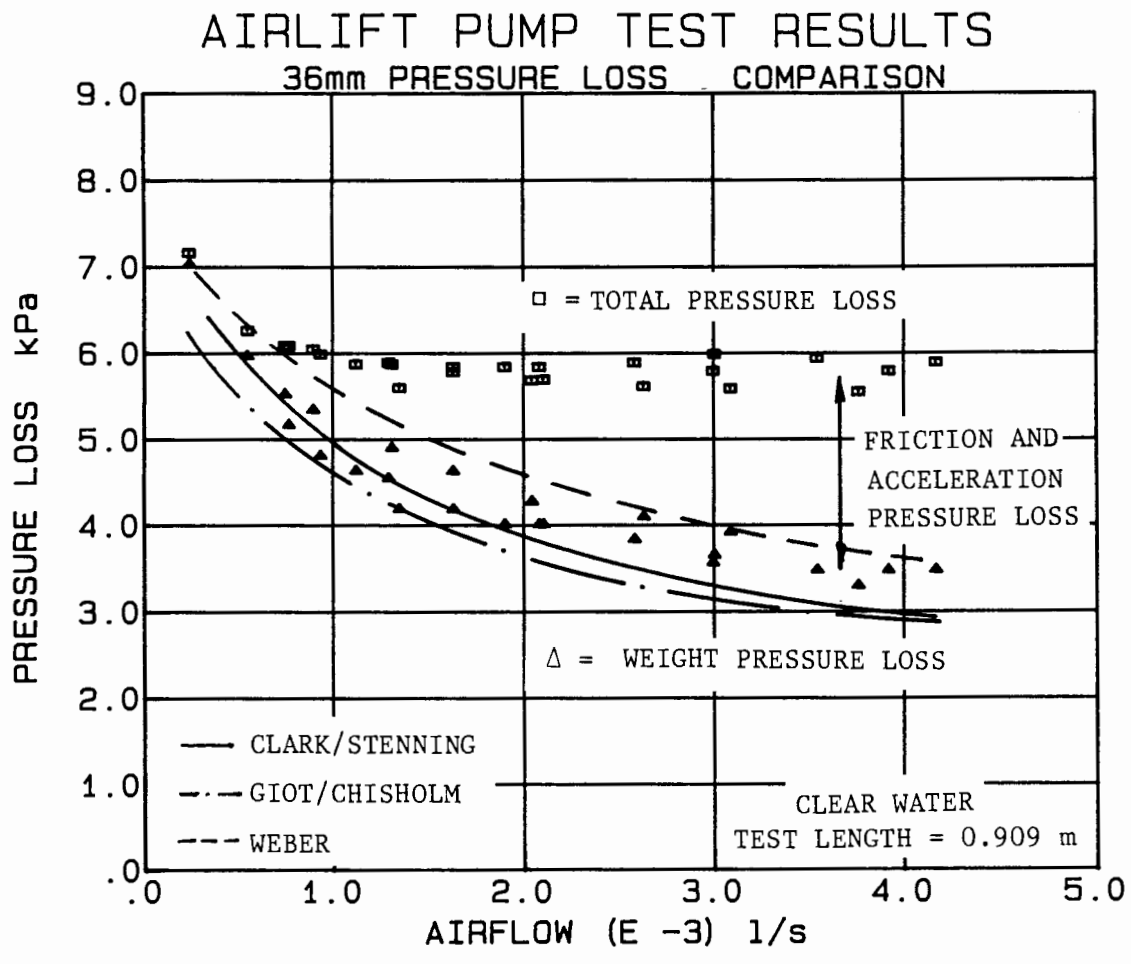

FIGURE 6.8

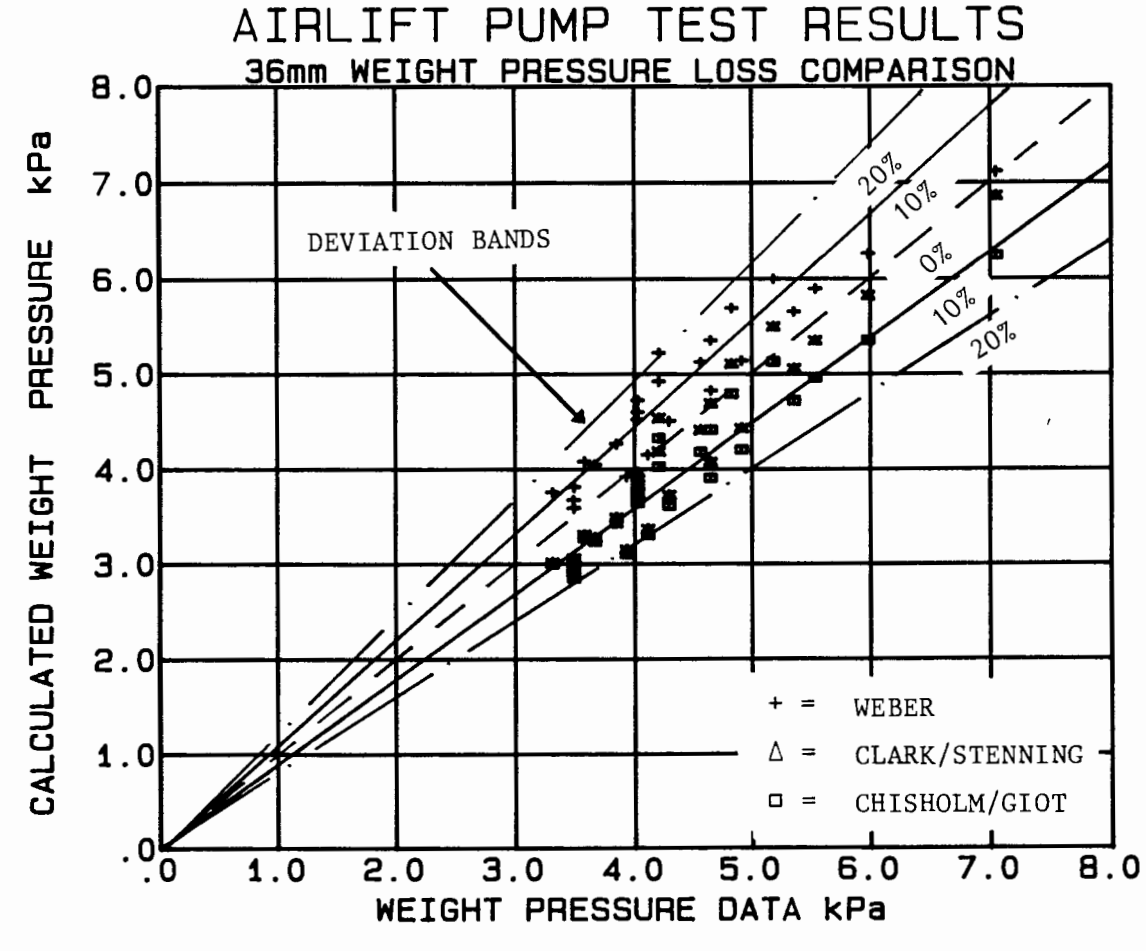

FIGURE 6.9

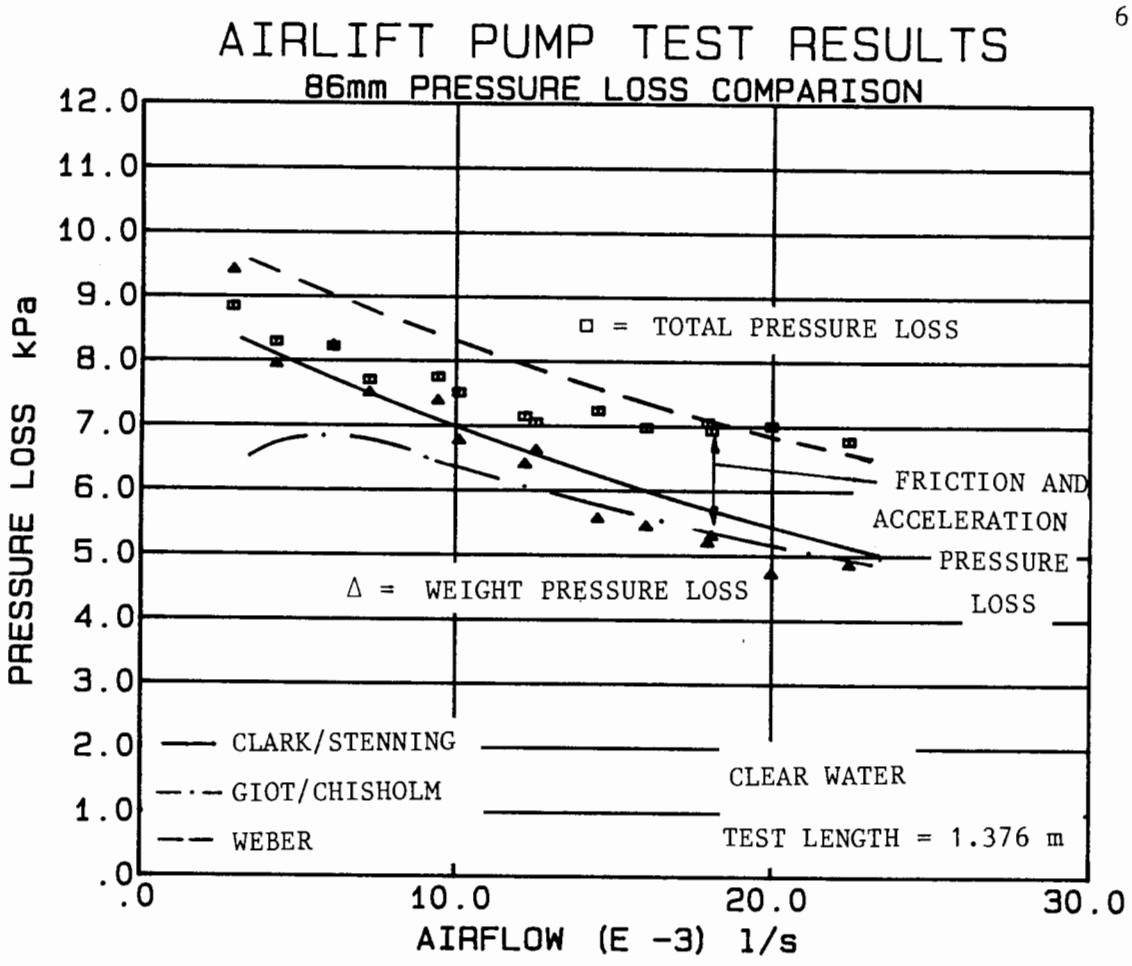

FIGURE 6.10

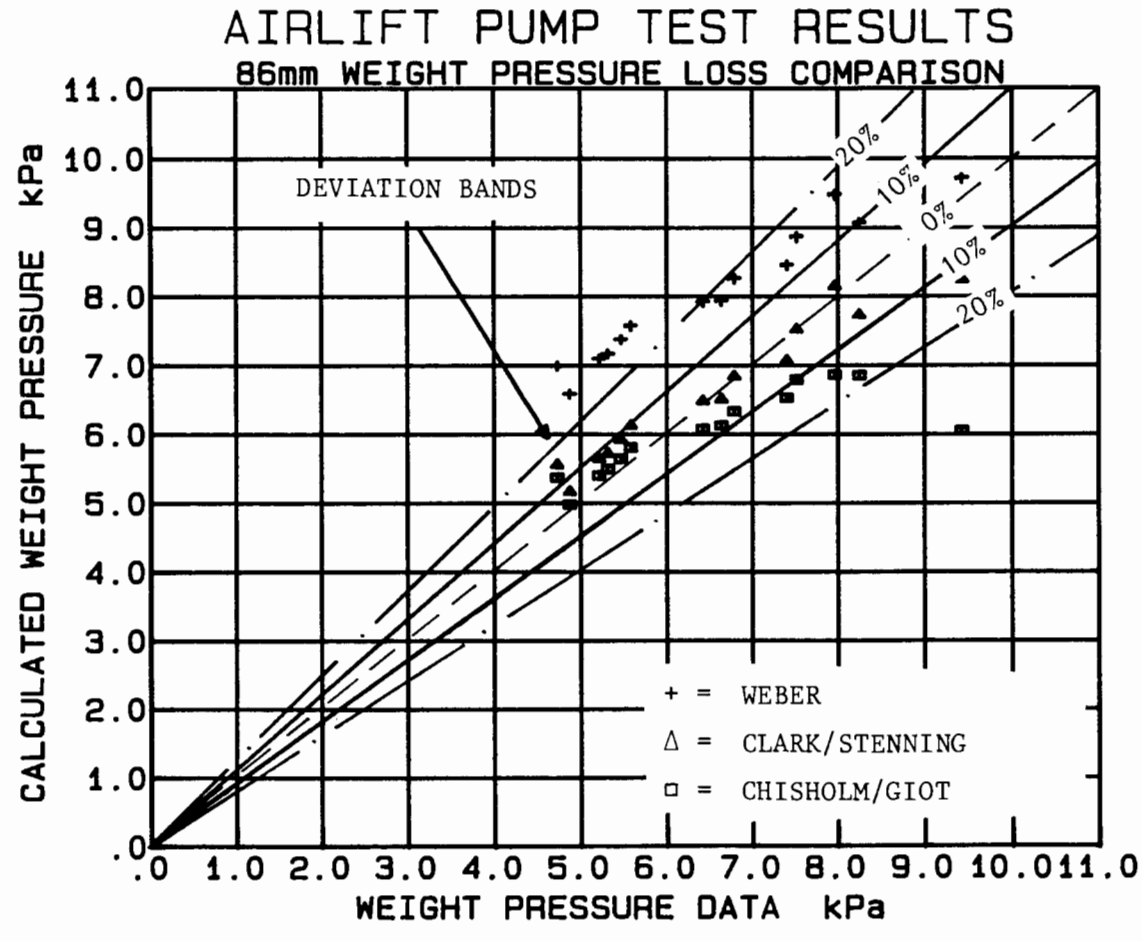

FIGURE 6.11

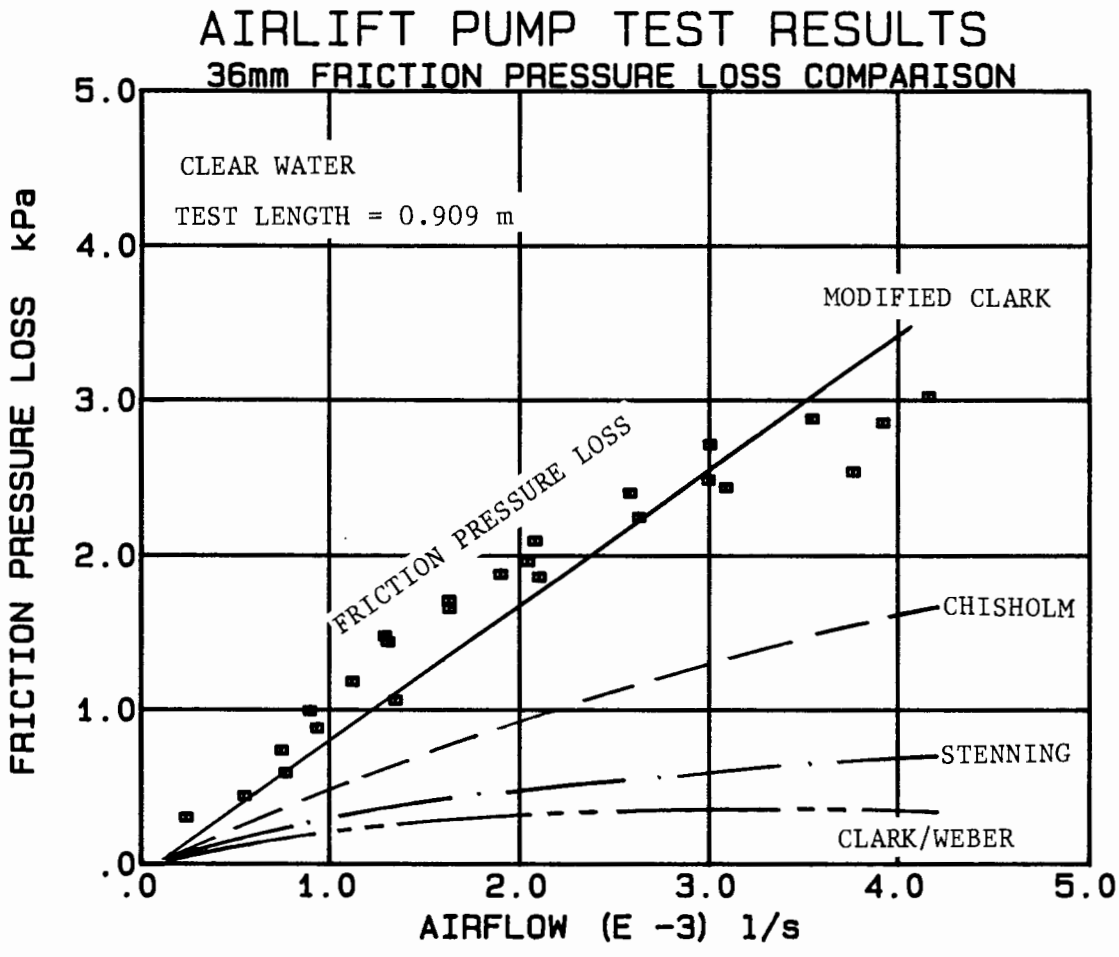

FIGURE 6.12

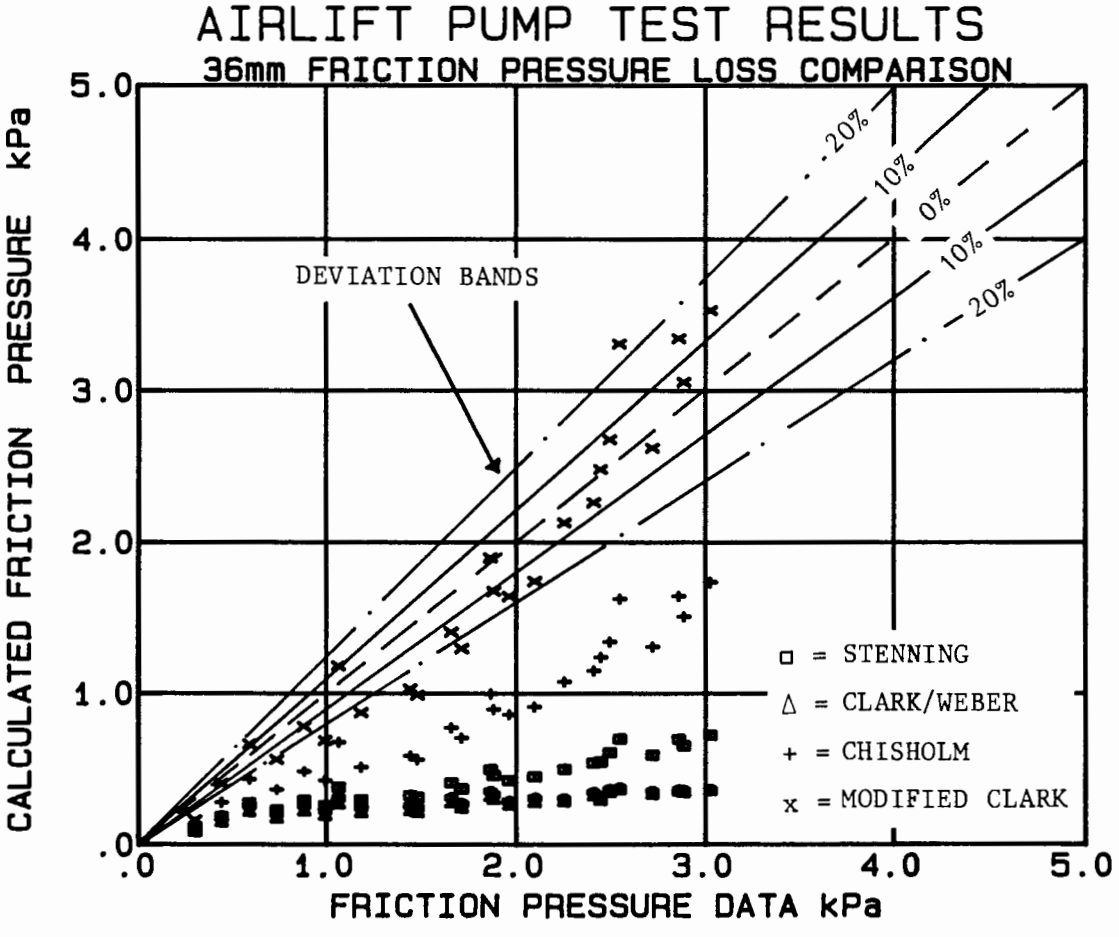

FIGURE 6.13

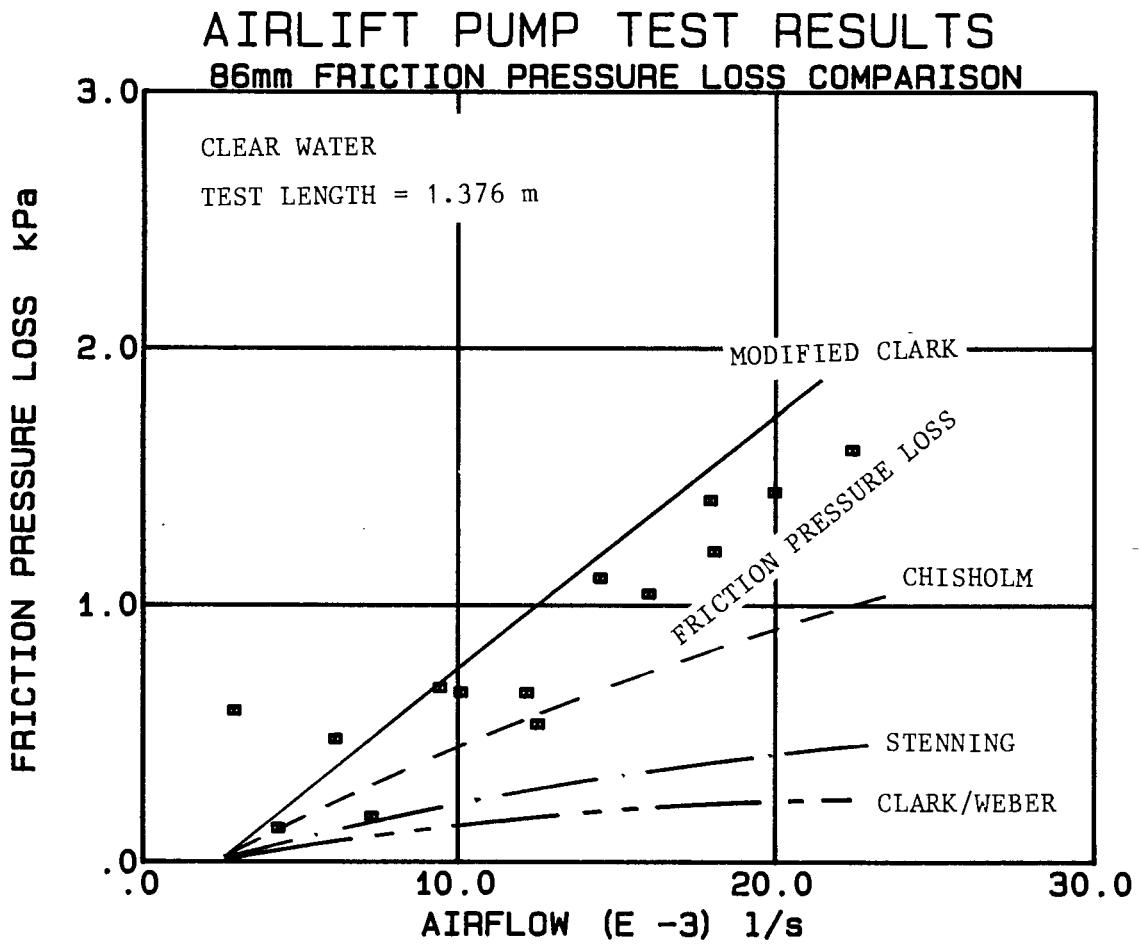

FIGURE 6.14

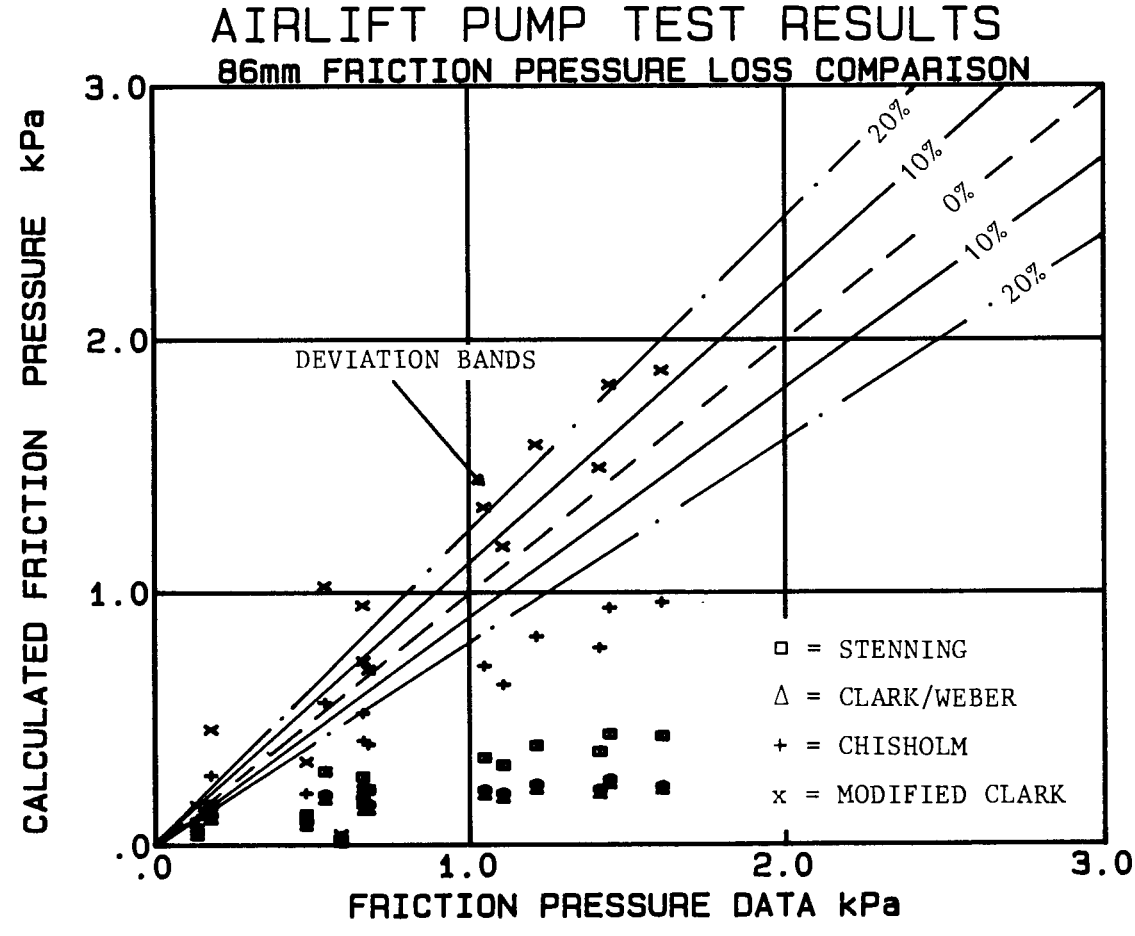

FIGURE 6.15

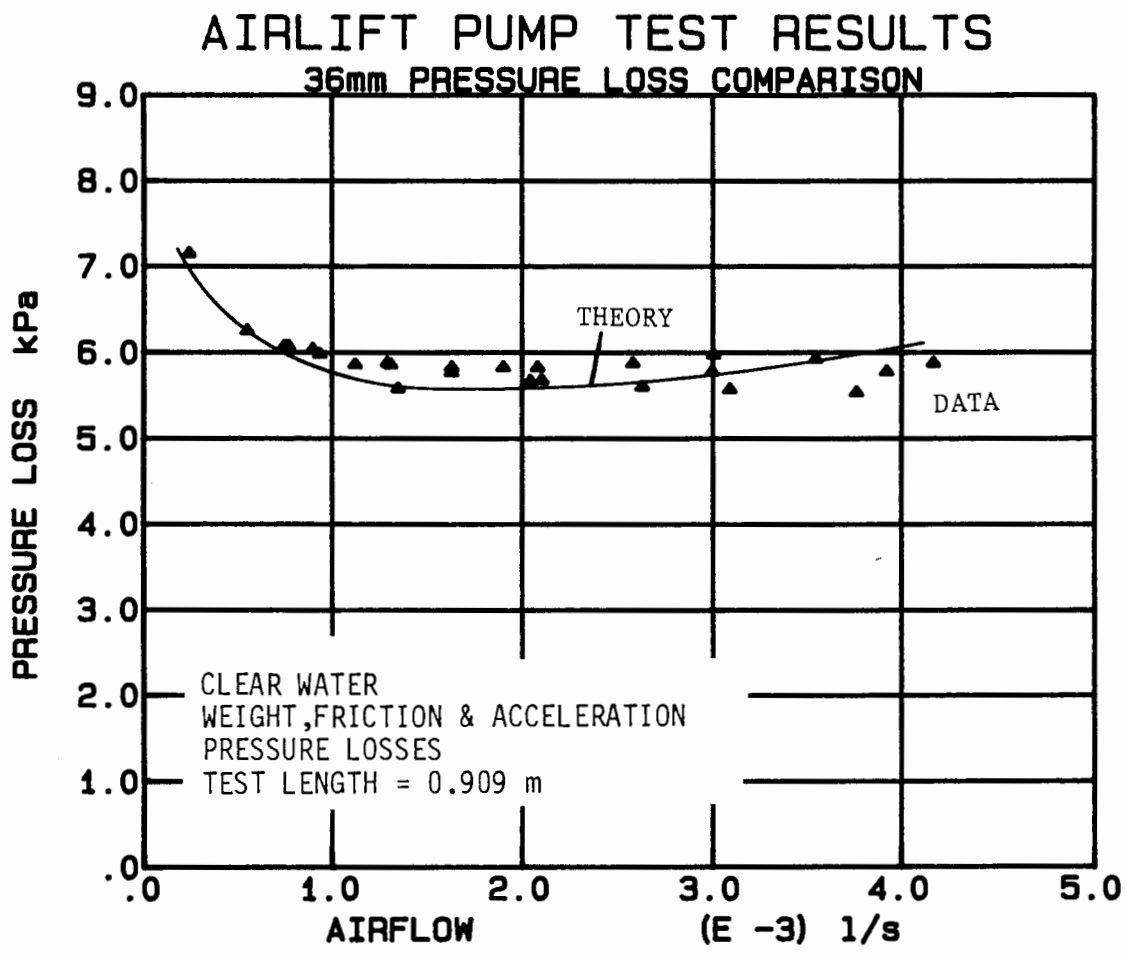

FIGURE 6.16

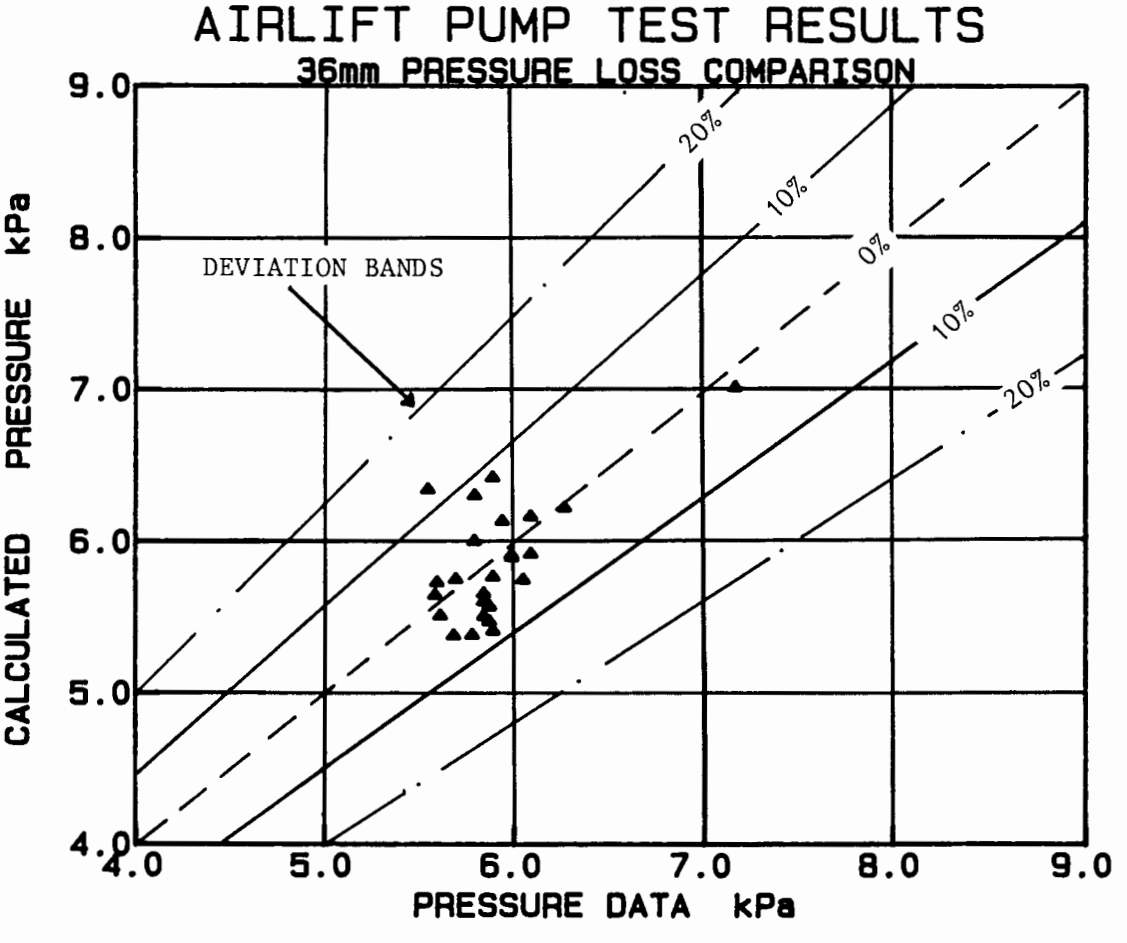

FIGURE 6.17

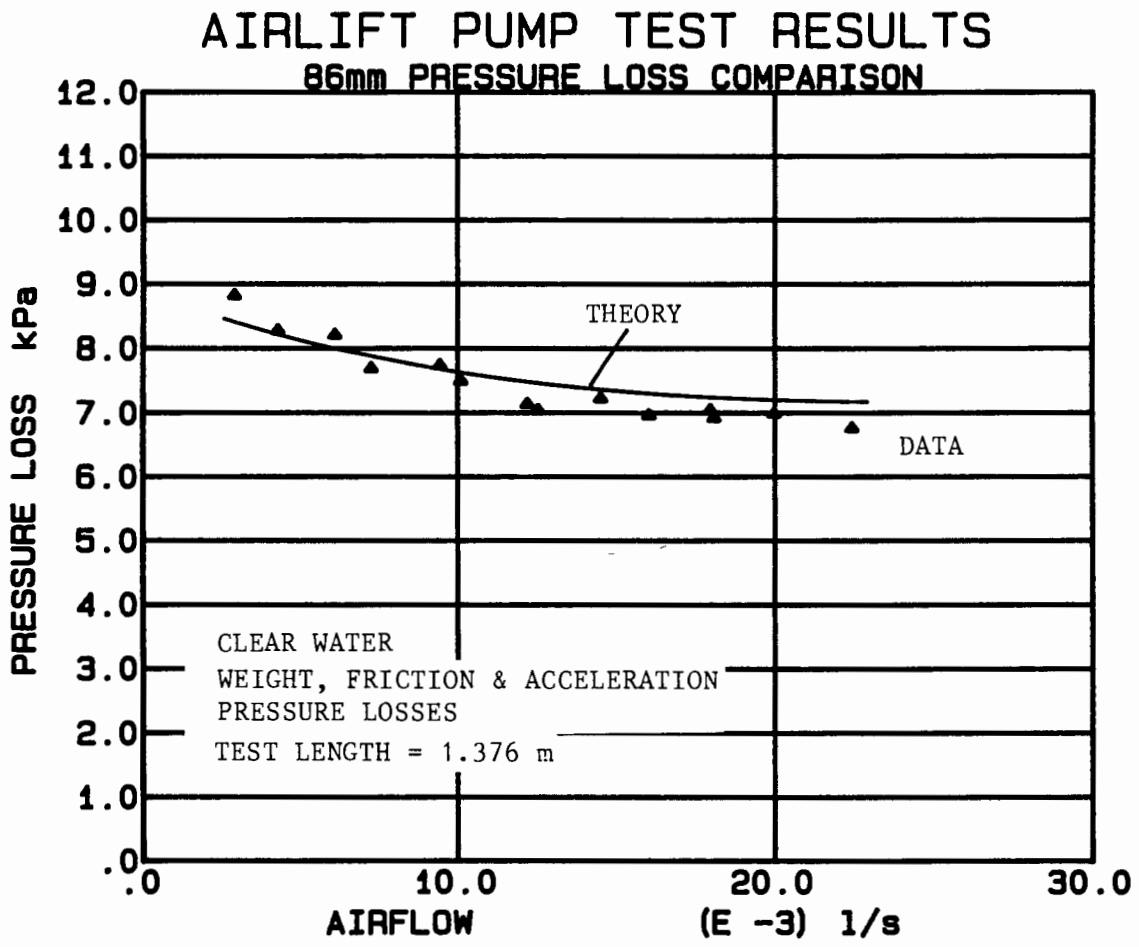

FIGURE 6.18

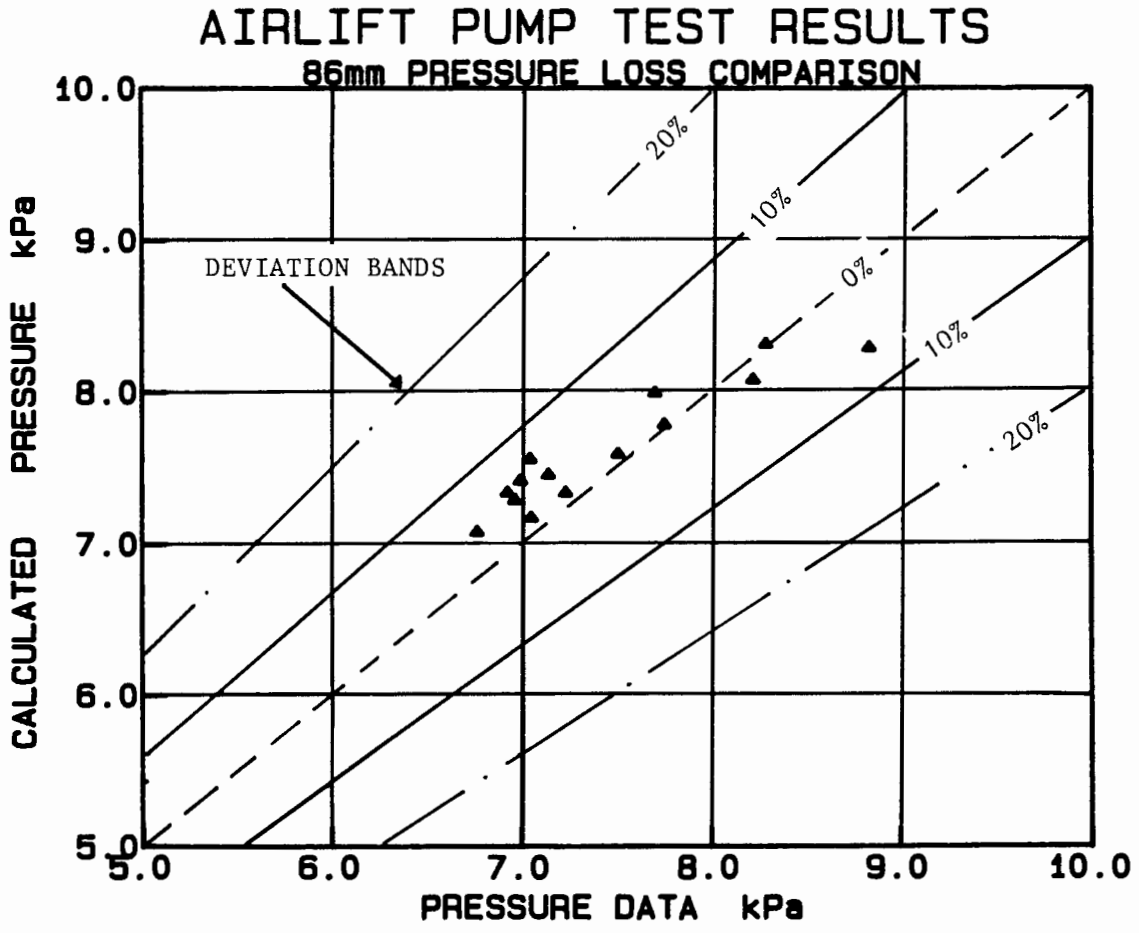

FIGURE 6.19

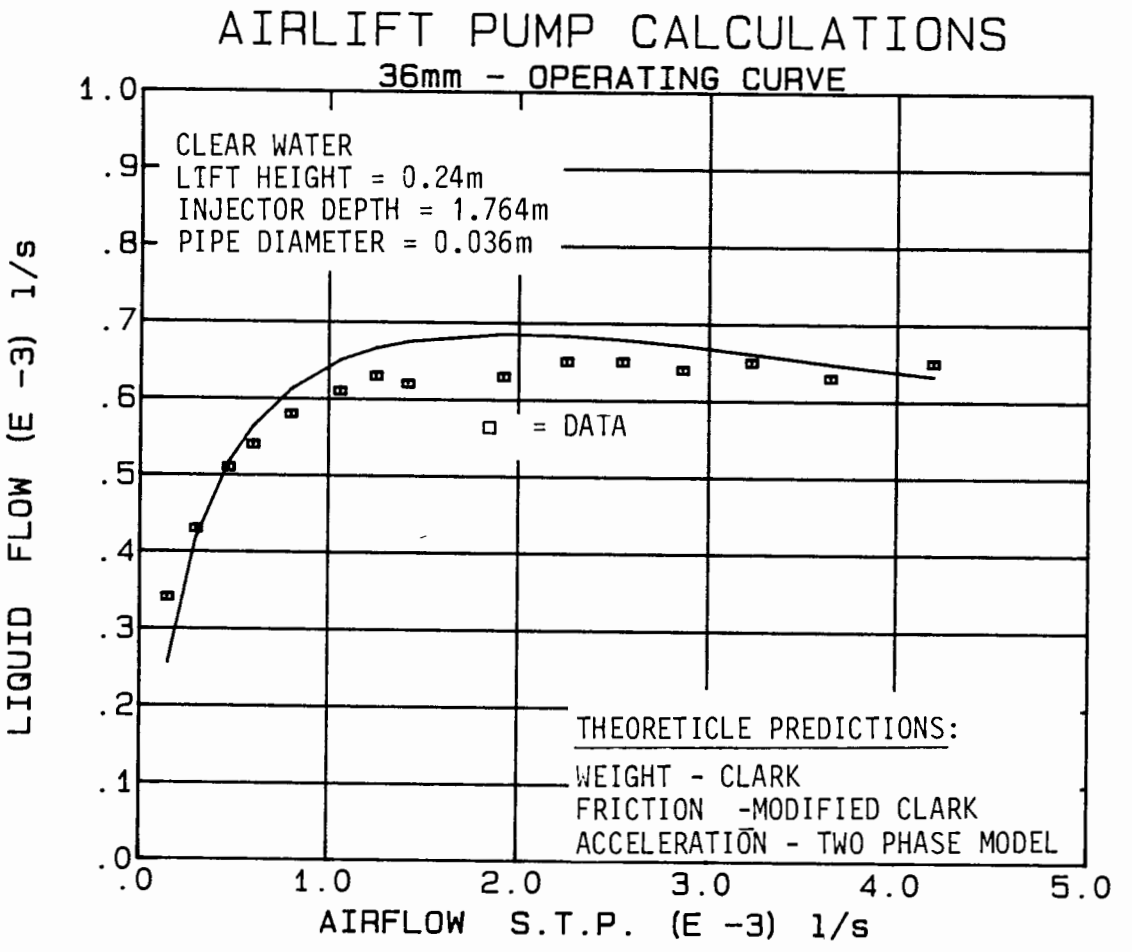

FIGURE 6.20

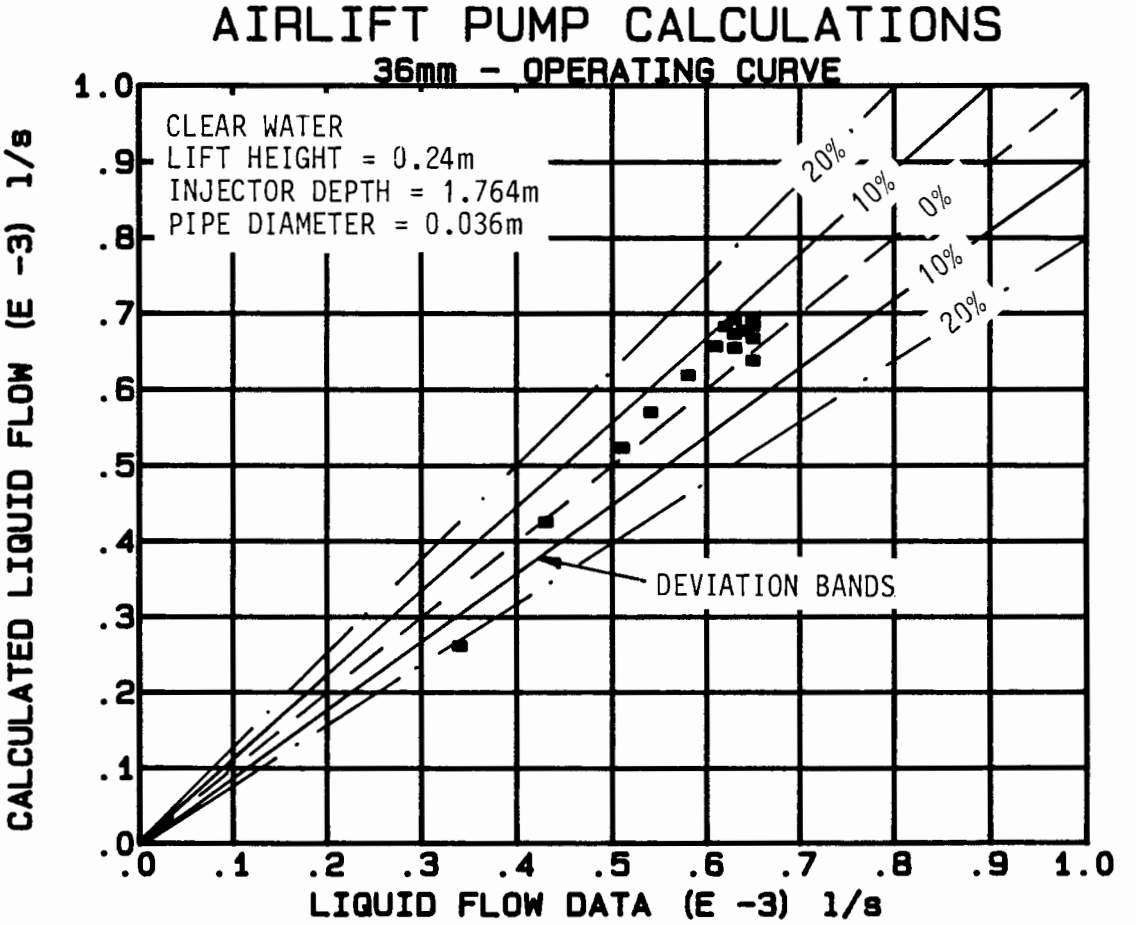

FIGURE 6.21

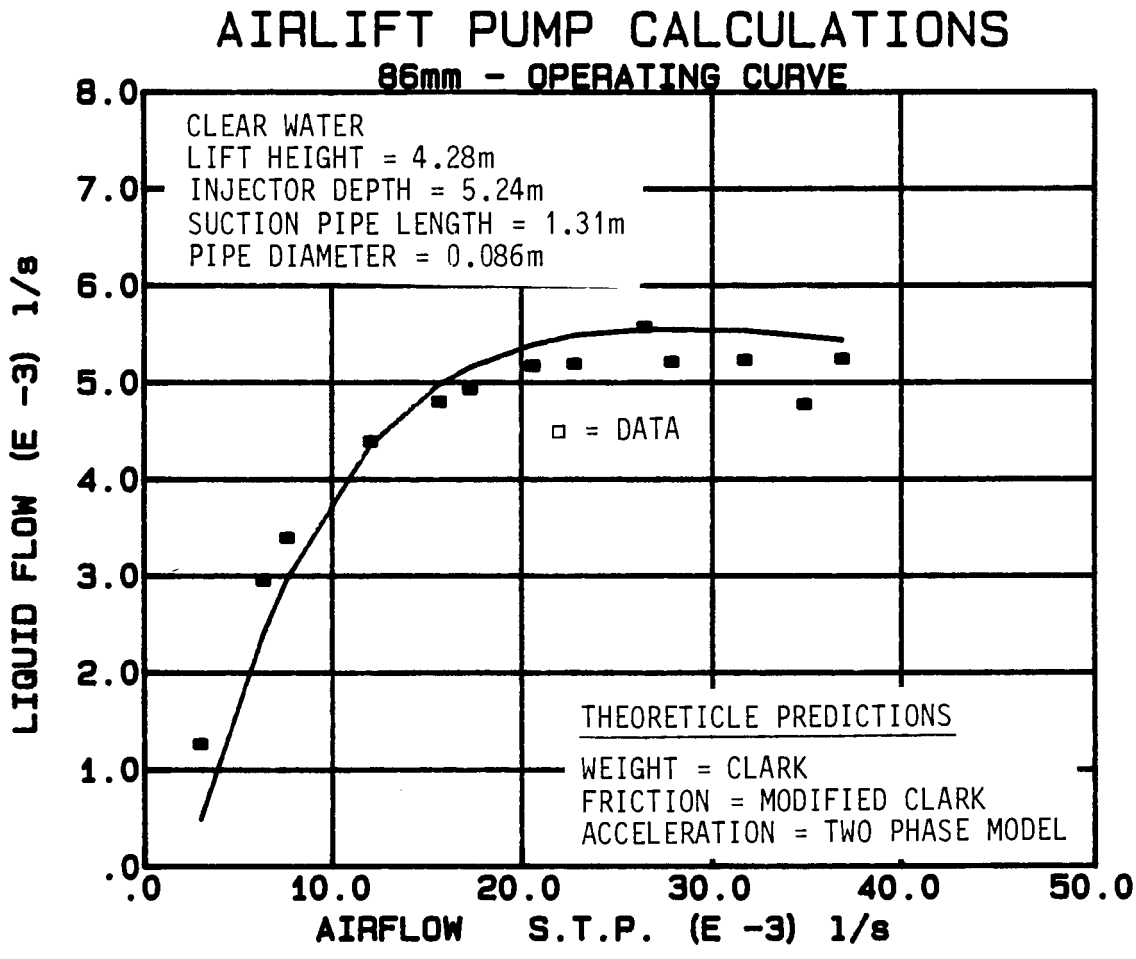

FIGURE 6.22

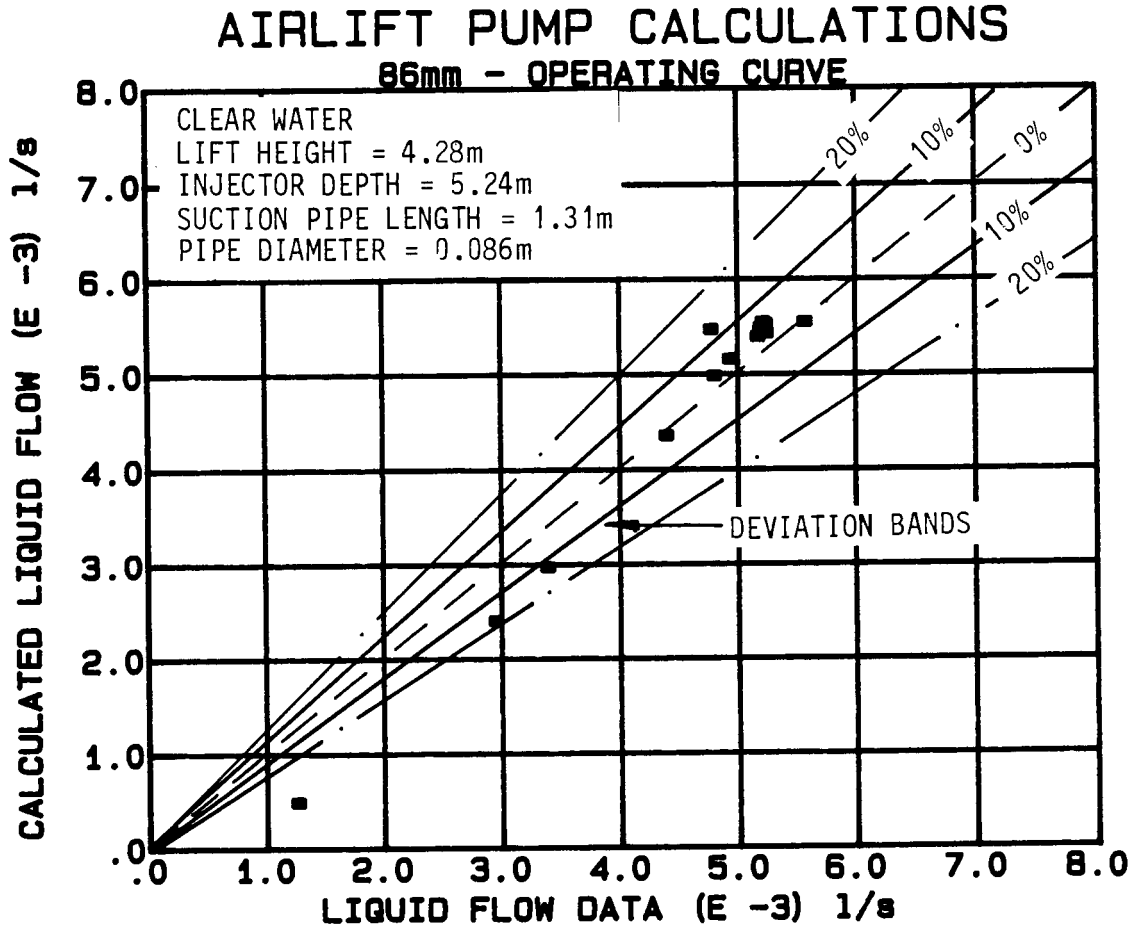

FIGURE 6.23

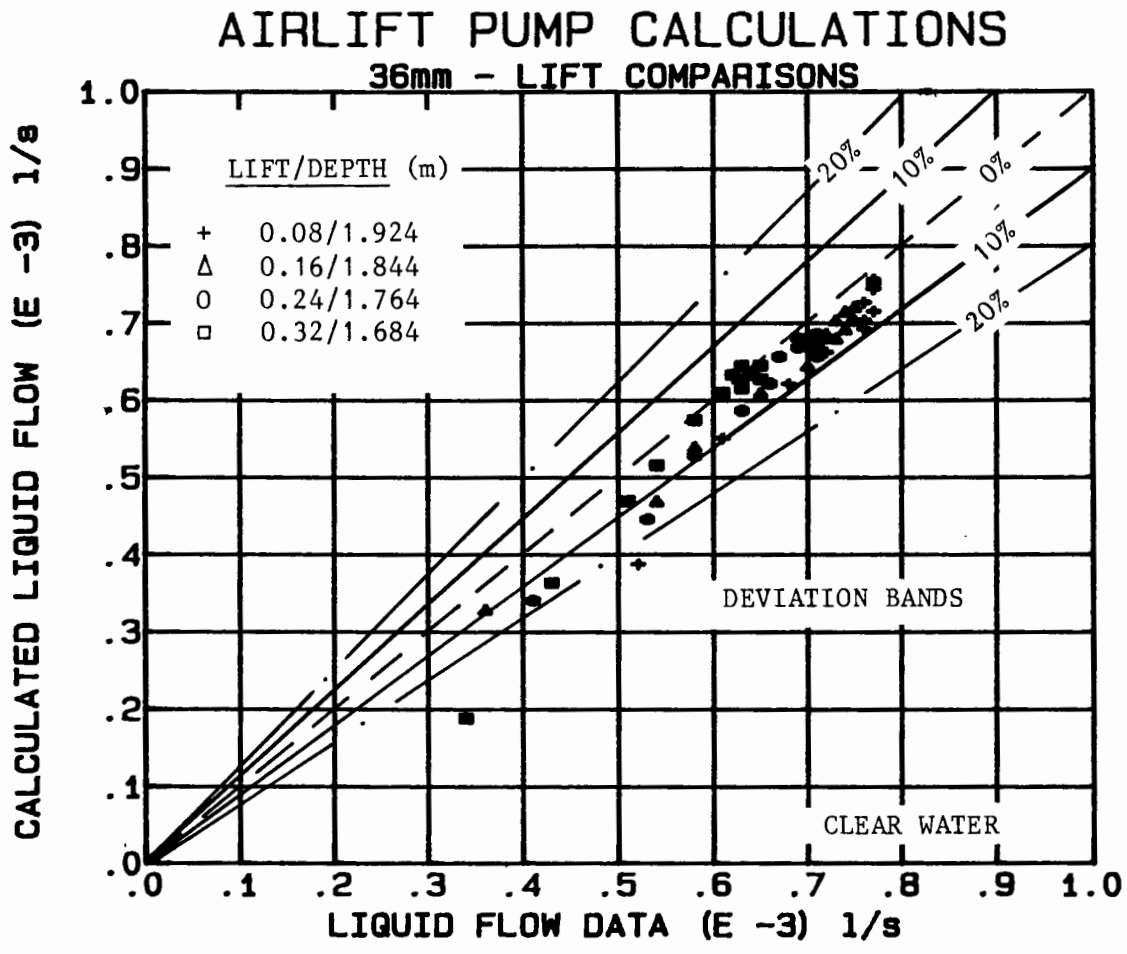

FIGURE 6.24

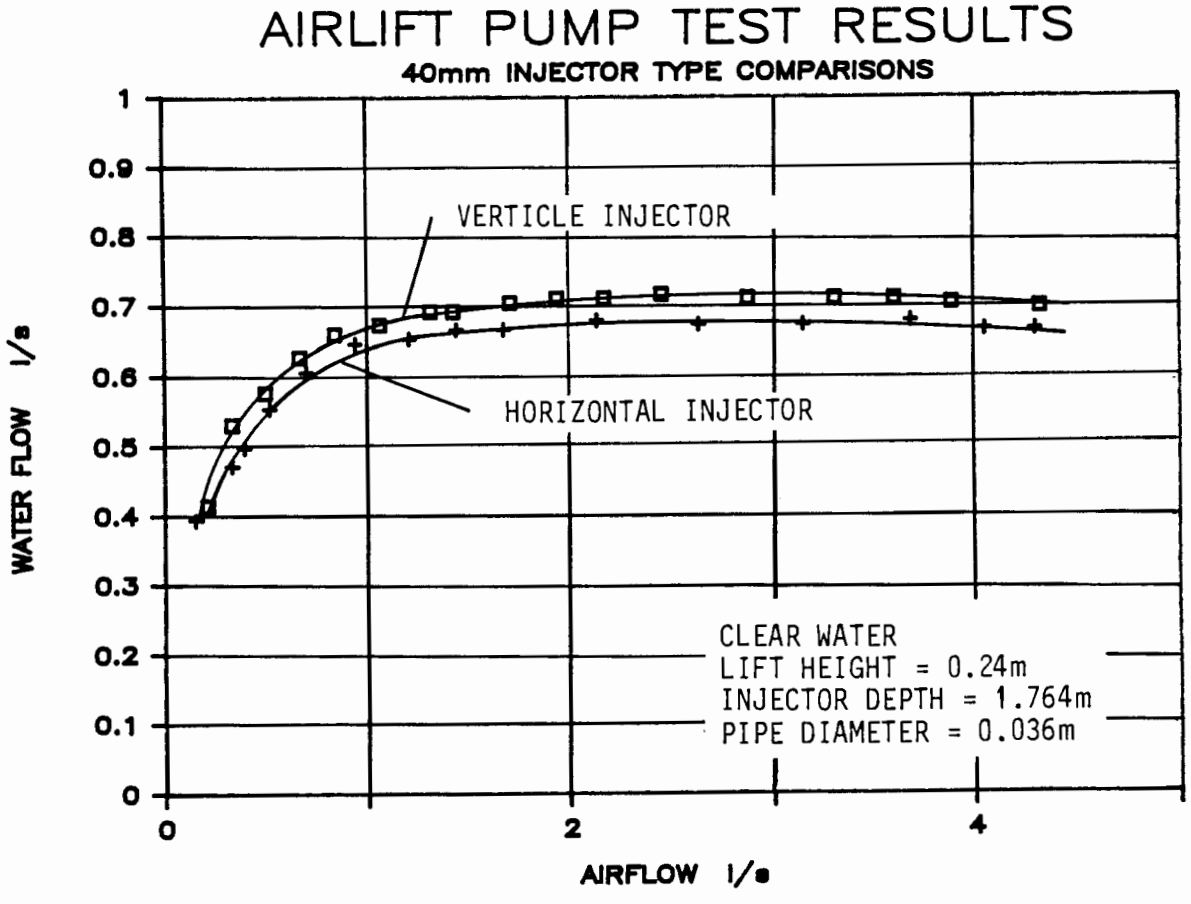

FIGURE 6.25

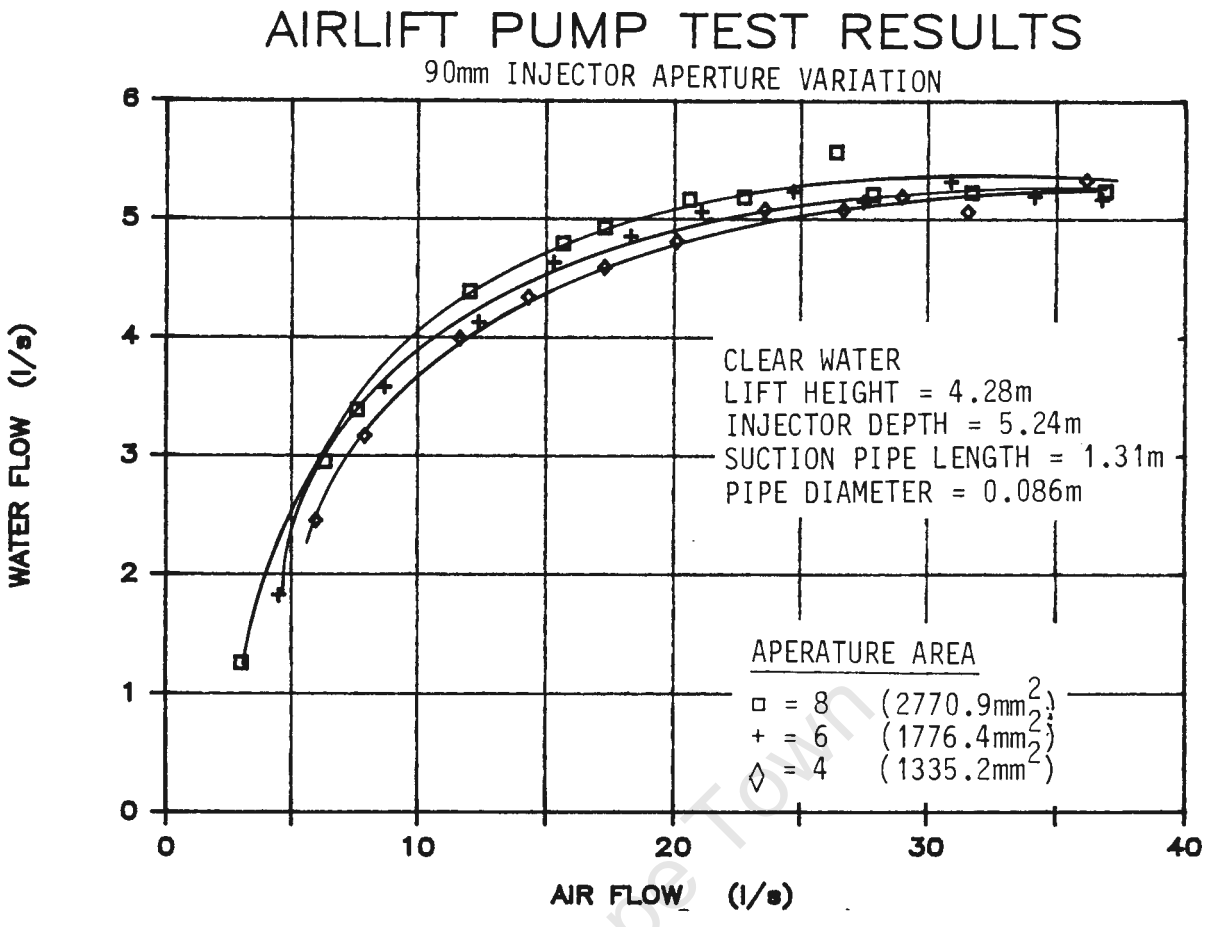

Figure 6.26

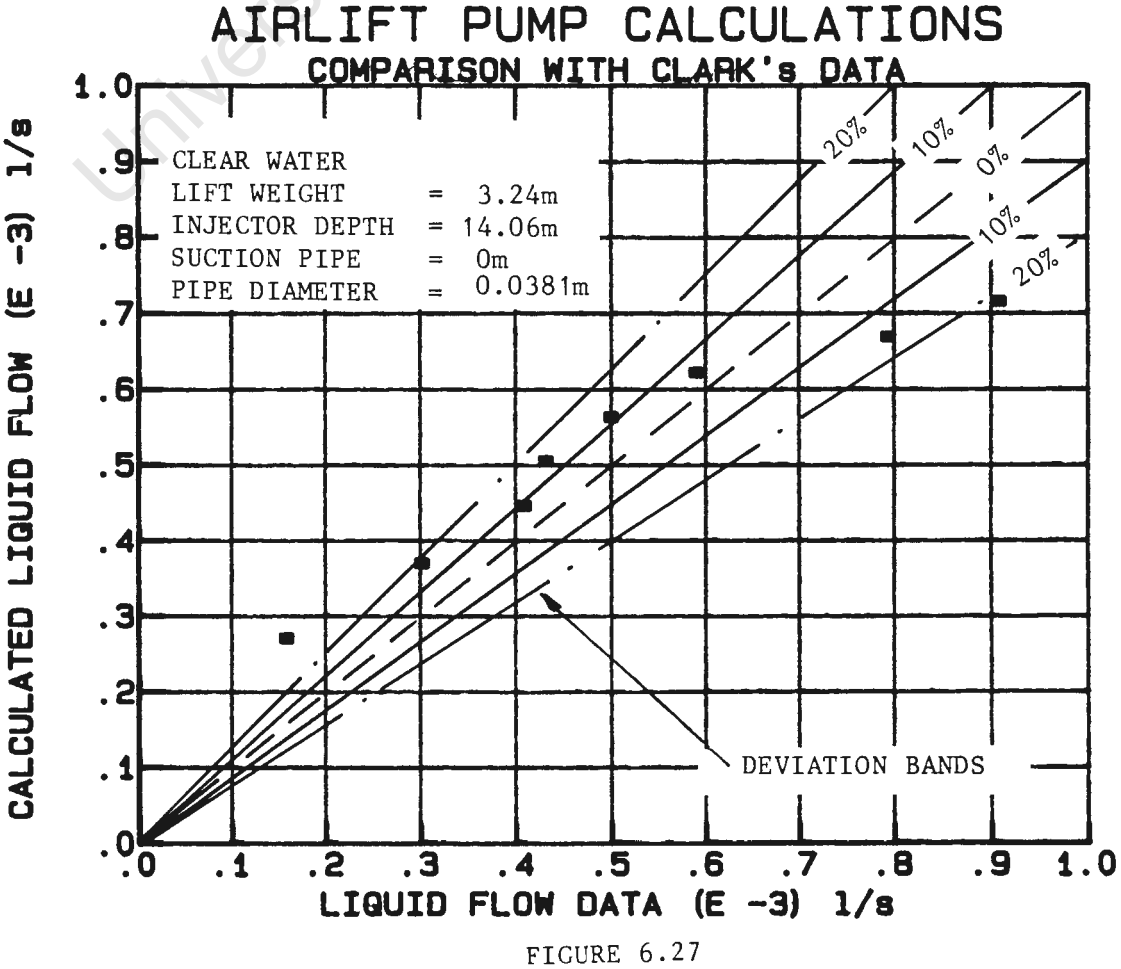

FIGURE 6.27

CHAPTER 7

DISCUSSION

7.1 Introduction

In this chapter, the results obtained from experiments and analysis on the 40 mm and 90 mm airlift pumps are discussed. These include the following component results used for the analytical model:

- **STATIC DILATIONS**
- **DYNAMIC VOID RATIOS**
- **WEIGHT PRESSURE LOSSES**
- **FRICTION PRESSURE LOSSES**
- **TOTAL PRESSURE LOSSES**

Also discussed are performance curves for the 40 mm and 90 mm airlift pumps operating under the conditions outlined in Section 3.1 as well as additional operating curves for airlift pumps presented in the literature.

7.2 Component Results

7.2.1 Static dilations

Referring to Figures 6.1(a) and (b), static dilations increase with increasing gas flow. At first the dilations increase rapdily and then tend to level out at higher gas flow rates. The static dilations investigated in the 36 mm, 86 mm and 142 mm pipe sizes all tended to level out at approximately 80%. This would indicate that a maximum volume concentration of gas can be enclosed in a static column of liquid and gas.

Figure 6.2 shows the method presented by Weber (1976) where the gas flow rate is divided by the pipe area in an attempt to produce a combined curve applicable to all pipe sizes. It is noticed that the pipe sizes researched, as well as additional pipe size data obtained from the literature do not combine well onto one curve.

Dividing the gas flow rate $\pi/4\ d^{2\cdot7}$, results in reducing the curves for the different pipe sizes to one curve, with the maximum dilation remaining approximately 80%. It will however be shown in section 7.2.2 that this is not required for the proposed analytical model.

7.2.2 Dynamic void ratios

Referring to Figure 6.4, at lower gas flow rates on the 40 mm airlift pump, the dynamic void ratio is best predicted using Clark's method. However, as the gas flow rate increases either Weber, Giot, Chisholm or Clark could be used to calculate the dynamic void ratio.

On the 90 mm airlift pump (Figure 6.6) Weber under-predicts the dynamic void ratio at all gas flow rates. Again Clark proves the most accurate at low gas flow rates with Chisholm's and Giot's predictions better at higher gas flow rates.

From a plot of calculated dynamic void ratios versus measured dynamic void ratios, for the 40 mm airlift pump (Figure 6.5), it is seen that most of Clark's predictions lie within 10% of the measured data. A large number of Weber, Giot and Chisholm's predictions tend to lie outside 10%.

On the 90 mm airlift pump (Figure 6.7) Clark's predictions again calculate the dynamic void ratios to within 10% of the measured data. Weber underpredicts by a percentage in excess of 15%, with Giot and Chisholm having good correlation at high gas flow rates.

For both systems it is clear that the dynamic void ratio component (ϵ_g) used to calculate the weight of the two phase mixture is best modelled by Clark's equation given below:

$$\left(\frac{1}{\epsilon_g}\right)\left(\frac{Q_g}{A}\right) = K_1\left(\frac{Q_g}{A} + \frac{Q_\ell}{A}\right) + K_2\,(gd)^{1/2} \qquad (2.33)$$

with $K_1 = 1.2$

$K_2 = 0.35$

7.2.3 Weight pressure loss

The weight pressure losses are calculated using the dynamic void ratios discussed in Section 7.2.2 as well as equation 2.21. For this reason the weight pressure losses assume the same trend discussed in Section 7.2.2.

Stenning's weight pressure loss calculation procedure does not make use of dynamic void ratios, and agrees well with Clark's predictions.

It is apparent from figures 6.8 and 6.10 that the weight pressure loss is best calculated using equation 2.21 given below, with the dynamic void ratio component calculated as discussed in section 7.2.2.

$$W = A\,g\,h\,(\rho_g\,\epsilon_g + \rho_\ell\,(1 - \epsilon_g)) \qquad (2.21)$$

Referring to Figures 6.8 and 6.9, the difference between the total pressure loss and the weight pressure loss consists of friction and acceleration pressure loss components. This difference is small at low gas flow rates, and increases at higher gas flow rates, where friction effects tend to become increasingly predominant.

On the 40 mm airlift pump, the friction and acceleration effects contribute up to 46% of the total pressure loss (Figure 6.8) at high gas flow rates. On the 90 mm airlift pump, these effects only contribute 26% (Figure 6.10).

The trend of the total pressure loss component is to decrease rapidly at low gas flow rates with levelling out at higher gas flow rates. This is due to a low percentage of gas at low gas flow rates, with the pressure loss component made up primarily of the weight of the liquid. As the gas flow rate is increased, the weight of the liquid decreases resulting in a decrease in the pressure loss. Included also is an increasing influence of the friction and acceleration components resulting in the levelling out of the total pressure loss.

7.2.4 Friction pressure loss

Figures 6.12 and 6.14 show the friction and acceleration pressure loss components of both the 40 mm and 90 mm airlift pumps. However, the acceleration component is in the order of 1% of the total pressure loss in this case, and is not significant.

Considering the friction pressure loss component as being the difference between the total pressure loss and the weight pressure loss, it is noticed that the literature under-predicts across the entire gas flow range (Figures 6.12 and 6.14).

The trend of the friction pressure loss curve is to increase due to a faster liquid velocity with increasing gas flow rate. It is expected that the friction pressure drop tends to level out slightly at higher gas flow rates as the total pressure loss and the weight pressure loss components level out.

The modification to Clark's calculation procedure, presented by the present author and discussed in Section 6.2.4, tends to predict the friction pressure loss component with higher accuracy on both airlift pumps. Referring to Figures 6.13 and 6.15, predictions with the modified method tend to lie within a 20% band of the measured data, whereas methods used in the literature show poor correlations. The friction pressure component can thus be calculated using:

$$\Delta p_f = \frac{2 f_\ell \rho_\ell h v_\ell^2}{D} (1 + 1.5 \epsilon_g) \qquad (7.1)$$

7.2.5 Total pressure loss

Both Figures 6.17 and 6.19 show how pressure losses are calculated to within 10% of the measured data across the entire gas flow range.

On both the 40 mm and 90 mm airlift pumps the calculated total pressure loss component assumes the trend discussed in Section 7.2.3.

Figures 6.16 and 6.18 show that the total pressure loss of the gas-liquid mixture in the delivery line is adequately predicted, using the component results discussed in Section 6.2.5. and the equation given below:

$$\Delta p_4 = [\epsilon_g \rho_g v_g^2 + (1 - \epsilon_g) \rho_\ell v_\ell^2]_E + [\epsilon_g \rho_g v_g^2 + (1 - \epsilon_g) \rho_\ell v_\ell^2]_F + W + p_f A \qquad (2.16)$$

7.3 Airlift Pump Performance Curves

7.3.1 General operating curves

From Figures 6.20 and 6.22 it can be concluded that the calculation procedure outlined in Section 2.4 using the two phase pressure loss models discussed in Section 6.3 adequately predicts both the 40 mm and 90 mm airlift pump performance curves.

Both graphs exhibit the characteristic airlift pump operating curve shape. With increasing gas flow rate, the liquid flow rate first increases rapidly and then tends to flatten out to a maximum liquid flow level characteristic of each system. The maximum liquid flow rate is maintained as the gas flow rate is increased and tends to drop off at extremely high gas flow rates.

This behaviour is due to the interaction between the weight, friction and acceleration pressure losses and is analogous to the discussion given in Section 7.2.3. The maximum liquid flow rate obtained in any airlift pump is dependent on the system characteristics:

- lift height
- gas injection depth
- pipe diameter
- suction pipe length
- gas flow rate
- liquid and gas properties

At low gas flow rates in the 90 mm airlift pump, liquid flow rates are slightly underpredicted to within 20% of the measured data. However, a large majority of the predicted liquid flow rates lie within 5% of the measured data.

From Figures 6.21 and 6.23 it can be seen that the calculation procedure used, adequately predicts liquid flow rates in the 40 mm and 90 mm airlift pumps to within 10% of the measured data.

7.3.2 40 mm Airlift pump-static lift and injector depth variation

Referring to Figure 6.24, the majority of the calculated liquid flow rates lie within 10% of the measured data for the lift heights and injector depths researched. The calculation procedure used tends to underpredict the liquid flow rates by a small percentage.

Being a recirculating system, various other small effects might influence the analysis which have not been accounted for, thus causing this slight under-prediction.

7.3.3 40 mm airlift pump-injection technique comparison

Referring to Figure 6.25, the vertical annular gas injector tends to lead to slightly larger liquid flow rates than the horizontal injector through holes. At its maximum, an increase of 5% was noticed on the 40 mm airlift pump. This increase in liquid flow tends to diminish at lower airflow values.

7.3.4 90 mm airlift pump-injector aperature

Referring to Figure 6.26, increasing the aperture area on the vertical annular gas injector tends to lead to an increase in the liquid flow rate.

This effect shows up to be more predominant at low gas flow rates than at higher gas flow rates, where an increased aperture area has little effect on the airlift pump performance curve.

7.3.5 Operating curves using literature sources compared with the present analysis

Referring to Figure 6.27, Clark's data is predicted to within 20% on a 38.1 mm airlift pump. Clark's research equipment consists of a recirculating system which could cause various secondary pressure losses to influence the airlift pump behaviour. These effects cannot be included in the analysis as not enough information is given in the literature.

Referring to Figure 6.28, Gibson's data is predicted to within 10% at low gas flow rates and to within 15% at higher gas flow rates in a 78 mm airlift pump.

Weber's data for a 300 mm airlift pump (Figure 6.29) operating at a depth of 125 m is predicted to within 10% throughout all gas flow rates.

Both Weber's and Gibson's airlift pumps are non-recirculating, indicating a higher accuracy.

It can be concluded that the present analysis applied to airlift pumps researched in the literature, adequately predicts the airlift pump performance curves.

CHAPTER 8

CONCLUSIONS

1. To analyse airlift pumps operating in two-phase gas-liquid flow, pressures and pressure losses have to be calculated. These include:

   - static pressure gains
   - pressure losses in the suction pipe
   - pressure losses across the gas injector
   - pressure losses in the delivery line

2. Static pressure gains and pressure losses in the suction pipe are concerned with liquid only and can be modelled using well-accepted methods.

3. Pressure losses across the gas injector are small with respect to the other pressure losses encountered in the analysis and can be modelled using equation 2.12.

4. Pressure losses in the delivery pipe are due to the two-phase gas-liquid mixture. These losses consist of:

   - the weight of the gas-liquid mixture
   - the friction of the gas-liquid mixture
   - the acceleration of the gas-liquid mixture caused by the expansion of the gas

5. Static dilations cause airlift pumps to operate. These increase rapidly with increasing gas flow rates. A combined static dilation curve can be obtained by dividing the gas flow rate by $\pi/4\ d^{2.7}$ which would be applicable to all pipe sizes.

6. Knowledge of the dynamic void ratio is required for calculating pressure losses due to the weight of the two-phase gas-liquid mixture in the delivery pipe. The dynamic void ratio is best predicted using Clark's calculation procedure (Section 2.5.5). Weight pressure losses of the two phase mixture can then be calculated using equation 2.21, which has given good correlation with measured data on two research facilities.

7. Pressure losses due to the friction of the two phase mixture in the delivery pipe becomes increasingly significant at high gas flow rates. The losses can be predicted using a modification to Clark's calculation procedure (section 6.2.4) developed by the present author (equation 7.1).

8. Pressure losses due to the acceleration of the two-phase mixture in the delivery pipe are small compared with weight and friction pressure losses. These losses are adequately predicted using a standard two-phase model.

9. The addition of the models recommended in items 6, 7 and 8 above lead to good prediction of the two-phase pressure losses in the delivery pipe.

10. The calculation procedure outlined in Section 2.4 is highly suitable for the prediction of airlift pump behaviour. Good agreement is obtained when using the present theory to analyse the airlift pumps researched at the University of Cape Town as well as airlift pump data from other authors and presented in the literature.

REFERENCES

1. Apazides, N. 1985 Influence of bubble expansion and relative velocity on the performance and stability of an airlift pump. International Journal of Multiphase Flow, Vol. 11(4), pp. 459 - 479.
2. Alves, G.E. March 1954 Two phase flow in pipes. Fluid and Particle Mechanics, Ch. 6.
3. Blevius, R.D. 1984 Applied fluid dynamics handbook. Van Nostrand and Company Inc.
4. Bergeaud, F. April 1973 How to calculate air lifts for marine dredging and mining. Ocean Industy, pp. 169 - 172.
5. Chisholm, D. Sutherland, L.A. proc. 1969 Prediction of pressure gradients in pipeline systems during two-phase flow. Institution of mechanical engineers, Vol. 184, part 3c, paper 4.
6. Chisholm, D. 1983 Two-phase flow in pipelines and heat exchangers. Pitman Press Ltd.
7. Clark, N.N. Meloy, T.P. Flemmer, R.L.C. Jan 1985 Predicting the lift of airlift pumps in the bubble flow regime. Chem S.A., Vol. 22, pp. 14-17.
8. Clark, N.N. Dabolt, R.J. Jan 1986 A general design equation for airlift pumps operating in slug flow. Aiche Journal, Vol. 32, No. 1, pp. 56-63.
9. Clauss, G. 1978 Hydraulic lifting in deep-sea mining. Marine Mining, Vol. 1, No. 3.
10. Dedegil, M.Y. June 1982 Increase of the suction head by means of the "airlift" method. Bulk solids handling, Vol. 2, No. 2, pp. 267-269.
11. Dedegil, M.Y. 1974 Feststoff Förderung Nach Dem Lufthebe Verhahren. Von Spezialisten für Spezialisten, pp. 1-5.
12. Dedegil, M.Y. 1978 Entwicklungs Stand Und Tendenzen Beim Feststoffordern Nach Dem Lufthebe Verfahren. Maschinenmarkt, Würzenburg, 34,39; pp.765-769.

13. Feldle, G. (dissertation) — Theoretische und Experimentelle Untersuchungen über die Vertikale Hydraulische feststaff förderung nach dem Strahlpumpverfahren.

14. Fritz, H.R. Feb. 1969 — Theoretical and practical aspects of the airlift reverse circulation boring system. Bohren, Sprengen, Räumen.

15. Gibson, L.A. 1925 — The Airlift Pump. Hydraulics and its applications, 3rd edition, Constable and Company Limited.

16. Giot, M; Berleur Oct. 1986 — Application of the Airlift principal to solve maintenance problems. Hydrotransport 10, Paper D2.

17. Giddings, T. 1983 — The use of airlift pumps to develop wells. Groundwater, V.21(4), pp. 521-522.

18. Giek, K. 1979 — A collection of technical formulae. 4th edition, Geick-verlag.

19. Golan, L.P. Stenning, A.M. Proc. 1969-70 — Two phase vertical flow maps. Institution of Mechanical Engineers, Vol. 184, Part 3c, Paper 14.

20. Halde, R; Svensson, M. 1981 — Design of airlift pumps for continuous sand filters. Chemical Engineering Journal (21); pp.223-227.

21. Hill, J.C.C. Dec. 1978 — Special dredging systems. Reprint from dredging and port construction.

22. Kytomaa, H.K. Brenen, C.E. Dec. 1986 — Some observations of flow patterns and statistical properties of three component flows. International Symposium on Slurry Flow, pp.95-101.

23. Kouremenous,D.A. Staicos, J. March 1985 — Performance of a small airlift pump. The International Journal of Heat and Flow, Vol. 6, No. 1, pp. 217 - 222.

24. Lazarus, J.H. Aug. 1982 — Pump and Pipeline Instrumentation. Hydrotransport 8, Paper 14.

25. Lazarus, J.H. Berg, R.R. March 1987 — Airlift Pumps for Ocean Mining Application. Research Report 1 for De Beers Marine, HTRU, University of Cape Town.

26. Lazarus, J.H. Berg, R.R. June 1987 — Airlift Pumps for Ocean Mining Application. Research Report 2 for De Beers Marine, HTRU, University of Cape Town.

27. Lazarus, J.H. June Airlift Pumps for Ocean Mining Application.
Berg, R.R. 1987 Preliminary to Research Report 3 for De Beers Marine, HTRU, University of Cape Town.

28. Lazarus, J.H. June Airlift pump investigation: "Static dilation
Berg, R.G. 1987 tests". Research Report 3 for De Beers Marine, HTRU, University of Cape Town.

29. Lazarus, J.H. Oct Airlift pump investigation: "Dynamic void ratios".
Berg, R.R. 1987 Research Report 4 for De Beers Marine, HTRU, University of Cape Town.

30. Lazarus, J.H. July CE 302 - Hydraulic Engineering Laboratory Manual,
1984 University of Cape Town.

31. Lazarus, J.H. 1987 Thesis 42 : 40 mm Airlift Pump.
Undergraduate thesis, University of Cape Town.

32. Loomis, A.W. 1980 Compressed Air and Gas Data. Chapter 31: Airlift pumping. Ingersoll-Rand Company, Washington.

33. Stenning, A.H. April An analytical experimental study of airlift pump
Martin, C.B. 1968 performance. Transactions of ASME, pp. 106-110.

34. Stone, J.H. 1987 A program to calculate airlift pump performance.
Microsoftware for engineers; Vol. 3; No. 3.

35. Stanislav, J.F. Dec Gas liquid flow in downward and upward inclined
Kokal, S. 1986 pipes. The Canadian Journal of Chemical Engi-
Nicholson, M.K. neering, Vol 64, pp. 881-886.

36. Shebatin, V.G. 1977 Air-lift conveying of liquids and suspensions.
Sokolov, N.N. Journal of Applied Chemistry of the USSR,
Domanskii, I.V. Vo. 50(4); pp. 823-826.
Davydov, I.V.

37. Shebatin, V.G. 1977 Gas content of a rising stream of three-phase
Domanskii, I.V. gas-liquid-solid mixture. Journal of Applied
Sokolov, V.N. Chemistry of the USSR, Vol. 50(4), pp. 810-814.

38. Stenning, A.H. April An analytical and experimental study of airlift
Martin, C.B. 1968 pump performance. Transactions of ASME, pp.106-110

39. Stone, I.N. 1987 A program to calculate air-lift pump performance.
Microsoftware for Engineers; Vol. 3; No. 3.

40. Tong, L.S. 1965 Boiling heat transfer and two phase flow.
John Wiley & Sons, Inc.

41. Unknown "A versatile Italian dredge pump system". Reprint from "World Dredging & Marine Construction Magazine.

42. Weber, M. Dedegil, M.Y. 1976 Transport of solids according to the airlift principle. Hydrotransport 4, paper III.

43. Weber, M. 1982 Vertical hydraulic conveying of solids by airlift. Journal of pipelines 3; No. 2; pp. 137-152.

44. Weber, M. Dec. 1976 Das Air-lift Verfahren und Seine einselzbarkeit zur förderung von mineralien aus der tiefsee. Meeres technique 7, 1976, pp. 189-199.

45. Weber, M. Schauki, N. 1967 Pneumatische unde hydraulische förderung. Auf bereitungs technik; Jahrgang 8; N10, pp.594-558.

CONTENTS OF APPENDIX

APPENDIX A

CALCULATION PROCEDURE AND COMPUTER PROGRAM

APPENDIX A

CALCULATION PROCEDURE AND COMPUTER PROGRAM

1. INTRODUCTION

To predict the performance of airlift pumps operating under different conditions, it is necessary to calculate liquid flow rates for a range of gas flow rates.

A computer program has been written in True Basic (Version 2), to aid in calculating the liquid flow rate for a specific gas flow rate. This chapter describes the calculation procedure used when analysing airlift pumps and gives a listing of the computer program.

2. CALCULATION PROCEDURE

To analyse an airlift pump, the technique discussed in section 2.4 is used. It is necessary to calculate:

(i) the static pressure at the suction inlet;
(ii) the pressure losses in the suction line;
(iii) the pressure losses across the gas injector;
(iv) the pressure losses in the delivery line.

Having calculated the above four pressures, a pressure balance is performed:

Atmospheric pressure at the external liquid level
\+ static pressure gain to the suction inlet
= Atmospheric pressure at the external liquid level
\+ pressure loss in the suction line
\+ pressure loss across the gas injector
\+ pressure loss in the delivery line (A1)

Thus if the airlift pump is in dynamic equilibrium, then the:

static pressure gain
= pressure loss in the suction line
+ pressure loss across the gas injector
+ pressure loss in the delivery line (A2)

and the two atmospheric pressures in equation A1 balance.

For calculating the pressures in equation (A2) it is necessary to know the gas flow rate and liquid flow rate as well as the independent variables. However, the liquid flow rate for a specific gas flow rate is the solution to the analysis and it is necessary to assume an initial liquid flow rate which is adjusted subject to the pressure balance. The following is the calculation procedure:

(i) Input independent variables (pipe diameter, gas injection depth, length of suction pipe and height of lift).
(ii) Assume an initial liquid flow rate.
(iii) Calculate all pressures (equation A1 or A2) using the assumed liquid flow rate.
(iv) Balance equation A1.
(v) If the two atmospheric presures do not balance within a prescribed accuracy, then adjust the liquid flow rate and reiterate from item (iii) above.
(vi) Continue this procedure until equation A1 is balanced. The liquid flow rate chosen is then the solution.

2.2 Pressure calculation

2.2.1 Static pressure gain

The static pressure gain is calculated as described in Section 2.4.1.

2.2.2 Pressure losses in the suction line

Pressure losses in the suction line are calculated as described in Section 2.4.2.

In the computer program, the above two pressures are used to calculate the pressure before the gas injection point which is given by:

pressure before gas injection = atmospheric pressure at external liquid level
+ static pressure gain to the suction inlet
- pressure losses in the suction line. (A3)

2.2.3 Pressure losses across the gas injector

Pressure loss across the gas injector are calculated using equation (2.12) and the following procedure:

(i) Calculate gas flow rate using the pressure at the gas injector (A3) and equation (2.14).
(ii) Calculate the dynamic void ratio.
(iii) Calculate the liquid and gas velocities.
(iv) Apply equation (2.12).

The pressure after the gas injection point is calculated using
pressure after gas injection = pressure before gas injection - pressure loss across the gas injectors (A4)

2.2.4 Pressure losses in the delivery pipe

Pressure losses in the delivery pipe are calculated using equation (2.16)

To allow for the isothermal expansion of the gas bubble up the delivery pipe, the pressure losses are calculated in incremental steps and then added.

In each incremental step the average weight and friction are calculated. For this reason, as well as to calculate the acceleration, it is necessary to determine the velocity of the gas and liquid phases and the void ratios at the beginning and end of each incremental step.

For the void ratios and gas velocities, it is necessary to determine the gas flow rate at the end of an incremental step. For this, the pressure at the end of the incremental step is required which is the solution to the calculation. To overcome this, the gas flow rate and void ratio at the end of the incremental step is aproximated.

This is done by calculating the void ratio at the gas injector and delivery outlet. Assuming a linear void ratio increase up the delivery pipe length, the end of each increment can be approximated.

Various incremental steps were used and it was found steps of 1 m length give sufficiently accurate results.

Thus the following procedure is used to calculate the pressure loss in the delivery pipe.

1. Choose incremental step distance.
2. Calculate the dynamic void ratio at the delivery outlet.
3. Calculate void ratio increase per incremental step.
4. Calculate gas flow rate at the beginning and end of each incremental step.
5. Calculate phase velocities at the beginning and end of each incremental step.
6. Calculate average weight and friction components for each incremental step.
7. Apply equation (2.16) and calculate pressure loss across each incremental step.
8. Sum all icnremental pressure losses up the delivery pipe.

The pressure at the delivery outlet is calculated using:

pressure at the delivery outlet = pressure after gas injection - total pressure loss up the delivery pipe.

(A5)

2.2.5 Pressure balance

If the initial gas flow rate chosen is correct, then the airlift pump is in dynamic equilibrium, and the pressure at the delivery outlet should balance atmospheric pressure to within a stipulated accuracy.

If the pressure at the delivery outlet is larger than atmospheric pressure, then the liquid flow rate must be adjusted to a larger value and the calculation procedure is repeated. For delivery outlet pressures less than atmospheric, liquid flow rates are reduced until a balance is obtained.

The accuracy stipulated in the pressure balance is 0.1% of the total pressure drop in the delivery pipe which is calculated using the gas injector pressure and atmospheric pressure at the delivery outlet.

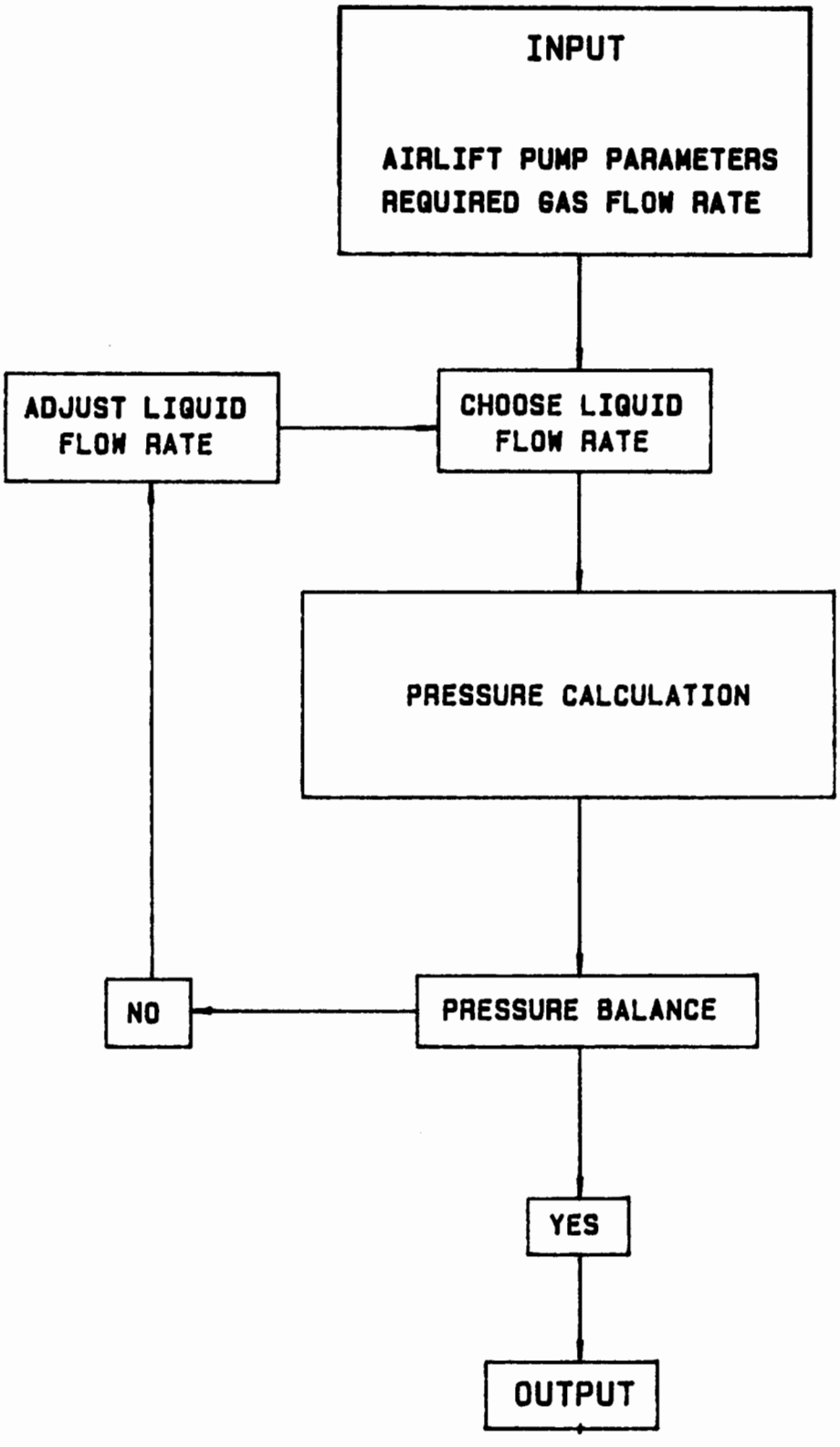
INPUT
AIRLIFT PUMP PARAMETERS
REQUIRED GAS FLOW RATE
CHOOSE LIQUID FLOW RATE
ADJUST LIQUID FLOW RATE
PRESSURE CALCULATION
PRESSURE BALANCE
NO
YES
OUTPUT

FIGURE A1

```
!##############################################################################
!
!                    AIRLIFT PUMP ANALYSIS
!                              program to calculate operating curves
!                              in two phase flow
!
!                                                        R R BERG  1987
!##############################################################################



! SETUP  ---------------------------------------------------------------------

LIBRARY "ENHANCE.TRU"
dim LIQUID(250),Qg(250),P11(250),Eg(250),dp(250)


! INTRODUCTION SCREEN  AND DATA INPUT ----------------------------------------

CALL OpeningScreen

CALL InputRoutine


! INCREMENTAL STEP DISTANCE --------------------------------------------------

LET N = INT(H1+H2)
LET COUNT = 1

CLEAR

! GAS FLOW RATE LOOP ---------------------------------------------------------

DO

! OUTPUT SCREEN --------------------------------------------------------------

CALL HiCenter (2, "      MAIN CALCULATION ROUTINE          ")
SET CURSOR 10,1
call HIon
PRINT "ENTER GAS FLOW RATE  S.T.P. l/s ?     "
SET CURSOR 10,33
      INPUT QGO
      let Qgo   = Qgo/1000
call HIOFF

CALL DRAWVLINE(5,20,40)
SET CURSOR 5,42
PRINT "GAS FLOW RATE"
SET CURSOR 6,42
PRINT "   l/s  S.T.P."
CALL DRAWhLINE(7,41,80)

SET CURSOR 5,62
PRINT "LIQUID FLOW RATE"
SET CURSOR 6,62
PRINT "       l/s      "
```

```
! INITIAL LIQUID FLOW RATE APPROXIMATION ------------------------------------

     let upper = 600e-3
     let lower = 0

! LIQUID FLOW RATE LOOP ------------------------------------------------------

do

call hionbl
CALL WRITERC (22,12,"                    CALCULATING ....              ")
call hiOFF

          let ql = (upper+lower) / 2

! CONSTANTS ------------------------------------------------------------------

          let po   = 101300
          let g    = 9.81
          let rhof = 1000
          let rhog = 1.204
          let w    = rhof*g
          let a    = pi*d^2/4
          let vls  = ql/a
          let x    = (h1+h2)/n
          let psum = 0
          let per  = 0

!INJECTOR PRESSURE CALCULATION ---------------------------------------------

               let re  = (ql)/a*d*1e6
               let f   = (.08/re^.25)

               let p1  = po+w*(h1)-w*vls^2*((1+1)/2/g+2*f*h3/g/d)

               let cut = p1

! INSITU GAS FLOW RATE CALCULATION -------------------------------------------

         for i =1 to (n+1)

    if i=1 then
          let Qg(i) = Qgo*po/p1

         else if i>1 then
             let Qg(i)=Qgo*po/(p2-psum-w*x*(1-(Eg(i-1)+CORR+Eg(i-1))/2))

    end if

! DYNAMIC VOID RATIO CALCULATION  --------------------------------------------


           call VOID_RATIO (Qg(i),ql,a,d,void)

      let Eg(i) = void
      let vl    = ql/a/(1-eg(i))
      let vg    = qg(i)/a/eg(i)
```

```
! VOID RATIO INCREASE PER INCREMENTAL STEP ----------------------------------

      let k1   = a*0.35*(9.81*d)^0.5
      let k2   = k1+1.2*ql
      let per  = k2*(Qgo-Qg(i))/(Qg(i)*(1.2*Qg(i)+k2))
      let corr = eg(i)*(1+per)/n

!  PRESSURE LOSS ACROSS GAS INJECTOR ----------------------------------------

       if i = 1 then
             let Qgh = 1e-99
             let Qgl = Qg(i)

       call ACCELERATION (Qgh,Qgl,ql,a,d,acc)

             let p2  = p1 - acc

         else if i>1 then

! PRESSURE LOSSES PER INCREMENT ---------------------------------------------

                let RE = vls*d/1e-6
                let F  = .08/RE^0.25

                let FRICTION = 2000*F*x*vl^2/d*(1+1.5*(eg(i-1)+eg(i))/2)


                let qgh = qg(i-1)
                let qgl = qg(i)

                call ACCELERATION (Qgh,Qgl,ql,a,d,acc)

                let WEIGHT=((eg(i-1)+eg(i))/2*1.204+(1-(eg(i-1)+eg(i))/2)*1000)*g*x



                       let dp(i)=FRICTION+WEIGHT+ACC

               let psum=psum+dp(i)
     end if

     next i

       let p3 = p2-psum

! PRESSURE BALANCE ----------------------------------------------------------

           let left  = po
           let right = p3
           let bal   = left - right

           if abs(bal) < ((CUT-po)*.001) then
                        exit do
                 else if bal < 0 then
                             let lower = ql
                       else if bal > 0 then
                                   let upper=ql
            end if

loop
```

```
! OUTPUT AND SUBROUTINES ------------------------------------------------

SET CURSOR COUNT+8,47
PRINT USING "#.##^^^^" : Qgo*1000
SET CURSOR COUNT+8,68
PRINT USING "#.##^^^^" : Ql*1000

CALL PROMPT
IF ANS$ = "N" THEN EXIT DO
LET COUNT = COUNT + 1
LOOP

!.....................................................................

 sub VOID_RATIO (qg,ql,a,d,void)

       let void  =( a*(1.2*(qg/a+ql/a)+.35*(9.81*d)^0.5)/qg)^(-1)

end sub

!.....................................................................

 sub ACCELERATION (Qgh,Qgl,ql,a,d,acc)


   let Egh = ( a*(1.2*(Qgh/a+ql/a)+.35*(9.81*d)^0.5)/Qgh)^(-1)
   let Egl = ( a*(1.2*(Qgl/a+ql/a)+.35*(9.81*d)^0.5)/Qgl)^(-1)
   let vlh = ql/a/(1-Egh)
   let vgh = Qgh/a/Egh
   let vll = ql/a/(1-Egl)
   let vgl = Qgl/a/Egl

   let pah = Egh*1.204*vgh^2 + (1-Egh)*1000*vlh^2
   let pal = Egl*1.204*vgl^2 + (1-Egl)*1000*vll^2

   let acc = pal-pah

end sub

!.....................................................................

SUB OpeningScreen

    CLEAR
    CALL DrawBox(2,8,10,70)
    CALL HiCenter(4," A I R L I F T  P U M P  A N A L Y S I S ")
    CALL HiCenter(6," T W O  P H A S E  -  G A S  L I Q U I D ")
    CALL HiOff
    CALL WriteCenter(12, "P R E D I C T I O N  O F  L I Q U I D")
    CALL WriteCenter(14, "F L O W  R A T E  F O R  A  G I V E N")
    CALL WriteCenter(16, "G A S  F L O W  R A T E  I N  A N Y")
    CALL WriteCenter(18, "A I R L I F T  P U M P")
    CALL DrawBox(21,23,25,55)
    CALL WriteCenter(22,"R R Berg  (c) 1988")
    CALL WriteCenter(25,"Press any key to continue")
    GET KEY c
    CLEAR

END SUB
```

```
!.....................................................................

SUB InputRoutine

CLEAR
CALL HiCenter(2, "        INPUT DATA SUBROUTINE             ")
CALL HiOn
set cursor 8,1
print "ENTER DEPTH OF THE GAS INJECTOR (m):          "
print "ENTER STATIC LIFT HEIGHT        (m):          "
print "ENTER LENGTH OF SUCTION PIPE    (m):          "
print "ENTER PIPE DIAMETER             (m):          "
SET CURSOR 8,36
INPUT H1
SET CURSOR 9,36
INPUT H2
SET CURSOR 10,36
INPUT H3
SET CURSOR 11,36
INPUT d
CALL HiOff

END SUB

!.....................................................................
SUB PROMPT

CALL HiCENTER (22,"Do you need further gas flow rates? - y or n ")
INPUT ANS$
LET ANS$ = UCASE$(ANS$)

END SUB

!.....................................................................

end
```

APPENDIX B

CHISHOLM (1983) - ARMAND COEFFICIENT DERIVATION

APPENDIX B

CHISHOLM'S (1983) ARMAND COEFFICIENT DERIVATION

1. Introduction

Chisholm uses equation 2.31 to calculate the Armand coefficient, which then is used in calculating the dynamic void ratio. The following Appendix shows how Chisholm derived equation 2.31.

2. Derivation

The volume flow ratio β is given by:

$$\beta = \frac{Q_g}{Q_g + Q_\ell} \tag{B1.1}$$

The velocity ratio (K) is the ratio of average gas velocity to average liquid velocity, given by

$$K = \frac{v_g}{v_\ell} \tag{B1.2}$$

The dynanmic void ratio is given by:

$$\epsilon = \frac{A_g}{A} \tag{B1.3}$$

From continuity the volume flow rates of the liquid and gas phases are given by:

$$Q_g = A_g v_g \tag{B1.4}$$

and $$Q_\ell = A_\ell v_\ell \tag{B1.5}$$

Multiplying equation (B1.3) by $\frac{v_g}{v_g}$, and substituting equations (B1.2), (B1.4) and (B1.5), the dynamic void ratio can be expressed as:

$$\epsilon_g = \frac{Q_g}{Q_g + K Q_\ell} \tag{B1.6}$$

Using the approach presented by Armand (1946) for dynamic void ratio calculation,

$$\epsilon_g = C_A \beta \tag{B1.7}$$

and substituting equation (B1.6) results in

$$\frac{1}{C_A} = \beta + \frac{K Q_\ell \beta}{Q_g} \tag{B1.8}$$

Further substitution of equation (B1.1) results in:

$$\frac{1}{C_A} = \beta + K(1 - \beta) \tag{B1.9}$$

For the calculation of K, Chisholm uses

$$K = \frac{1}{\left[1 - \beta\left(1 - \frac{\rho_g}{\rho_\ell}\right)\right]^{1/2}} \tag{B1.10}$$

which he derives from the empirical equation

$$K = \left(\frac{\rho_L}{\rho_H}\right)^{1/2} \tag{B1.11}$$

and equations (B1.6), B1.1) and (B1.11).

Substituting equation (B1.10) into (B1.9) results in

$$\frac{1}{C_A} = \beta + \frac{(1 - \beta)}{\left[1 - \beta\left(1 - \frac{\rho_g}{\rho_\ell}\right)\right]^{1/2}} \tag{B1.12}$$

which is the same as equation 2.31.

APPENDIX C

DETAILED COMPONENT RESULTS

AIRLIFT PUMP DATA SHEET

results of STATIC DILATION

SHEET No : 1
PIPE SIZE mm : 36
TEST/THEORY : TEST RESULTS OPERATOR: R.R.BERG
MATERIAL DESCRIP : CLEAR WATER DATE: 5/10/1987
DENSITY kg/m^3 : 1000

TEST NUMBER	ORIFICE PLATE H mm	ORIFICE PLATE L mm	GAS FLOW Qg l/s	COLUMN DILA. Ego %
1	533	532	0.15	33
2	535	530	0.33	46
3	538	525	0.54	49
4	545	520	0.75	57
5	552	514	0.92	68
6	564	500	1.19	69
7	586	480	1.54	70
8	602	462	1.77	71
9	635	426	2.16	74
10	706	357	2.79	77
11	767	295	3.24	78
12				
13				
14				
15				

AIRLIFT PUMP DATA SHEET

results of STATIC DILATION

SHEET No : 2
PIPE SIZE mm : 86
TEST/THEORY : TEST RESULTS OPERATOR: R.R.BERG
MATERIAL DESCRIP : CLEAR WATER DATE: 5/10/1987
DENSITY kg/m^3 : 1000

TEST NUMBER	ORIFICE PLATE H mm	ORIFICE PLATE L mm	GAS FLOW Qg l/s	COLUMN DILA. Ego %
1	988	980	4.22	48
2	995	973	7.00	59
3	1003	963	9.44	64
4	1023	942	13.44	70
5	1035	930	15.30	71
6	1060	906	18.53	74
7	1085	884	21.17	76
8	1102	865	22.99	76
9	1121	841	24.99	77
10	1169	798	28.76	79
11				
12				
13				
14				
15				

AIRLIFT PUMP DATA SHEET

results of STATIC DILATION

SHEET No : 3
PIPE SIZE mm : 142
TEST/THEORY : TEST RESULTS OPERATOR: R.R.BERG
MATERIAL DESCRIP : CLEAR WATER DATE: 6/10/1987
DENSITY kg/m^3 : 1000

TEST NUMBER	ORIFICE PLATE H mm	ORIFICE PLATE L mm	GAS FLOW Qg l/s	COLUMN DILA. Ego %
1	990	981	4.48	22.0
2	994	978	5.97	27.0
3	1002	969	8.58	34.5
4	1019	951	12.31	41.0
5	1035	933	15.08	45.7
6	1062	905	18.71	50.0
7	1086	881	21.38	53.8
8	1137	829	26.21	59.4
9	1167	796	28.76	60.6
10	1215	747	32.30	63.1
11	1265	695	35.65	64.9
12	1300	660	37.78	65.6
13				
14				
15				

AIRLIFT PUMP DATA SHEET

result of DYNAMIC VOID RATIO COMPARISONS

SHEET No	:	1					
PIPE SIZE mm	:	36mm ID					
TEST/THEORY	:	both			OPERATOR:	R.R.BERG	
MATERIAL DESCIP	:	clear water			DATE:	26/10/1987	
DENSITY kg/m^3	:	1000					

GAS FLOW	LIQUID FLOW	DYNAMIC VOID RATIO PREDICTIONS				
Qg l/s	Ql l/s	GIOT & CHISHOLM	CLARK	WEBER	DATA	
0.24	0.45	30.0	23.0	20.0	21.0	
0.55	0.59	40.0	34.0	29.0	33.0	
0.74	0.63	44.5	40.0	34.0	38.0	
0.77	0.72	42.5	38.4	32.6	42.0	
0.90	0.65	47.0	43.0	36.0	40.0	
0.93	0.71	46.0	42.7	36.0	46.0	
1.12	0.67	50.6	47.4	40.0	48.0	
1.29	0.66	53.0	50.6	42.6	49.0	
1.30	0.68	53.0	50.0	42.0	45.0	
1.34	0.76	52.0	49.0	41.0	53.0	
1.62	0.69	56.0	54.0	45.0	48.0	
1.62	0.75	55.0	53.0	45.0	53.0	
1.89	0.77	57.0	55.6	47.0	55.0	
2.04	0.70	59.0	58.0	49.0	52.0	
2.08	0.73	59.0	58.0	49.0	55.0	
2.10	0.79	58.0	57.0	48.5	55.0	
2.57	0.77	61.6	61.0	52.0	57.0	
2.62	0.71	63.0	62.0	53.0	54.0	
2.99	0.79	63.4	63.0	54.3	60.0	
3.00	0.77	63.8	63.3	54.7	59.0	
3.08	0.71	65.0	64.7	56.0	56.0	
3.54	0.77	66.1	66.0	57.0	61.0	
3.76	0.79	66.5	66.0	58.0	63.0	
3.91	0.77	67.4	67.0	58.9	61.0	
4.16	0.77	68.2	67.9	59.8	61.0	

AIRLIFT PUMP DATA SHEET

result of DYNAMIC VOID RATIO COMPARISONS

SHEET No	:	2				
PIPE SIZE mm	:	86mm ID				
TEST/THEORY	:	both			OPERATOR:	R.R.BERG
MATERIAL DESCIP	:	clear water			DATE:	27/10/1987
DENSITY kg/m^3	:	1000				

GAS FLOW	LIQUID FLOW	DYNAMIC VOID RATIO PREDICTIONS			
Qg l/s	Ql l/s	GIOT & CHISHOLM	CLARK	WEBER	DATA
2.88	1.03	58.9	44.0	34.0	36.0
4.27	2.16	53.0	44.5	35.6	46.0
6.09	3.07	53.5	47.0	38.4	44.0
7.25	3.56	54.0	48.8	39.8	49.0
9.42	4.14	55.7	52.0	42.6	49.0
10.08	4.07	57.0	53.5	44.0	54.0
12.16	4.40	59.0	55.9	46.2	56.5
12.50	4.62	58.5	55.7	46.1	55.0
14.45	4.62	60.6	58.3	48.6	62.2
15.90	4.74	61.7	59.7	49.9	63.0
17.92	4.74	63.0	61.6	51.8	64.7
18.04	4.99	63.0	61.0	51.4	64.0
19.95	5.20	63.6	62.2	52.8	68.0
22.43	4.81	66.0	64.0	55.0	67.0

AIRLIFT PUMP DATA SHEET

result of WEIGHT PRESSURE LOSS COMPARISON

SHEET No : 1
PIPE SIZE mm : 36mm ID
TEST/THEORY : both OPERATOR: R.R.BERG
MATERIAL DESCIP : clear water DATE: 28/10/1987
DENSITY kg/m^3 : 1000

GAS FLOW Qg l/s	LIQUID FLOW Ql l/s	WEIGHT PRESSURE LOSS in kPa				TOTAL PRESSURE LOSS kPa
		GIOT & CHISHOLM	CLARK & STENNING	WEBER	DATA	
0.239624	0.45	6238	6864	7111	7047	7161
0.548378	0.59	5346	5822	6261	5978	6259
0.745737	0.63	4954	5351	5888	5533	6082
0.76577	0.72	5127	5498	5995	5177	6082
0.896258	0.65	4711	5056	5651	5355	6043
0.934265	0.71	4785	5109	5688	4820	5984
1.12068	0.67	4411	4689	5351	4642	5867
1.29218	0.66	4173	4412	5119	4553	5886
1.30936	0.68	4198	4430	5133	4909	5866
1.34887	0.76	4321	4536	5216	4197	5592
1.62886	0.69	3901	4072	4821	4642	5778
1.62961	0.75	4020	4185	4915	4197	5837
1.89949	0.77	3838	3963	4715	4019	5837
2.04163	0.7	3607	3724	4499	4286	5680
2.08011	0.73	3639	3748	4519	4019	5837
2.10116	0.79	3733	3833	4594	4019	5689
2.57732	0.77	3425	3489	4263	3841	5886
2.62497	0.71	3298	3369	4146	4108	5611
2.99372	0.79	3267	3306	4074	3573	5788
3.0005	0.77	3232	3275	4043	3662	5984
3.08782	0.71	3098	3151	3914	3930	5582
3.54511	0.77	3030	3059	3806	3484	5935
3.76221	0.79	2990	3012	3751	3306	5544
3.91921	0.77	2913	2939	3667	3484	5788
4.16499	0.77	2844	2869	3584	3484	5886

AIRLIFT PUMP DATA SHEET

result of WEIGHT PRESSURE LOSS COMPARISON

SHEET No : 2
PIPE SIZE mm : 86mm ID
TEST/THEORY : both OPERATOR: R.R.BERG
MATERIAL DESCIP : clear water DATE: 27/10/1987
DENSITY kg/m^3 : 1000

GAS FLOW	LIQUID FLOW	WEIGHT PRESSURE LOSS in kPa				TOTAL PRESSURE
Qg l/s	Ql l/s	GIOT & CHISHOLM	CLARK & STENNING	WEBER	DATA	LOSS kPa
2.88	1.03	6045	8258	9718	9424	8838
4.27	2.16	6862	8166	9480	7954	8289
6.09	3.07	6851	7751	9070	8248	8221
7.25	3.56	6789	7533	8863	7513	7700
9.42	4.14	6523	7081	8452	7396	7750
10.08	4.07	6324	6853	8255	6778	7505
12.16	4.40	6072	6492	7916	6411	7141
12.50	4.62	6121	6516	7931	6631	7044
14.45	4.62	5798	6134	7573	5573	7230
15.90	4.74	5637	5930	7370	5456	6965
17.92	4.74	5395	5652	7090	5206	7050
18.04	4.99	5488	5728	7160	5309	6926
19.95	5.20	5364	5565	6986	4721	6995
22.43	4.81	4974	5175	6578	4868	6769

AIRLIFT PUMP DATA SHEET

result of FRICTION PRESSURE LOSS COMPARISON

SHEET No : 1.00
PIPE SIZE mm : 36mm ID
TEST/THEORY : both OPERATOR: R.R.BERG
MATERIAL DESCIP : clear water DATE: 28/10/1987
DENSITY kg/m^3 : 1000.00

GAS FLOW	LIQUID FLOW	FRICTION PRESSURE LOSS in kPa				DATA
Qg l/s	Ql l/s	STENNING	CLARK & WEBER	CHISHOLM	MODIFIED CLARK	kPa
0.24	0.45	97	82	130	160	300
0.55	0.59	185	147	277	404	441
0.75	0.63	228	174	362	564	735
0.77	0.72	276	217	432	664	588
0.90	0.65	256	191	424	688	992
0.93	0.71	293	222	483	782	880
1.12	0.67	295	211	514	876	1183
1.29	0.66	310	213	562	990	1480
1.31	0.68	324	224	587	1032	1441
1.35	0.76	378	269	678	1184	1061
1.63	0.69	369	242	707	1297	1712
1.63	0.75	409	276	772	1406	1657
1.90	0.77	457	299	896	1676	1880
2.04	0.70	424	262	861	1642	1962
2.08	0.73	451	281	913	1742	2095
2.10	0.79	498	319	999	1897	1862
2.58	0.77	542	322	1152	2259	2404
2.62	0.71	498	284	1078	2125	2249
2.99	0.79	609	347	1341	2674	2488
3.00	0.77	592	334	1309	2613	2716
3.09	0.71	549	295	1238	2477	2438
3.55	0.77	656	346	1510	3052	2883
3.76	0.79	700	366	1629	3306	2539
3.92	0.77	698	354	1646	3342	2856
4.16	0.77	725	358	1735	3526	3024

AIRLIFT PUMP DATA SHEET

result of WEIGHT PRESSURE LOSS COMPARISON

SHEET No : 2.00
PIPE SIZE mm : 86mm ID
TEST/THEORY : both OPERATOR: R.R.BERG
MATERIAL DESCIP : clear water DATE: 27/10/1987
DENSITY kg/m^3 : 1000.00

GAS FLOW	LIQUID FLOW	FRICTION PRESSURE LOSS in kPa				DATA
Qg l/s	Ql l/s	STENNING	CLARK & WEBER	CHISHOLM	MODIFIED CLARK	kPa
2.88	1.03	6045	8258	9718	9424	8838.00
4.27	2.16	6862	8166	9490	7954	8289.00
6.09	3.07	6851	7751	9070	8248	8221.00
7.25	3.56	6789	7533	8863	7513	7700.00
9.42	4.14	6523	7081	8452	7396	7750.00
10.08	4.07	6324	6853	8255	6778	7505.00
12.16	4.40	6072	6492	7916	6411	7141.00
12.50	4.62	6121	6516	7931	6631	7044.00
14.45	4.62	5798	6134	7573	5573	7230.00
15.90	4.74	5637	5930	7370	5456	6965.00
17.92	4.74	5395	5652	7090	5206	7050.00
18.04	4.99	5488	5728	7160	5309	6926.00
19.95	5.20	5364	5565	6986	4721	6995.00
22.43	4.81	4974	5175	6578	4868	6769.00

APPENDIX D

EXAMINATIONS WRITTEN BY THE AUTHOR TO COMPLETE THE REQUIREMENTS OF THE DEGREE

APPENDIX D

Examination		Credit Rating
CIV 540Z	Finite Element Analysis	4
CIV 536Z	Coastal Engineering Practice	5
CIV 516Z	Coastal Hydraulics	5
SEA 200F	Physical Oceanography	5
CIV 542Z	Irrigation Systems	3
THESIS	"Hydro-pneumatic conveying of liquid by means of an airlift pump"	20
	Total	42

Credit requirements for degree = 40